INTERACTIONS BETWEEN SOUND AND LONG PARTIAL ENCLOSURES

CHU, HO KIN

Ph.D

The Hong Kong

Polytechnic University

2018

The Hong Kong Polytechnic University

Department of Building Services Engineering

INTERACTIONS BETWEEN SOUND AND LONG PARTIAL ENCLOSURES

CHU, HO KIN

A thesis submitted in partial fulfilment of the requirements for the degree of

Doctor of Philosophy

February 2017

CERTI F ICATE OF ORIGINALITY

I hereby declare that this thesis is my own work and that, to the best of my knowledge and belief, it reproduces no material previously published or written, nor material that has been accepted for the award of any other degree or diploma, except where due acknowledgement has been made in the text.

(Signed)

CHU, Ho Kin (Name of student)

Abstract

This thesis aims at filling the missing research works in the current literatures concerning the field of sound and long partial enclosures. The first part of the thesis is to set up theoretical models for the internal sound field generated by a flush-mounted circular piston in an infinitely long and rigid rectangular duct with apertures such as side opening(s) and a slot. The apertures are modelled as vibrating air pistons. Simultaneous equations of the vibrating air piston velocities at these apertures are derived. The radiation impedance of a square air piston in terms of wave-number, piston size and aperture thickness is also derived.

The leaky sound behaviour of an open slot at the duct wall has been modelled. The air in the slot is modelled as a linear array of air pistons, which oscillate under the action of the sound excitation. A theory is developed to model in details the asymmetric sound radiation from the slot. This results in the introduction of a complex wave-number which is used to model the sound propagation inside the leaky duct.

The second part of the thesis demonstrates the finite element numerical modelling of leaky duct. In-duct modal decomposition technique is adopted to analyse the computed sound pressures. Contributions of discrete propagating modes are examined. Numerical results show excellent agreement with the predictions from the new mathematical model developed in the first part of this study.

A method to predict the abovementioned complex wave-number for different slot dimensions is derived. The findings show that the complex wave-number correlates closely with the propagation constant and the slot length. The present research formulates

the theoretical prediction of sound propagation phenomena along a leaky duct. This breakthrough generalizes current understanding on acoustical properties in tube-like cavity.

Publications arisen from this thesis

Some ideas and figures have appeared previously in the following publications:

Chu, S.H.K. & Tang, S.K., 2017. Analytical model and numerical simulation of internal sound fields of an infinitely long duct with aperture array. *INTER-NOISE Hong Kong*. (Full paper)

Chu, S.H.K. & Tang, S.K., 2014. Theory and three-dimensional numerical simulation of sound propagation along a long enclosure with side opening. *INTER-NOISE Melbourne Australia*. (Full paper)

Chu, S.H.K. & Tang, S.K., 2013. Three-dimensional numerical modelling of sound propagation in a long partial enclosure. *INTER-NOISE Innsbruck Austria*. (Full paper)

Chu, S.H.K. & Tang, S.K., 2012. Theoretical prediction and experimental modal analysis of sound propagation along a long enclosure. *The 19th International Congress on Sound and Vibration*. (Full paper)

Chu, S.H.K. & Tang, S.K., 2012. Sound propagation along a long partial enclosure, Acoustics 2012 Hong Kong. *Journal of the Acoustical Society of America*, 131(4), 3333, (2012). (Abstract)

Acknowledgements

First and foremost, I would like to express my sincere gratitude to my supervisor Professor S. K. Tang for his supervision, advice, guidance and support during my course of study. I am really grateful to his patient and willingness to discuss my research with me. I have benefited greatly from his expertise and insightful comments.

Thanks also go to all the professors at the Department of Building Services Engineering of The Hong Kong Polytechnic University for their teaching and guidance which nourished the acquisition of advanced knowledge in the field of my specialization.

Moreover, I would like to thank my colleagues Ms. Y. G. Tong, Ms. Louisa Cheung and Mr. K. E. Piippo for sharing of their learning experiences and professional knowledge with me.

Furthermore, I own credit to Mr. David Sze, Mr. Kenneth Yau and Ms. Yvonne Chan, the university mates of the undergraduate study for providing me some experimental data collection in laboratory and their work reports.

Lastly, I would like to offer my deepest thanks to my family for their unconditional love and support. I owe thanks to my parents for their care and encouragement. I would like to express my heartfelt thanks to my wife Yoko Poon and my daughter Chu Tik, motiving me to persevere.

Contents

Chapter 1

Introduction and outline

Chapter 2

Sound field in a long rectangular enclosure by a flush-mounted circular piston

Chapter 3

Radiation impedance of aperture and theoretical model of wave motion at the open slot

Chapter 4

Mathematical model of sound propagation along a rectangular duct with side opening(s) or an open slot

Chapter 5

Validation of the three-dimensional numerical modelling

Chapter 6

Prediction of the complex wave-number for the open slot cases

Chapter 7

Conclusions

References

Nomenclature

Symbol	*Description*
a	Duct interior height
A_{mn+}	Modal amplitude of waves traveling in $+x$ direction
A_{mn-}	Modal amplitude of waves traveling in $-x$ direction
b	Duct interior width
c	Speed of sound
c_{mn}	Modal wave speed
d	Square aperture length
d_i	Centre-to-centre distance from the sound source to *i*th piston
d_j	Centre-to-centre distance from the sound source to *j*th piston
D	An oscillating component defined as k_{x0}/k
E	Grid elements (numerical model)
f_{mn}	Modal frequency of the duct with an infinitely long gap
$f(y,z)$	A function of position (duct cross-section)
$F(x,y)$	A function for the average pressure of the single *i*th air piston
gth	Gap width
$G(x,y)$	A function for the average pressure of the mutual contribution from *j*th to *i*th air piston
h	Aperture height
$H(y,z)$	Acoustic pressure over a rectangular cross-section
$H_0(x)$	Struve function of zero order
$H_{-1}(x)$	Struve function of order -1

Symbol	*Description*
$H(\theta)$	Directional factor
i	Imaginary unit, $\sqrt{-1}$
I	Incident wave pressure amplitude
$J_0(x)$	Bessel function of zero order
$J_1(x)$	Bessel function of first order
k	Acoustic wave-number
k_r	Real part of wave-number
k_i	A real number (ik_i imaginary part of wave-number)
k_{mn}	Transverse component of propagation vector
$k_{n,c}$	Wave-number of infinitely long duct (without side opening)
$k_{n,o}$	Wave-number of duct with single side opening
k_x	Propagation constant (duct longitudinal direction)
k_{x0}	Complex wave-number of x-component at the open slot surface
k_{y0}	Complex wave-number of the normal vector of the open slot surface
$\vec{k}$	Vector of wave-number
L	Slot length
L_f	Length of free space (numerical model)
m	Transverse (vertical) mode order of rectangular duct
n	Spanwise (horizontal) mode order of rectangular duct
	Outward normal direction of a boundary
$\hat{n}$	Normal unit vector

Symbol	*Description*
N	Number of points allocated in an internal cross-section
p	Acoustic pressure
p_{mn}	Modal acoustic pressure
p_s	Acoustic pressure at the aperture contributed by the source
$\bar{p}$	Average acoustic pressure at an aperture
P	Wave pressure amplitude of sound source
P_0	Wave pressure at $z = 0$ (aperture)
P_i	Incident wave pressure (aperture)
	Average pressure of the source contribution to *i*th air piston
P_r	Reflected wave pressure (aperture)
P_δ	Wave pressure at $z = \delta$ (aperture)
P_{in}	Incident wave pressure (duct)
q	Dipole source strength
Q	Monopole source strength
Q_0	Source strength with even normal velocity distribution
r	Radial coordinate of circular piston
r_0	Distance between the source element to a far field point
R	Radius of circular piston;
	Reflected wave pressure amplitude
R_f	Radius of free space (numerical model)
s	Number of fitted points (percentage deviation)

Symbol	*Description*
S	Cross-section area of aperture
	Surface area
S'	Surface area of the sound source
t	Time
T	Free field perfectly matched layer (PML) thickness
U_0	Volume velocity at $z = 0$ (aperture)
	Amplitude of the slot oscillating flow
U_i	Incident volume velocity (aperture)
U_r	Reflected volume velocity (aperture)
U_δ	Volume velocity at $z = \delta$ (aperture)
$U(x)$	Velocity distribution function (slot surface)
V	Air piston velocity
V_i	Air piston velocity contributed by the *i*th piston
V_j	Air piston velocity contributed by the *j*th piston
V_s	Sound source velocity
$\dot{V}_s$	Sound source acceleration
V_C	Values obtained from COMSOL 3-D numerical model
V_M	Values predicted by mathematical model (MATLAB)
w	Aperture width
x, y, z	Cartesian coordinates
x', y', z'	Cartesian coordinates for the sound source
x_1	Centre-to-centre distance from sound source to an opening

Symbol	*Description*
y_1, z_1	Cartesian coordinates for a duct cross-section (initial discrete point)
Δy	Regular intervals of a for a duct cross-section
z_0	Acoustic impedance at $z = 0$ (aperture)
z_a	Acoustic impedance, $\rho_o c/S$
z_r	Acoustic impedance at $z = \delta$ (aperture)
Z	Specific radiation impedance
Z_r	Specific radiation impedance with the effect of aperture thickness
Δz	Regular intervals of b for a duct cross-section
$\alpha_{i,j}$	Matrix of total impedance for multiple air pistons
β	Decaying rate of internal duct pressure
δ	Aperture thickness
δ_{ij}	Kronecker delta function
ε	Amplitude adjustment of an oscillating component D
λ	Wavelength
η	Membrane displacement
θ	Polar angle
θ'	Inclination measured from the normal vector of an open slot
$\theta(x)$	A function of x for a rectangular radiation impedance (in real part)
ρ_o	Fluid density

Symbol	*Description*
$\varphi(x)$	A function of x for a rectangular radiation impedance (in imaginary part)
ϕ	Phase angle of an oscillating component D
ω	Angular frequency
ω_{mn}	Modal angular frequency
ψ_{mn}	Normalized modal function
$\psi_{\mu\nu}$	Normalized modal function $(\mu, \nu = m, n)$ or $(\mu, \nu \neq m, n)$

{This page is intended to be blank}

Chapter 1

Introduction and outline

1.1 Literature survey

This thesis deals with the problem of predicting the sound propagation in partial enclosures and the acoustical behaviours inside such structures. The results will be useful in many areas including the architectural design of buildings, environmental noise propagation and active noise control where long tube-like structures are involved.

Long partial enclosures can be found in many building developments. Examples include the long corridors on the perimeter zone of a building opened partially through small windows to the atmosphere, covered corridors like a long covered walkway/ bridge, and long corridors in some large churches/ university colleges having architecture similar to those built in the medieval periods. The urban street canyon in a congested high-rise city and the road flanked by roadside barriers are two other examples of long partial enclosures. There are also tube-like structures inside which the sound propagation is of concern. A typical example is the cavity under the walkway along a train via-duct which tends to enhance relatively long distance sound propagation due to reflective nature of its

internal surfaces. The rolling noise, impact noise and squeal noise can go into the cavity under the walkway on the via-duct, which is of the partially enclosed form.

It should be noted that one major difference between a full enclosure and a partial enclosure is that the internal acoustical environment of the latter is seriously affected by the environment external to it. Sound from a nearby sound source can go into the long partial enclosure and then propagate along the structure to a distance much longer than that in the free field where the spherical spreading of sound energy can result in a 6dB sound attenuation per doubling the distance from source (Morse & Ingard 1968).

However, studies related the acoustical characteristics and the propagation of noise inside long partial enclosures are rarely found. This appears to be due to the misunderstanding that sound propagation in such sound-leaky structures is not important. The reverberation observed in covered walkways with two sides opened to the atmosphere tends to suggest the possibility that sound can propagate over a distance longer and/or stay within the enclosure longer than generally expected. The associated sound radiation from the partial enclosures to the atmosphere also requires attention as this has an implication on environmental noise control (Environmental Protection Department 2002).

This section offers the overview of acoustical literatures related to some kinds of long partial enclosure, aperture, long duct with flushed-mounted finite membrane and acoustical damping phenomena. Effects of mean flow are ignored. Such theoretical background and principles of these related aspects form the basis of this research.

1.1.1 Acoustical behaviour in long enclosure

Noise propagation and reverberation in long enclosures or ducts have been studied extensively in the past few decades. Doak (1973a) provided a high quality paper on the theoretically closed form solutions for sound propagation along these hard-wall structures without mean flow. The wave equation for simple harmonic waves in a long enclosure is:

$$\nabla^2 p + k^2 p = 0 \tag{1.1}$$

where p and k denote the sound pressure and the wave-number respectively.

For an infinitely long, straight, hard-walled duct of constant area of cross-section, wave field contains standing waves in the y and z directions and traveling wave in the x direction. The solution takes the form of:

$$p(x,y,z,t) = f(y,z)e^{\pm ik_x x}e^{i\omega t} \tag{1.2}$$

This form of equation with function $f(y,z)$ can be solved by separation of variables. Suppose the duct interior height is a and width is b, the boundary condition associated with all internal surfaces of the duct follows that of a rigid wall of vanishing normal acoustic particle velocity.

$$\left.\frac{\partial p}{\partial y}\right|_{\mathrm{y=0}} = \left.\frac{\partial p}{\partial y}\right|_{\mathrm{y=a}} = \left.\frac{\partial p}{\partial z}\right|_{\mathrm{z=0}} = \left.\frac{\partial p}{\partial z}\right|_{\mathrm{z=b}} = 0 \tag{1.3}$$

The sound pressure can be expressed as an expansion of the eigen-functions of the partial differential equation. The eigen-functions are called the modes of the system, and the eigen-function expansion is the modal solution. In the case of a duct section constrained, the modal solution is

$$p(x,y,z,t) = \sum_{mn} \psi_{mn}\,(y,z)(A_{mn+}e^{-ik_x x} + A_{mn-}e^{ik_x x})e^{i\omega t} \tag{1.4}$$

where

$$k_x = \sqrt{k^2 - (\frac{m\pi}{a})^2 - (\frac{n\pi}{b})^2} \tag{1.5}$$

A_{mn+} and A_{mn-} are the modal amplitudes of the waves traveling in the $+x$ direction and $-x$ direction respectively. ψ_{mn} is called the normalized modal function.

$$\psi_{mn}(y,z) = \sqrt{(2-\delta_{0m})(2-\delta_{0n})}\cos\left(\frac{m\pi y}{a}\right)\cos\left(\frac{n\pi z}{b}\right) \tag{1.6}$$

δ_{ij} is the Kronecker delta function which becomes unity when $i=j$,

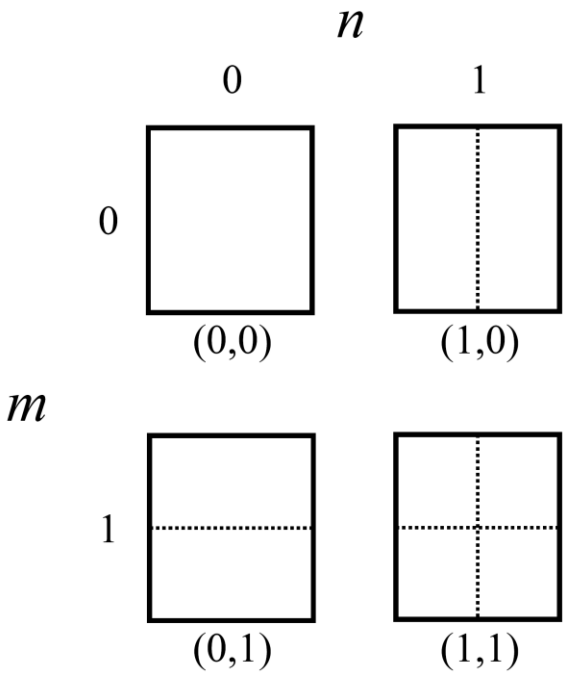

Figure 1.1 - Notation of mode index

There is a frequency at which k_x is zero for each (*n,m)* mode indices where *n* and *m* denote the spanwise (horizontal) and transverse (vertical) mode order of rectangular duct respectively. Such frequency is called the cut-on or cut-off frequency. When k_x is real, sound wave propagates in the $\pm x$ direction and the eigen-function is on a propagating mode. The mode is evanescent when the frequency is below the cut-off frequency and k_x becomes imaginary. An evanescent wave decays exponentially with x. The negative root of k_x has to be taken into account in any theoretical formulation (Kinsler *et al.* 2000).

In addition to the regular form of long duct, the analytical solutions for bended duct without mean flow is available from Cummings (1974). Numerical and experimental results for analysis of sound propagation of a mitred duct bend were verified (Cabelli & Shepherd 1984). Studies related sound propagation along ducts with non-uniform cross-sections have also been carried out by many researchers, for instance, Alfredson (1972), Utsumi (1999, 2001), Tang & Lau (2002), Sadamoto *et al.* (2004) and Lau & Tang (2005).

Kang (1996a, 1996b) determined the formulae for calculating the sound energy of reverberation in rectangular long enclosures with geometrically reflecting boundary. Yang & Shield (2000) also developed a ray tracing computer model for prediction of the sound field inside a long enclosure. Numerical investigation on the sound propagation inside long fully enclosures with diffusive cross-section boundaries has been done (Kang 2002a, 2002b). Sound response in a damped rectangular enclosure can be noted in Pan *et al.* (1999). In addition, Lam & Li (2007) offered a coherent model for predicting noise reduction in long enclosures with impedance discontinuities.

There were also researches concerning in-duct sound properties under other wall boundary conditions and configurations of long enclosure. Cummings (1978) derived a

theoretical model and carried out experiment of sound transmission through the duct wall. Assumption was made that sound radiated as finite length line source on the basis of coupled acoustic/ structural wave system. Flexible-walled duct coupled with acoustic/ structural modes were investigated (Martin *et al.* 2004). Huang's studies (2006) showed the broadband sound reflection by plates covering side-branch cavities in a long duct and discussed the corresponding silencing performance. Sound propagation from a slanted side branch into an infinitely long rectangular duct was examined by Tang & Lam (2008). A critical slant angle was noted and such phenomenon was explained by a simplified model.

1.1.2 Sound radiation from opened duct end

The acoustics of axisymmetric opening of an opened duct was considered in the past. The radiation efficiency of an opened duct ending was presented by Morfey (1969a, 1969b). Special focus was made on the higher order modes. On this basis, Doak (1973b) derived the duct interior sound field and the total radiated acoustic power of open duct end in terms of modal reflection coefficients, modal termination impedances and the like.

The opened ducts with and without flange were examined by researchers. Acoustically treated circular duct and annular duct with infinite flange were considered by Zorumski (1973). The topic of end correction for plane wave motion for opened duct was well known (Kinsler *et al.* 2000). The theory is that the end correction increases proportionally to the duct radius as long as the wavelength is large compared to the

transverse dimension. It is independent of frequency but affects the resonance frequencies of the duct.

The radiative directivity patterns of acoustic modes were discussed by Homicz & Lordi (1975). Rice (1978) also studied the multimodal far field acoustic radiation theory for a circular duct. In 1990s and 2000s, Chapman (1994) determined the ray structure of propagating acoustic modes at and the sound radiation from a cylindrical duct end. Comparisons between the theory of multimode and high-frequency asymptotic results were done by Joseph & Morfey (1999). Hocter (1999, 2000) was interested in the exact and approximate sound radiation and its pattern in the proximity of an opened cylindrical duct end. Comparisons between finite element numerical model and analytical solutions for the near field sound pressure level and the far field directivity of opened duct end could be found in Chen *et al.* (2004). Apart from abovementioned studies of sound radiation without mean flow, the sound radiation and directivity function with mean axial flow were derived theoretically, for instance, by Johnston & Ogimoto (1980) and Sinayoko *et al.* (2010).

The radiation of sound through the open end of other geometry like conical pipe was also examined (Ting & Keller 1977). A particular case of curved duct geometry was presented by Malbéqui *et al.* (1996). The directivity patterns were found quantifiable and not axisymmetric around the exit centreline.

1.1.3 Sound propagation of opened waveguide and street canyon

Models for calculating sound distribution in urban areas can be divided into macro scale and micro scale. Noise mapping software is based on simplified algorithms and is applicable for macro urban areas. This section includes a general review of the typical micro scale acoustical models and the related principles which have well been published in top journals.

There are models developed for accurate prediction of sound distribution at a micro scale, such as in a street canyon (Kang 2005, 2007). The adopted simulation techniques and related principles on the acoustics in street canyons include energy-based image source method, radiosity model, transport theory and wave-based models. Some scale model experiments and site measurements for street canyons as the validation were reviewed and discussed.

Kang (2000) presented the sound propagation behaviour of an idealized rectangular urban street canyon with buildings along both sides of constant height. By summing the energy from all the image sources in groups and taking direct sound transfer into account, the energy response at receiver can be obtained. Consequently, the reverberation time (RT), early decay time (EDT) and steady-state sound pressure level (SPL) at receiver could be determined by this energy-based image source method.

There were studies in relation to noise propagation in open channel type of structure using image source method (for instance, lu & Li 2002). They addressed the problem of predicting sound propagation in narrow street canyons, assuming that the

height of the buildings was much greater than the street width. A point source was considered and it simulated, for example, air conditioners installed on building façades and powered mechanical equipment for repair and construction work. Starting from the Helmholtz equation, the solution at a receiver was derived. The sound fields due to the point source and its images were summed coherently such that mutual interference effects between contributing rays could be included in the analysis.

The radiosity method is an effective way of dealing with diffusely reflecting boundaries. This method divides boundaries of a street canyon into a number of elements. It replaces the elements and receivers with nodes in a network. The sound propagation in the canyon could be simulated by energy exchange between nodes (Kang 2000). It is assumed that the ground is diffusely reflective, but the formulation was modified to consider geometrically reflecting ground by Kang (2002a).

Le Polles *et al.* (2004) applied the model of transport theory to an empty street canyon as two infinite and perfectly reflecting planes with partially diffusely reflecting surfaces characterized by Lambert's Law. Since there is no exact analytical solution for such a system, an asymptotic solution was explored (Börgers *et al.* 1992), showing that the transport equation with the appropriate boundary conditions might be reduced to a diffusion equation. It was assumed that the street width was much smaller than the length and height of the street. If the sound source was located on the ground, the sound propagation in a street canyon would be similar to the propagation between two parallel planes.

Researchers studied two-dimensional numerical modelling of sound propagating in an infinitely long duct. Perfectly matched layer absorbing boundary condition were

adopted to the opened interface by Koch (2005). Acoustical properties in the cavity, especially the discrete resonance modes, were examined. Pelat *et al.* (2009) were interested in a multimodal formalism and acoustic field was decomposed.

Scale model experiments were carried out, for example, Horoshenkov *et al.* (1999), Ismail & Oldham (2005) and Picaut & Simon (2001). Site measurements inside street canyons were also done by Ko & Tang (1978) and Picaut *et al.* (2005).

1.1.4 Sound transmission through aperture

Many researchers, such as Wilson & Soroka (1965a, 1965b), Gomperts (1965) and Sauter & Soroka (1970) were interested in the prediction of diffuse sound field transmission through apertures which were in circular, rectangular shape/ slit. The normal incidence transmission loss with a certain factor could be adopted to estimate the diffuse field transmission loss through aperture (Sgard *et al.* 2007). Furne (1990) and Chen (1995) considered both the direct and diffused components of the sound field in a reverberant room. Particularly, Pàmies *et al.* (2011) investigated sound radiation out from the aperture of a rectangular box with interior sound field expressed in cavity modes.

Studies concern about the propagating and evanescent modes within the finite thickness aperture are available (for instance, Wassef 1985). The predictions of oblique incidence sound transmission through aperture were also discussed by Park & Eom (1997).

Oldham & Zhao (1993) conducted a series of experiments and compared the results with theoretical predictions of sound transmission loss across circular and slit

apertures. Trompette *et al.* (2009) also described an experimental transmission loss tests in diffuse field for slit in comparison with analytical model.

Researches of the acoustic impedances of tone holes of geometry like woodwind musical instrument by Benade (1960) and Keefe (1982) were noted. The impedances in series of various sizes or positions of the woodwind tone holes without air flow was examined. Such pipes, provided with side openings, constitutes sound transmission as a high-pass filter. Similarly, duct acoustics with hole on the side wall has been explored as well. Dubos & Kergomard (1999) and Dalmont & Nederveen (2002) investigated the sound transmission across a three-port junction in two-dimensional rectangular geometry by using equivalent circuit network and modal decomposition.

The radiation impedance of a piston on the side wall of a duct was examined by other researchers such as Lapin (2000) and Komkin & Mironov (2013). They assumed the air piston was oscillating with uniform velocity normal to the piston and derived the self-impedance. Such approach was also adopted by Huang (2000). In addition, the sound transmission modelling through a mixed separation of flexible structure with an aperture were formulated by Yu *et al.* (2014). The characteristic of aperture was assumed to be a virtual panel with averaged vibrating velocity normal to the panel.

Kim & Kim (2002) studied the sound field of a two-dimensional and partially opened cavity coupled with a membrane and an external free field. The directional radiation pattern of a cavity with plates and opening was examined by Seo & Kim (2005). The solutions were obtained numerically.

1.1.5 Sound propagation of duct with a flush-mounted finite membrane

The presence of side opening or open boundary of a long partial enclosure is the key feature of the duct configuration in this research. The insight of similar duct model with a flexible plate or membrane is considered helpful. The physical interpretation of flush-mounted finite membrane in an infinitely long duct is reviewed before working on the open boundary model.

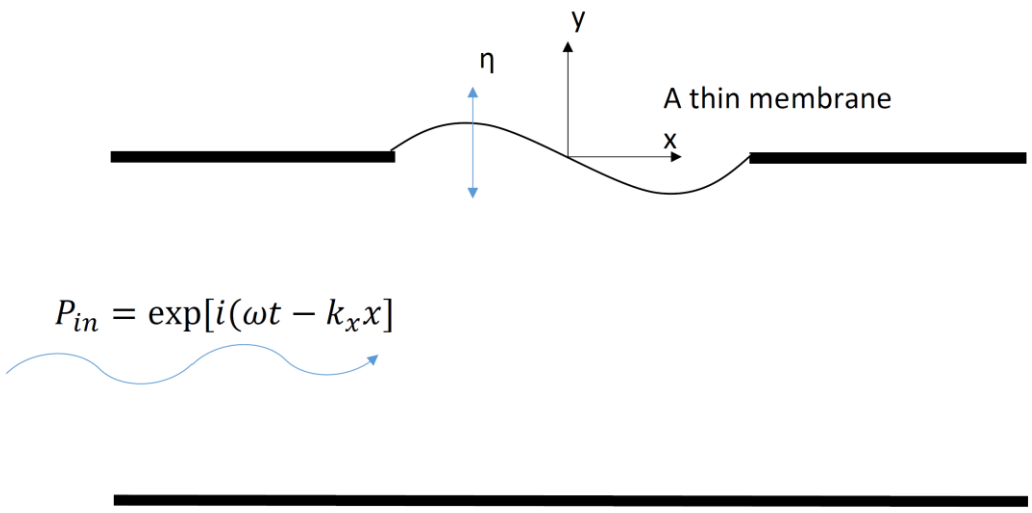

Figure 1.2 – Illustration of a flush-mounted finite membrane in a long duct

A two-dimensional duct with a very thin finite membrane is illustrated in Figure 1.2. P_{in} is the known incident wave pressure. The membrane displacement is $\eta(x,t)$. Such

thin membrane is an element forms the mechanism of a damping model with energy dissipation. The eigenvalue of the damping dynamics is expressed mathematically as,

$$k = k_r + ik_i \tag{1.7}$$

which is a complex number. In view of the flexible membrane itself, there is a damping term represents the energy loss from a flat membrane under a heaving motion like a piston. For lossless condition, eigenvalues exist only as follows (Huang *et al.* 2000):

(1) Pure real $k = k_r$ means free wave propagating along the duct axial direction. Otherwise,

(2) Pure imaginary $k = ik_i$ means standing waves between the membrane and rigid lower wall.

The cross-sections of the leading and trailing edges of the finite membrane represent the discontinuity in acoustic properties across. Wave reflections occur at the upstream edge of the membrane.

The physical interpretation of complex wave-number can also be found from the sound attenuation in lined ducts by researchers, such as Bokor (1969) and Kurze & Vér (1972). The complex propagation constant in duct axial direction was evaluated. Studies of leaky surface wave of electro-acoustics or geoscience (Schröder & Scott 2001) discussed physical meanings of complex wave-number as well. Interaction of an inhomogeneous plane wave with a corrugated surface and diffraction was investigated by Declercq *et al.* (2005) and Molinet (2011).

1.1.6 Acoustical damping

The previous section discusses the damping phenomenon of membrane which noticeably affects acoustical behaviour inside a duct. Further review of acoustical damping becomes necessary.

Acoustical damping mechanisms can be separated into the non-radiative damping and radiation damping (Kerwin 1961). Wallace (1987) discussed that the non-radiative acoustical damping is situated in the near-field of the structure and energy is lost through dissipative mechanisms including sound-absorbing materials, damped cavity resonators or damped structure. In reality, sound waves traverse along a long duct should have physical loss. A damping term is put on for a part of energy loss by absorption in the air throughout the duct, by viscous friction impeding the air nearest the walls of the duct and/or absorption at the walls (Morse 1976). The formulation of modal damping coefficient was also presented and discussed by Lau & Tang (2000).

For the radiation damping, the acoustical energy is removed irreversibly from the vibrating modes. Pretlove (1965) was interested in the actions of the air through flexible plate vibration. The reactive part of the acoustical radiation called virtual mass attached to the plate was studied. In the meantime, the resistive part of acoustical radiation was concerned in the far field which was in phase with the surface velocity of the vibrating plate (Mangiarotty 1963). Radiation damping model for structural acoustic interactions of baffled membrane could be found in Kriegsmann & Scandrett (1989) as well. The theoretical approach related an impedance approximation and membrane displacement. Besides, Cummings *et al.* (1999) derived models of radiation damping of a plate mounted

in a rigid baffle with a slab of absorbent layer. The acoustical characteristic impedance and propagation coefficient of absorbent layer were modelled in form of complex number. It was noted that the radiation damping varied remarkably between different plate modes. Also the loss factor of a plate was strongly dependent on the air space depth if air gap between a plate and an absorbent layer was available.

1.2 Objectives and research scopes

Although literatures regarding opened waveguides are found as per Section 1.1.3, the image source method is not executed well when there is discontinuity along any boundary such that the image cannot be definitely constructed. Such discontinuity which exists in a partial enclosure adds to the complexity of the problem. Moreover, energy-based model, which ignores wave effects, may be inherently inaccurate at lower frequencies.

Studies on sound transmission through aperture are discussed in Section 1.1.4. They were usually focused on the transmission loss factor in various cases of sound source field or single aperture configuration. Uniform velocity profile through the aperture was assumed conventionally. A certain model for the propagation of sound and its leaky characteristics inside long partial enclosures has not been tackled thoroughly so far.

The major objective of the present study is to develop a reliable sound propagation model in a long partial enclosure due to stationary sources inside the enclosure, which is a generalization of the existing knowledge. The research scopes include as below:

(1) To review current literatures related to long partial enclosures and find relevant missing research works;

(2) To study the sound propagation along a leaky duct/ long partial enclosure;

(3) To develop mathematical models for the estimation of leaky sound behaviour of a long duct with aperture(s);

(4) To build up a finite-element computation assisted analytical model for the prediction of leaky sound phenomenon of a narrow rectangular side opening, namely "open slot".

Knowledge on how sound propagates along this long partial enclosure and how sound interacts with the cavity and the surrounding could allow for the development of an appropriate active control method (Kang & Kim 1997, Tang & Cheng 1998).

1.3 Approach of investigations

The present investigations are done theoretically and by numerical finite-element computation. The theoretical part of the study consists of prediction of sound field generated in an infinitely long duct by a circular sound source and sound propagation along a leaky duct, while the numerical models are generated for the assist of analytical modelling.

It is expected that the sound propagates in form of modes inside the cavity of the partial enclosure as in the rigid-wall duct case (Morse & Ingard 1968). Analytical modelling of the internal sound field generated by an vibrating boundary in an enclosure

by modal function expansion is noted (Jayachandran *et al.* 1998). In the study of Potel & Bruneau (2008), the sound pressure in a duct of non-homogeneously shaped walls had been reviewed with modal analysis. For simplicity, the present research focuses on the interaction of sound with smooth and rigid duct walls.

Finite element numerical models for evaluation of acoustic modes in trapezoidal cavities were made by Li & Cheng (2004) and Sum & Pan (2006). They offered the formulations for the distorted mode shapes. However, the mode forms and the eigen-frequencies are not easy to determine because of the existence of discontinuous boundaries in this study. Attempt is made to determine such modes analytically. Similar to the determination of solutions for a point source in an infinitely long hard-walled rectangular duct (Doak 1973a), the solutions of the three-dimensional wave equation within the cavity are required. Vanishing normal acoustic particle velocity is adopted as the boundary condition for the rigid walls involved as usual, while the opening(s) are treated as virtual air piston(s). The whole enclosure is then assumed to subject to excitation simultaneously. The sound propagation due to air pistons or distributed sources inside the duct cavity or on the wall of the cavity (opened boundary) can then be estimated.

Tang *et al.* (2005) explained the sound radiation due to unsteady interaction between an inviscid vortex and a finite length flexible boundary mounted on a rigid plane. Air flow was in a direction parallel to the plane. Their results suggest that there are two longitudinal dipoles biased radiation directivities on both sides of the flexible boundary.

In this research, the sound radiation from the duct cavity interior to the external environment through the duct wall openings is predictable to a certain extent. An open slot along the long duct cavity is supposed to be an interface oscillation while sound is

propagating along the duct. Sound radiation from the slot to the free field should unlikely be in a direction normal to the slot surface. In this study, the slot is modelled as a linear array of air pistons oscillating with different velocities. The theoretical slot radiation model can be worked out by integrating the acoustical contributions of the piston radiations. Since the particular wave motion or physical slot interface oscillation is not exactly known, finite-element computation is adopted to generate the acoustic pressure inside duct to assist the determination of analytical solutions.

1.4 Organization of the thesis

Chapter 1 introduces the literature survey and objectives of the thesis. It contains the literature review on sound properties along a long enclosure, duct and its radiated sound behaviour from opened duct end. Surveys of acoustical damping, sound transmission through aperture, sound propagation along opened waveguides and duct with a finite membrane are also discussed.

Afterwards, the main contributions of this thesis is organized in two parts. The first part is the investigation of the mathematical models for the long partial enclosure with a circular sound source and side openings or slot (Chapters 2, 3 and 4). The second part is Chapters 5 and 6 which describe the finite element computational modelling (3-D model) for such long partial enclosures.

In Chapter 2, the sound propagation in an infinitely long duct of rectangular cross-section is described as the basis of relevant mathematics and physics for the present research. The corresponding wave field generated by a circular sound source is derived

theoretically. Besides, this chapter discusses the technique of in-duct modal decomposition for the finite element computational result analysis. Chapter 3 emphasises the sound radiation properties of the long partial enclosure. Radiation impedance of rectangular/ square aperture and the theoretical wave motion of in the presence of open slot on the duct wall are formulated. These are the crucial part in the mathematical model of sound propagation along a rectangular duct with side opening(s) and slot. Subsequently, simultaneous equations and solutions for the average sound pressure at the opening(s) are elaborated in Chapter 4.

Subsequent to the formulation of the mathematical models for the leaky duct in the first part, the next step is the construction of finite element computational models. Chapter 5 describes the set-up and validation of the 3-D models by adoption of the fundamental theories of infinitely long duct and grid sensitivity test of a model with two finite size openings on the duct wall. Thereafter, comparisons between numerical results and mathematical predictions of the long duct with a single/two opening(s) on the wall are evaluated. The implementation of finite element computational modelling for the infinitely long gap model is presented in Chapter 6. Discussion of results of modal frequencies of ducts are given. Further analysis of sound field in frequency domain for single aperture model is done. Besides, the cases of various slot sizes and frequencies are examined and discussed. This chapter is the significant linkage between the theoretical models and finite element computational models in this research. Formulations of leaky wave motion of open slot on the side wall of a duct are then established.

Lastly, Chapter 7 of this thesis states the achievements and conclusions of this study. Further works are suggested.

Chapter 2

Sound field in a long rectangular enclosure by a flush-mounted circular piston

2.1 Introduction

The excitation and transmission of sound by a source inside a rigid duct with non-reflecting terminations and no mean flow is controlled by two relatively independent parameter sets as below (Doak 1973a).

(1) The nature of source distribution; and

(2) Duct modes.

It is common that the sound sources for noise control applications and acoustical performance test are circular loudspeakers (Fontaine & Shepherd 1985, Shepherd 1986, Hsu & Poornima 2001 and Piippo & Tang 2011). This chapter describes the sound propagation in waveguide with rectangular cross-section as the basis of mathematics and physics for the current study. The corresponding wave field generated by a circular sound source is derived and the modal decomposition technique is reviewed for the numerical result analysis.

2.2 Wave field by a flush-mounted circular piston

A mathematical model for the pressure wave generated by a flush-mounted vibrating circular piston as the sound source for the case of a rigid duct will be derived. As illustrated in Figure 2.1, a circular piston of radius *R* is flush-mounted on the top of a rectangular duct with height *a* and width *b*. The case to consider is the wave field excited by a circular sound source in a straight, hard-walled duct of infinite length.

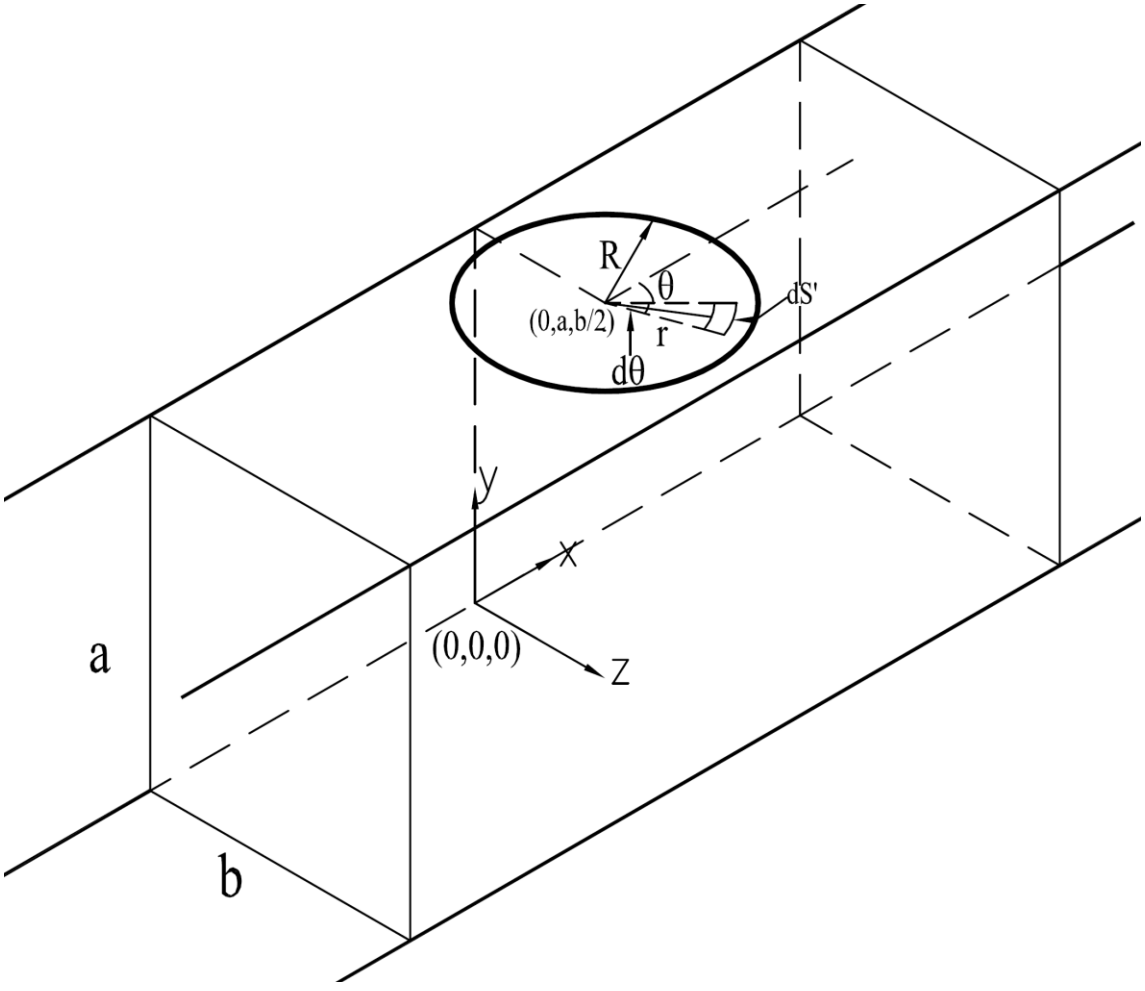

Figure 2.1 - The geometry of a flush-mounted circular piston.

The pressure wave generated by a volume source on the surface S can be calculated in terms of acoustic modes (Huang 2000). The general solution for the wave propagation downstream of a wall-mounted source is:

$$p(x,y,z,t) = \frac{\rho_o}{2ab}\sum_{m,n} c_{mn}\psi_{mn}(y,z)\oint \psi^*_{mn}(y',z')V(x',y',z',t)e^{-i\omega(x-x')/c_{mn}}dS \tag{2.1}$$

where V the source vibration velocity is constant, ρ_0 is the fluid density, c the speed of sound, (x',y',z') the Cartesian coordinates of the sound source, and

$$\left(\frac{c}{c_{mn}}\right)^2 = 1-\left(\frac{\omega_{mn}}{\omega}\right)^2; \quad \left(\frac{\omega_{mn}}{c}\right)^2 = \left(\frac{m\pi}{a}\right)^2+\left(\frac{n\pi}{b}\right)^2$$

Since the loudspeaker is mounted on the upper wall,

$$y' = a,\ x' = r\cos\theta \text{ and } z' = \frac{b}{2}+r\sin\theta$$

The integral of Eq. (2.1) is:

$$\begin{aligned}&\oint \psi^*_{mn}(y',z')e^{\frac{-i\omega(x-x')}{c_{mn}}}dS \\ &= \int_0^R\int_0^{2\pi}\sqrt{(2-\delta_{0m})(2-\delta_{0n})}\cos\left(\frac{m\pi y'}{a}\right)\cos\left(\frac{n\pi z'}{b}\right)e^{\frac{-i\omega(x-x')}{c_{mn}}}d\theta r dr\end{aligned} \tag{2.2}$$

For convenience of later calculations, we express the parameters as follows:

$$k_x = \frac{\omega}{c_{mn}} = \sqrt{\left(\frac{\omega}{c}\right)^2-\left(\frac{m\pi}{a}\right)^2-\left(\frac{n\pi}{b}\right)^2} \text{ and } k_{0n} = \frac{n\pi}{b} \tag{2.3}$$

After some mathematical manipulation, Eq. (2.2) is effectively:

$$\sqrt{(2-\delta_{0m})(2-\delta_{0n})}\cos(m\pi)\int_0^R\int_0^{2\pi}\cos\left(k_{0n}\left(\frac{b}{2}+r\sin\theta\right)\right)e^{-ik_x(x-r\cos\theta)}d\theta r dr$$

$$=\sqrt{(2-\delta_{0m})(2-\delta_{0n})}(-1)^m e^{-ik_x x}\int_0^R\int_0^{2\pi}\cos\left(k_{0n}\left(\frac{b}{2}+r\sin\theta\right)\right)e^{ik_x r\cos\theta}d\theta r dr \tag{2.4}$$

Firstly, the integral from 0 to 2π of Eq. (2.4) is considered:

$$\int_0^{2\pi}\cos\left(k_{0n}\left(\frac{b}{2}+r\sin\theta\right)\right)e^{ik_x r\cos\theta}\,d\theta=\int_0^{2\pi}\cos\left(k_{0n}r\sin\theta+\frac{n\pi}{2}\right)e^{ik_x r\cos\theta}\,d\theta$$

$$=\int_0^{2\pi}\left(\cos\left(\frac{n\pi}{2}\right)\cos(k_{0n}r\sin\theta)-\sin(k_{0n}r\sin\theta)\sin\left(\frac{n\pi}{2}\right)\right)e^{ik_x r\cos\theta}\,d\theta \tag{2.5}$$

It is noted that

$$\int_0^{2\pi}\sin(k_{0n}r\sin\theta)\sin\left(\frac{n\pi}{2}\right)e^{ik_x r\cos\theta}\,d\theta=0$$

for all n. Then, Eq. (2.5) becomes:

$$\int_0^{2\pi}\cos\left(\frac{n\pi}{2}\right)\cos(k_{0n}r\sin\theta)\,e^{ik_x r\cos\theta}\,d\theta\ .$$

For n an odd number, the integral of Eq. (2.4) vanishes. For even n by dropping the factor $(-1)^{n/2}$,

$$\int_0^{2\pi}\cos(k_{0n}r\sin\theta)e^{ik_x r\cos\theta}d\theta=2\int_0^{\pi}\cos(k_{0n}r\sin\theta)e^{ik_x r\cos\theta}\,d\theta \tag{2.6}$$

Consider

$$\int_{-\pi}^{\pi} e^{(ia\sin\theta+ib\cos\theta)}d\theta = \int_{-\pi}^{0} e^{(ia\sin\theta+ib\cos\theta)}d\theta + \int_{0}^{\pi} e^{(ia\sin\theta+ib\cos\theta)}d\theta$$

$$= -\int_{\pi}^{0} e^{(-ia\sin\theta+ib\cos\theta)}d\theta + \int_{0}^{\pi} e^{(ia\sin\theta+ib\cos\theta)}d\theta$$

$$= 2\int_{0}^{\pi} \cos(a\sin\theta)\, e^{ib\cos\theta}d\theta,$$

therefore (Gradshteyn & Ryzhik 2007, 8.411-1), Eq. (2.6) is:

$$\int_{0}^{2\pi} \cos(k_{0n}r\sin\theta)e^{ik_x r\cos\theta}d\theta = \int_{-\pi}^{\pi} e^{i(k_x r\cos\theta+k_{0n}r\sin\theta)}\,d\theta$$

$$= \int_{-\pi}^{\pi} e^{ir\sqrt{k_x^2+k_{0n}^2}\cos(\theta+\phi)}d\theta = 2\pi J_0\left(r\sqrt{k_x^2+k_{0n}^2}\right)$$

The original integral (Eq. 2.2) becomes, for even *n*:

$$2\pi\sqrt{(2-\delta_{0m})(2-\delta_{0n})}(-1)^{m+n/2}e^{-ik_x x}\int_{0}^{R} rJ_0\left(r\sqrt{k_x^2+k_{0n}^2}\right)dr \qquad (2.7)$$

Next, the integral from 0 to *R* of Eq. (2.7) is considered. By 6.561-5 of Gradshteyn & Ryzhik (2007),

$$\int_{0}^{R} rJ_0\left(r\sqrt{k_x^2+k_{0n}^2}\right)dr = R^2\int_{0}^{1} r'J_0\left(r'R\sqrt{k_x^2+k_{0n}^2}\right)dr'$$

$$\Rightarrow \frac{R}{\sqrt{k_x^2+k_{0n}^2}}J_1\left(R\sqrt{k_x^2+k_{0n}^2}\right)$$

The whole integral (Eq. 2.7) is, for even *n*:

$$\sqrt{(2-\delta_{0m})(2-\delta_{0n})}(-1)^{m+n/2}\frac{2\pi R}{\sqrt{k_x^2+k_{0n}^2}}J_1\left(R\sqrt{k_x^2+k_{0n}^2}\right)e^{-ik_x x} \qquad (2.8)$$

Consider Eq. (2.3),

$$k_x^2+k_{0n}^2=\left(\frac{\omega}{c}\right)^2-\left(\frac{m\pi}{a}\right)^2=k^2-k_{m0}^2,$$

the wave solutions of an infinitely long duct with a circular sound source:

$$\begin{aligned}&p(x,y,z,t)\\&=\pi\omega R\frac{\rho_o V e^{-i\omega t}}{ab}\\&\times\sum_{m,n}\sqrt{(2-\delta_{0m})(2-\delta_{0n})}(-1)^{m+\frac{n}{2}}\frac{J_1\left(R\sqrt{k^2-k_{m0}^2}\right)}{\sqrt{k^2-k_{mn}^2}\sqrt{k^2-k_{m0}^2}}\psi_{mn}(y,z)e^{-ix\sqrt{k^2-k_{mn}^2}}\end{aligned} \qquad (2.9)$$

Eq. (2.9) yields the solutions of sound field for discrete propagating modes (*n*,*m*). By consideration of Eq. (1.4), the solution of wave equation for simple harmonic waves in positive *x* direction of duct:

$$p(x,y,z,t)=\sum_{mn}A_{mn+}\psi_{mn}\,(y,z)e^{-ik_x x}e^{i\omega t} \qquad (2.10)$$

By comparing Eq. (2.9) and (2.10), one can note that the modal amplitude:

$$A_{mn+}=\pi\omega R\frac{\rho_o V}{ab}\sqrt{(2-\delta_{0m})(2-\delta_{0n})}(-1)^{m+\frac{n}{2}}\frac{J_1\left(R\sqrt{k^2-k_{m0}^2}\right)}{\sqrt{k^2-k_{mn}^2}\sqrt{k^2-k_{m0}^2}} \qquad (2.11)$$

It shows that the internal sound pressure magnitude in an infinitely long rectangular enclosure with a circular source flush-mounted on top wall of duct includes the expression of $(-1)^{m+n/2}$. In this connection, the odd modes in the spanwise direction will not be excited. In Eq. (2.11), there are factors namely,

$$\frac{1}{\sqrt{k^2 - k_{mn}^2}} \quad \text{and} \quad \frac{J_1\left(R\sqrt{k^2 - k_{m0}^2}\right)}{\sqrt{k^2 - k_{m0}^2}},$$

Apparently, the former is the indication of resonance when the driving frequency approaches an eigen-frequency. For the latter, one can note that change of the argument $R\sqrt{k^2 - k^2{}_{m0}}$ in Bessel function regulates mode amplitudes excited above and close to eigen-frequencies. At resonance (wave-number $k = k_{mn}$),

$$k^2 = k^2{}_{mn} = k^2{}_{m0} + k^2{}_{0n},$$

the argument in the Bessel function becomes $R \times k_{0n}$, where k_{0n} is the wave-number of the purely spanwise (horizontal) mode except the plane transverse (vertical) mode, $m = 0$. Due to the properties of Bessel function, the increase of R and/or n can moderate the mode amplitude at above and close to eigen-frequencies.

2.3 Modal analysis and modal decomposition

The preceding shows a mathematical model of the infinitely long duct with circular sound source and it is useful for the substantiation of finite element computational modelling in Chapter 5. The question is that what techniques can be applied for analysis of results from numerical modelling? Acoustic modal analysis of cavity or duct in experiment is a significant process of extracting characteristics, such as resonance frequencies and mode shapes, from the transfer functions measured at distribution points within the space of interest (Nieter & Singh 1982, Kung & Singh 1985). The experimental modal analysis for rectangular cavity can be found in many researches, for instance, Peretti & Dowell (1992),

Kubota & Dowell (1992) and Montazeri *et al.* (2007). Rectangular open cavity sound modelling with experimental validation of acoustic resonances in three-dimensional can be found in Ortiz *et al.* (2013). Moreover, Snakowska (1996) reviewed the prediction of acoustic field radiated from a semi-finite cylindrical duct without flange by modal analysis.

In the present research, finite element computational model simulating an elementary long duct and circular sound source is applied instead of physical experiment. This work helps to obtain further insight of the interior sound properties and development of the mathematical models for long partial enclosure. The details of numerical modelling and modal analysis are given in Chapter 5. Internal duct data computed show the distributions of sound pressure over selected cross-sections along the duct. The sound pressure spectra at regular points across duct cross-sections are analysed as shown in Chapters 5 and 6. The procedure and technique can identify the possible mode frequencies and corresponding acoustic mode patterns.

Owing to the orthogonal property of the functions (Morse & Feshbach 1953) :

$$\cos\left(\frac{m\pi y}{a}\right)\cos\left(\frac{n\pi z}{b}\right),$$

in-duct modal decomposition technique is adopted for the experimental sound pressure data over a concerned rectangular cross-section (Åbom 1989). The modal decomposition technique has been widely used in numerous researches of wave propagation in duct or waveguide, such as Pagneux *et al.* (1996), Amir *et al.* (1997), and Allam & Åbom (2006). Schultz (2006) examined the acoustic impedance boundary in square ducts by experiments. However, the elementary series of equations were not expressed

comprehensively. This section elaborates on the relevant principles of modal decomposition to suit the current configurations of numerical data collected.

By consideration of the solution of wave equation for simple harmonic waves in positive *x* direction of duct, Eq. (2.10), the acoustic pressure or relevant transfer function measurement over a rectangular cross-section in *y* and *z* direction is

$$H(y,z) = \sum_{mn} A_{mn}\psi_{mn}\,(y,z) \tag{2.12}$$

where A_{mn} is the modal amplitude of the section.

The eigen-functions $\psi_{\mu\nu}(y,z)$ depend on the cross-sectional shape of the duct and are orthogonal (Morse & Feshbach 1953). Thus,

$$\frac{1}{S}\iint_S \psi_{mn}(y,z)\psi_{\mu\nu}(y,z)\,dydz = \begin{cases} 0, & \mu,\nu \neq m,n \\ 1, & \mu,\nu = m,n \end{cases} \tag{2.13}$$

By multiplying $\psi_{\mu\nu}(y,z)$ for both sides of Eq. (2.12),

$$H(y,z)\psi_{\mu\nu}(y,z) = \psi_{\mu\nu}(y,z)\sum_{mn} A_{mn}\psi_{mn}\,(y,z) \tag{2.14}$$

$$\Rightarrow \frac{1}{S}\iint_S H(y,z)\psi_{\mu\nu}(y,z)\,dydz = \frac{1}{S}\iint_S \psi_{\mu\nu}(y,z)\sum_{mn} A_{mn}\psi_{mn}\,(y,z)\,dydz$$

$$= \frac{1}{S}\iint_S \psi_{\mu\nu}(y,z)\cdot[A_{01}\,\psi_{01}(y,z) + A_{10}\psi_{10}(y,z) + A_{11}\psi_{11}(y,z) + \cdots$$

$$+ A_{mn}\psi_{mn}(y,z)]dydz$$

According to Eq. (2.13),

$$\Rightarrow \frac{1}{S}\iint_{S} H(y,z)\psi_{mn}(y,z)\,dydz = A_{mn} \tag{2.15}$$

The above shows that the corresponding modal amplitude for the (n,m) mode is the multiplication of acoustic pressure data $H(y,z)$ and $\psi_{mn}(y,z)$ over the concerned rectangular cross-section area $S = ab$.

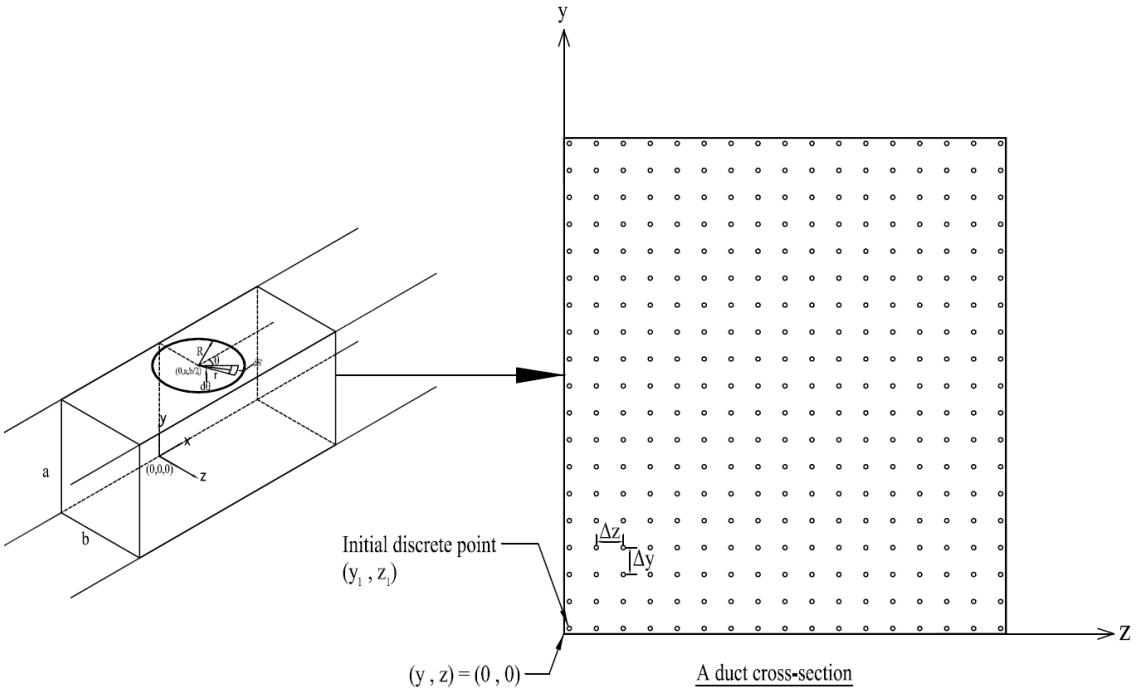

Figure 2.2 – Discrete points of a rectangular duct cross-section.

The acoustic pressures can be extracted from numerical results. Figure 2.2 illustrates the discrete points of a duct cross-section in a grid form. The configurations of the data for each cross-section are set as below:

$$H(y,z)\begin{Bmatrix} H(y_1+\Delta y, z_1+\Delta z) & H(y_1+2\Delta y, z_1+\Delta z) & \cdots \\ H(y_1+\Delta y, z_1+2\Delta z) & H(y_1+2\Delta y, z_1+2\Delta z) & \cdots \\ \vdots & \vdots & \ddots \end{Bmatrix}$$

where $(y_{1,}\ z_1)$ is the initial discrete point of a duct cross-section in Cartesian coordinates. Δy and Δz are the regular intervals in the y and z direction respectively.

$$\psi_{mn}(y,z)\begin{Bmatrix} \psi_{mn}(y_1+\Delta y, z_1+\Delta z) & \psi_{mn}(y_1+2\Delta y, z_1+\Delta z) & \cdots \\ \psi_{mn}(y_1+\Delta y, z_1+2\Delta z) & \psi_{mn}(y_1+2\Delta y, z_1+2\Delta z) & \cdots \\ \vdots & \vdots & \ddots \end{Bmatrix}$$

It is noted that mode amplitudes can be found by Eq. (2.15):

$$\frac{1}{S}\iint_S H(y,z)\psi_{mn}(y,z)\,dydz = A_{mn}$$

$$\Rightarrow \frac{1}{N}\sum_{\mathrm{uv}}[H(y_1+\mathrm{u}\Delta y, z_1+\mathrm{v}\Delta z)\cdot\psi_{mn}(y_1+\mathrm{u}\Delta y, z_1+\mathrm{v}\Delta z)] = A_{mn} \qquad (2.16)$$

where N is number of points allocated in an internal duct cross-section. $N = (\mathrm{u}+1)\times(\mathrm{v}+1)$. Consequently, Eq. (2.16) presents the discrete form of the in-duct modal decomposition techniques. Such technique is adopted to determine the mode amplitudes from numerical modelling studied in later chapters. Results are prepared for comparing the theoretical predictions.

2.4 Concluding remarks

A flush-mounted circular piston vibration on the top horizontal side of long duct is applied and a mathematical model of the corresponding internal sound field is derived. The theory shows that the spanwise odd modes do not excited. Above and close to eigen-frequencies excited, the increase of loudspeaker radius and/or spanwise mode order can moderate the mode amplitude.

Such mathematical model of the circular sound source contribution offers a checking of the finite element computational model. This is a part of the theoretical prediction of leaky ducts (discussed later). In addition, the in-duct modal decomposition technique is discussed and tied up for the present research.

Chapter 3

Radiation impedance of aperture and theoretical model of wave motion at the open slot

3.1 Introduction

Apart from the review presented in Section 1.1.4 concerning the sound transmission through apertures, the radiation impedance of apertures with rigid infinite baffle are explored in details in existing literature, for instance, Wood & Thurston (1953), Mechel (1988), Bank & Wright (1990), Pierce *et al.* (2002) and etc. Some authors focused on the effects of aperture geometry (circular, square or rectangular shape/ slit). Studies on radiation impedance of a square shape apertures was done by Swenson & Johnson (1952) and Lee & Seo (1996). Researches on rectangular shape apertures are also available (Burnett & Soroka 1972, Stepanishen 1977, Levine 1983, Nelisse *et la.* 1998). Stepanishen (1971) and Kinsler *et al.* (2000) described the calculation of the radiation impedance of a circular piston. Sound radiation and impedance of a rectangular piston on a corner were also examined (Mangulis 1965a, 1965b).

However, due to the fairly complicated formulations and infinite series form of the radiation impedance solution, approximations or numerical approach were introduced

for practical applications by the researchers. The accuracy of results should be governed by the sound frequency.

In order to estimate the sound transmission properties through apertures, one can consider the condition over the aperture surface as a piston vibrating with uniform normal velocity (Morfey 1969a). Kinsler *et al.* (2000) outlined the radiation impedance as the ratio of the normal force component to velocity component. The integrated pressure at the aperture area can be determined but non-uniform radiation of side walled opening of long duct is expected in this study. Such phenomenon is examined in this study.

3.2 Radiation impedance of a rectangular and square air piston for the mathematical model

Numerical expression in term of the mutual radiation impedance of square and rectangular piston was presented by Arase (1964). Sha *et al.* (2005) adopted mathematical modelling in calculating the self-impedance and mutual radiation impedance of uniformly and flexibly vibrating patches. In addition, Aarts & Janssen (2003) have done the Struve function H1 approximation for the evaluation of radiation impedance. In recent research, plots of radiation impedances and far field directivity patterns of sound radiation from infinitely long strips were presented (Mellow & Kärkkäinen 2011).

Nevertheless, a simple formula in terms of square size and wave-number is not established yet. An objective of next sub-sections is to find a proper radiation impedance of a square piston for the mathematical model to be used later.

3.2.1 Rectangular aperture

A flat rectangular piston mounted flush on an infinite baffle is assumed in the present study. The specific radiation impedance is as below but the width to height ratio (*w/h*) is neither very large nor very small (Morse and Ingard 1968).

$$Z = \frac{w^2\theta(kw) - h^2\theta(kh) - iw^2\varphi(kw) + ih^2\varphi(kh)}{w^2 - h^2} \tag{3.1}$$

where

$$\theta(x) = 1 - \frac{4[1 - J_0(x)]}{x^2}$$

$$\varphi(x) = \frac{8}{\pi x}[1 - \frac{\pi}{2x}H_0(x)]$$

3.2.2 Square aperture

Set $f(x) = x^2\theta(x)$; $g(x) = x^2\varphi(x)$, for square air piston w tends to h, Eq. (3.1) becomes:

$$Z = \frac{(kw)^2\theta(kw) - (kh)^2\theta(kh)}{(kw)^2 - (kh)^2} - i\frac{(kw)^2\varphi(kw) - (kh)^2\varphi(kh)}{(kw)^2 - (kh)^2}$$

$$= \lim_{x \to kh}[\frac{x^2\theta(x) - (kh)^2\theta(kh)}{x^2 - (kh)^2} - i\frac{x^2\varphi(x) - (kh)^2\varphi(kh)}{x^2 - (kh)^2}]$$

$$= \lim_{x \to kh}[\frac{f(x) - f(kh)}{(x + kh)(x - kh)} - i\frac{g(x) - g(kh)}{(x + kh)(x - kh)}]$$

$$= \lim_{x\to kh} \frac{1}{x+kh} \times \lim_{x\to kh} \frac{f(x)-f(kh)}{x-kh} - i \lim_{x\to kh} \frac{1}{x+kh} \times \lim_{x\to kh} \frac{g(x)-g(kh)}{x-kh}$$

$$= \frac{1}{2kh} \times \frac{df(x)}{dx}\Big|_{x=kh} - i\frac{1}{2kh} \times \frac{dg(x)}{dx}\Big|_{x=kh}$$

One can note that:

$$f(x) = x^2 - 4 + 4J_0(x); \quad g(x) = \frac{8x}{\pi} - 4H_0(x)$$

By 8.473-4 and 8.553-2 of Gradshteyn & Ryzhik (2007)

$$Z = \frac{1}{2kh}[2kh - 4J_1(kh)] - i\frac{1}{2kh}[\frac{8}{\pi} - 4H_{-1}(kh)]$$

$$Z = 1 - \frac{2J_1(kd)}{kd} - \frac{i}{kd}\left[\frac{4}{\pi} - 2H_{-1}(kd)\right], \qquad (h = d)$$

(3.2)

3.3 Aperture thickness consideration

In consideration of the finite aperture thickness δ, the incident and reflected waves are indicated in Figure 3.1.

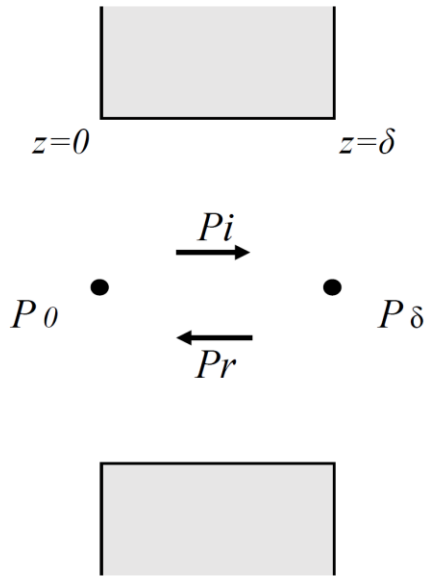

Figure 3.1 – Incident and reflected wave in an aperture with finite thickness.

$P_i = Ie^{-ikz}$, $P_r = Re^{ikz}$ (Kinsler *et al.* 2000)

At $z = 0$,

Continuity of pressure: $I + R = P_0$ (3.3)

Continuity of volume velocity: $U_i + U_r = U_0$ (3.4)

$$\frac{I - R}{z_a} = \frac{P_0}{z_0} \tag{3.5}$$

where $z_a = \rho_o c/S$ and S is the cross-section area of aperture. Substitute Eq. (3.3) into (3.5), one can note that:

$$Z = \frac{z_0}{z_a} = \frac{I + R}{I - R}$$

$$\frac{R}{I} = \frac{Z-1}{Z+1} \tag{3.6}$$

At $z = \delta$,

Continuity of pressure: $P_i + P_r = P_\delta$ (3.7)

Continuity of volume velocity: $U_i + U_r = U_\delta$ (3.8)

$$\frac{Ie^{-ik\delta} - Re^{ik\delta}}{z_a} = \frac{P_\delta}{z_r} \tag{3.9}$$

Substitute Eq. (3.7) into Eq. (3.9),

$$\Longrightarrow \frac{e^{-ik\delta} - (\frac{R}{I})e^{ik\delta}}{z_a} = \frac{e^{-ik\delta} + (\frac{R}{I})e^{ik\delta}}{z_r}$$

Thus, the specific radiation impedance, with the effect of aperture thickness included, is:

$$Z_r = \frac{z_r}{z_a} = \frac{e^{-ik\delta} + (\frac{R}{I})e^{ik\delta}}{e^{-ik\delta} - (\frac{R}{I})e^{ik\delta}} = \frac{Z - itan(k\delta)}{1 - iZtan(k\delta)} \tag{3.10}$$

3.4 Theoretical model of wave motion at the open slot of long duct

Morse & Rubenstein (1938) investigated the problem of diffraction of wave by ribbon and slit for different angles of incidence. Polar diagrams showing the angular sound pressure distributions of waves diffracted by a slit as a function of wavelength were

illustrated. Diffraction of wave due to duct openings or a slot on a duct wall is expected in the present research.

Howe (1980, 1981, 1997) and Grace *et al.* (1998) studied the diffraction of sound by screen with different aperture shapes, such as circle, rectangle, square, triangle and etc., in the presence of grazing flow. The motion in the aperture is modelled by a vortex sheet. Self-sustained oscillations and shear layer instabilities of the aperture flow were represented by Rayleigh conductivity (Rayleigh 1945) in complex form. Other studies on sound diffraction and scattering through an aperture can be found in Huang *et al.* (1955), Bladel (1967), Filippi (1977), Hongo & Serizawa (1999), Davy (2009) and Kim (2010). In their studies, apertures were on a single hard screen or wall as well.

In order to examine the physical propagation phenomenon of a leaky duct, literatures regarding sound radiation directivity of an vibrating plate and characteristics of that in a flow duct are reviewed for further insights. Mathematical analysis of sound radiation of vibrating surfaces can be found in Copley (1968) and Feit (1970). Formulations of the far field directivity pattern were derived. Three types of oscillation namely Gaussian, cosine and plane oscillation of a circular piston in an infinite plane were introduced by Cheong & Lee (2001) in their 3-D numerical simulation. It concerned the situation of uniform velocity air flow parallel to the infinite plane and sound directivity patterns were determined analytically. Sucheendran *et al.* (2014) also derived an analytical solution for the coupled acoustic-structural response of an elastic thin plate mounted on the wall of a rectangular duct with grazing flow.

3.4.1 Far field acoustics of a slot like sound source

In this research, a specific velocity distribution of the air piston at an aperture is suggested. A theoretical approach for modelling acoustic wave motion at the slot of duct is prepared. The emphasis here is to show how the transition of discontinuity in acoustical properties from the rigid wall to the open slot.

Initially, the far field created by a simple source is reviewed. The pressure field of a simple source is known (Kinsler et al. 2000).

$$p(r_0, t) = \frac{i\rho_0 cQ}{2\lambda r_0} e^{i(\omega t - k r_0)} \tag{3.11}$$

where Q is the source strength, r_0 the wave traveling distance between the source element to a far field point, ρ_0 the fluid density, c the speed of sound, λ wavelength which is equal to $2\pi/k$.

$$p(r_0, t) = \frac{i\rho_0 ckQ}{4\pi r_0} e^{i(\omega t - k r_0)} \tag{3.12}$$

The pressure amplitude of a simple source,

$$P = \frac{\rho_0 ckQ}{4\pi r_0}$$

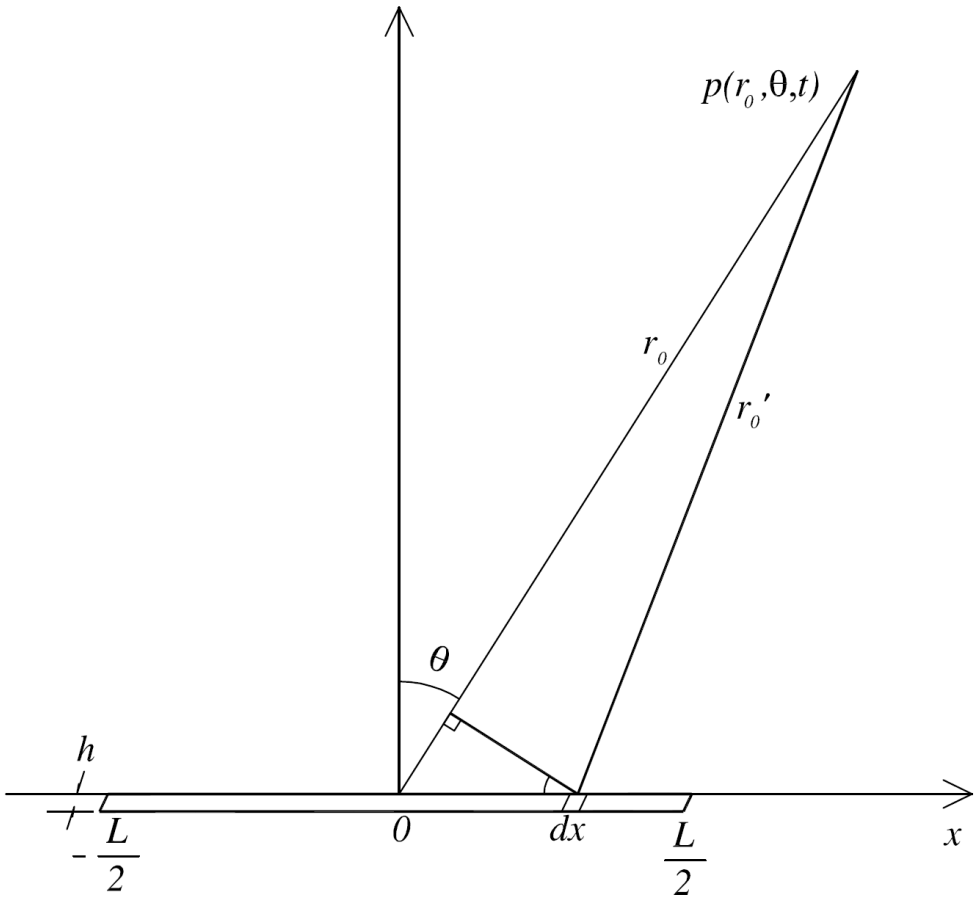

Figure 3.2 - The far field acoustics at (r_0, θ) of a slot like sound source of length L and height h.

Consider a slot like sound source as illustrated in Figure 3.2 (h is slot height; L is slot length), the volume velocity of an element at x is:

$$dQ = U(x)hdx \tag{3.13}$$

where $U(x)$ is the velocity distribution function along the slot surface.

In view of the physical manner of self-sustained oscillations, the open slot surface as the interface vibrates radially with an oscillating component of velocity distribution described by $U(x)$. That is,

$$U(x) = U_0 e^{-ik_{xo}x} \tag{3.14}$$

where U_0 is a constant, representing the amplitude of the slot oscillating flow, the wave-number of x-component wave propagation at the open slot surface is k_{xo}.

For far field, the acoustic pressure field is found by summing the contributions of sources of length dx with height h,

$$p(r_0, \theta, t) = \int_{-L/2}^{L/2} \frac{i\rho_0 ckU_0 e^{-ik_{xo}x} h}{4\pi r_0'} e^{i(\omega t - kr_0')} dx \tag{3.15}$$

Consider the geometry of Figure 3.2, in the far field approximation,

$$\frac{1}{r_0'} \approx \frac{1}{r_0}; \qquad r_0' \approx r_0 - x\sin\theta$$

Therefore, Eq. (3.15) takes the form as:

$$p(r_0, \theta, t) = \frac{i\rho_0 ckhU_0}{4\pi r_0} \int_{-\frac{L}{2}}^{\frac{L}{2}} e^{-ik_{xo}x} e^{i[\omega t - k(r_0 - x\sin\theta)]} dx$$

$$= \frac{i\rho_0 ckhU_0}{4\pi r_0} e^{i(\omega t - kr_0)} \int_{-L/2}^{L/2} e^{-ik_{xo}x} e^{ikx\sin\theta} dx$$

$$= \frac{i\rho_0 ckhU_0}{4\pi r_0} e^{i(\omega t - kr_0)} \int_{-L/2}^{L/2} e^{i(k\sin\theta - k_{xo})x} dx$$

$$= \frac{i\rho_0 ck(hLU_0)}{4\pi r_0} e^{i(\omega t - kr_0)} \frac{\sin[\frac{1}{2}(k\sin\theta - k_{xo})L]}{\frac{1}{2}(k\sin\theta - k_{xo})L} \tag{3.16}$$

Let the source strength be:

$$Q_0 = hLU_0, \tag{3.17}$$

it is known that the pressure amplitude in the far field is defined as:

$$p(r_0, \theta) = p_n(r_0)H(\theta)$$

where $p_n(r_0)$ represents the far field pressure magnitude. $H(\theta)$ is called as the directional factor and

$$H(\theta) = \left|\frac{\sin(v)}{v}\right|$$

$$v = \frac{1}{2}kL\sin\theta$$

Therefore, Eq. (3.16) becomes:

$$p(r_0, \theta, t) = \frac{i\rho_0 ckQ_0}{4\pi r_0} e^{i(\omega t - kr_0)} \frac{\sin(v - \frac{k_{xo}L}{2})}{v - \frac{k_{xo}L}{2}} \tag{3.18}$$

Eq. (3.18) shows that there is a shift of $\frac{k_{xo}L}{2}$ in v of the directional factor. The directional factor of "inclined radiation" is introduced and can be read as:

$$\left|\frac{\sin(v - v')}{v - v'}\right|$$

$$v' = \frac{1}{2}kL\sin\theta' = \frac{k_{xo}L}{2}$$

$$\sin\theta' = \frac{k_{xo}}{k} \tag{3.19}$$

3.4.2 Modified wave-number at the open slot

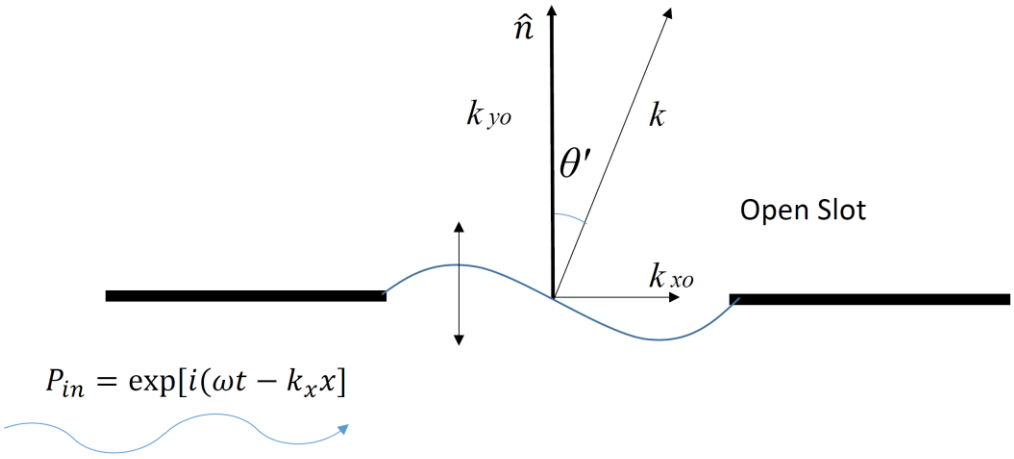

Figure 3.3 - The model of complex wave-number at the open slot of long duct

The question here is what the particular wave-number or the normal vector of the surface of slot is?

In connection with the above evaluation and Eq. (3.19), an illustration of the complex wave-number at the open slot of long duct is shown in Figure 3.3. It is more appropriate to suggest a vector of wave-number in x-y plane making an inclined angle θ' with the normal given:

Definition of propagation vector: $\vec{k} = k_{xo}\hat{x} + k_{yo}\hat{y}$ (3.20)

Along the open slot there is an interface oscillation. The acoustic waves are partly propagating in axial direction and partly radiated away in the normal direction of the slot in principle. Such physical understanding indicates the leaky wave behaviour of long duct. The interpretation of k_{xo} becomes crucial. It is recognized that sound waves propagate

when the propagation constant (k_x) of Eq. (1.4) is real number and alternatively a standing wave decays exponentially with x when k_x is imaginary. For the open slot model, the real part of k_{xo} can explain the sound propagating behaviour while it controls the angle θ' and affects the magnitude of k_{yo} of leaky duct. One can set an open slot model as below with ε a real number.

$$\varepsilon = \sin\theta' = \left|\frac{k_{xo}}{k}\right|$$

$$\varepsilon e^{i\phi} = \frac{k_{xo}}{k}$$

$$k_{xo} = \varepsilon k e^{i\phi} \tag{3.21}$$

where ε and ϕ are the amplitude and phase angle of an oscillating component respectively.

An oscillating component of $D = \varepsilon e^{i\emptyset}$ for leaky duct is now introduced. The surface of the opening is a plane parallel to x-z plane. The 2-D diffracted wave at the opening travelling in x-y plane is expected. By consideration of Eq. (3.20), one can note that:

$$k^2 = {k_{yo}}^2 + {k_{xo}}^2 \tag{3.22}$$

Substitute Eq. (3.21) into Eq. (3.22),

$$k^2 = {k_{yo}}^2 + (\varepsilon k e^{i\emptyset})^2$$

After some manipulation,

$$\Rightarrow k_{yo} = k\sqrt{1 - (\varepsilon k e^{i\emptyset})^2}$$

Thus,

$$k_{yo} = \vec{k} \cdot \hat{n} = k\sqrt{1 - D^2} \tag{3.23}$$

where $D = \varepsilon e^{i\emptyset}$.

According to the above theoretical model of leaky duct and Eq. (3.23), the "modified wave-number" in complex form is established. By the theoretical set-up of k_{yo} as abovementioned, the radiation impedance of a square air piston without thickness as Eq. (3.10) turns out to be:

$$Z_r = \frac{Z - itan(k\delta\sqrt{1 - D^2})}{1 - iZtan\left(k\delta\sqrt{1 - D^2}\right)} \tag{3.24}$$

where

$$Z = 1 - \frac{2J_1(kd\sqrt{1 - D^2})}{(kd\sqrt{1 - D^2})} - \frac{i}{(kd\sqrt{1 - D^2})}\left[\frac{4}{\pi} - 2H_{-1}\left(kd\sqrt{1 - D^2}\right)\right]$$

3.5 Concluding remarks

Literatures review of radiation impedance of apertures are presented in this chapter. A proper formula of radiation impedance of a square air piston in terms of square size and wave-number is derived for the mathematical model. The thickness of air piston is also included in the formula to enhance the accuracy of theoretical prediction.

In the analysis of physical propagation phenomenon of a leaky duct, the "inclined radiation" of the proposed slot like sound source is modelled by simulating a slot

oscillating flow in x direction. It demonstrates that sound field directivity is biased to the positive x direction. A theoretical model of the wave motion at the open slot of long duct is developed. A complex wave-number with real dimensionless variables of amplitude adjustment (ε) and phase angle (ϕ) is introduced to model the sound propagation of leaky duct, namely "leaky duct mode". This "modified wave-number" is a significant part of the mathematical model of this research.

Chapter 4

Mathematical model of sound propagation along a rectangular duct with side opening(s) or an open slot

4.1 Introduction

The sound propagation along a long rectangular enclosure with a circular source on the top wall and rectangular opening or multiple square openings on the side wall are studied in this chapter. By solving the simultaneous equations of the vibrating air piston velocities at the opening(s), a mathematical model of an internal duct sound field can be derived.

Sound pressures of discrete propagating modes are investigated. Interactions between an internal sound source and the effect of the opening(s) on the wall of an infinitely long duct are demonstrated.

4.2 Average acoustic pressure at the opening(s)

The next sub-sections present the general equations for the average acoustic pressure at a single rectangular opening and multiple square openings on the side wall of a rectangular duct.

4.2.1 A single rectangular opening

As illustrated in Figure 4.1, a rectangular air piston of size $w \times h$ is flush-mounted on the side wall of the duct with height a and width b. A circular sound source is fixed on the top wall of the rectangular duct. The case for consideration is the sound field excited by the sound source in the presence of a side wall opening along a straight hard-walled infinitely long duct of constant cross-section area.

The fluid loading in term of average pressure acting on a single air piston at the opening can be set as follows Huang (2000) and Tang (2012):

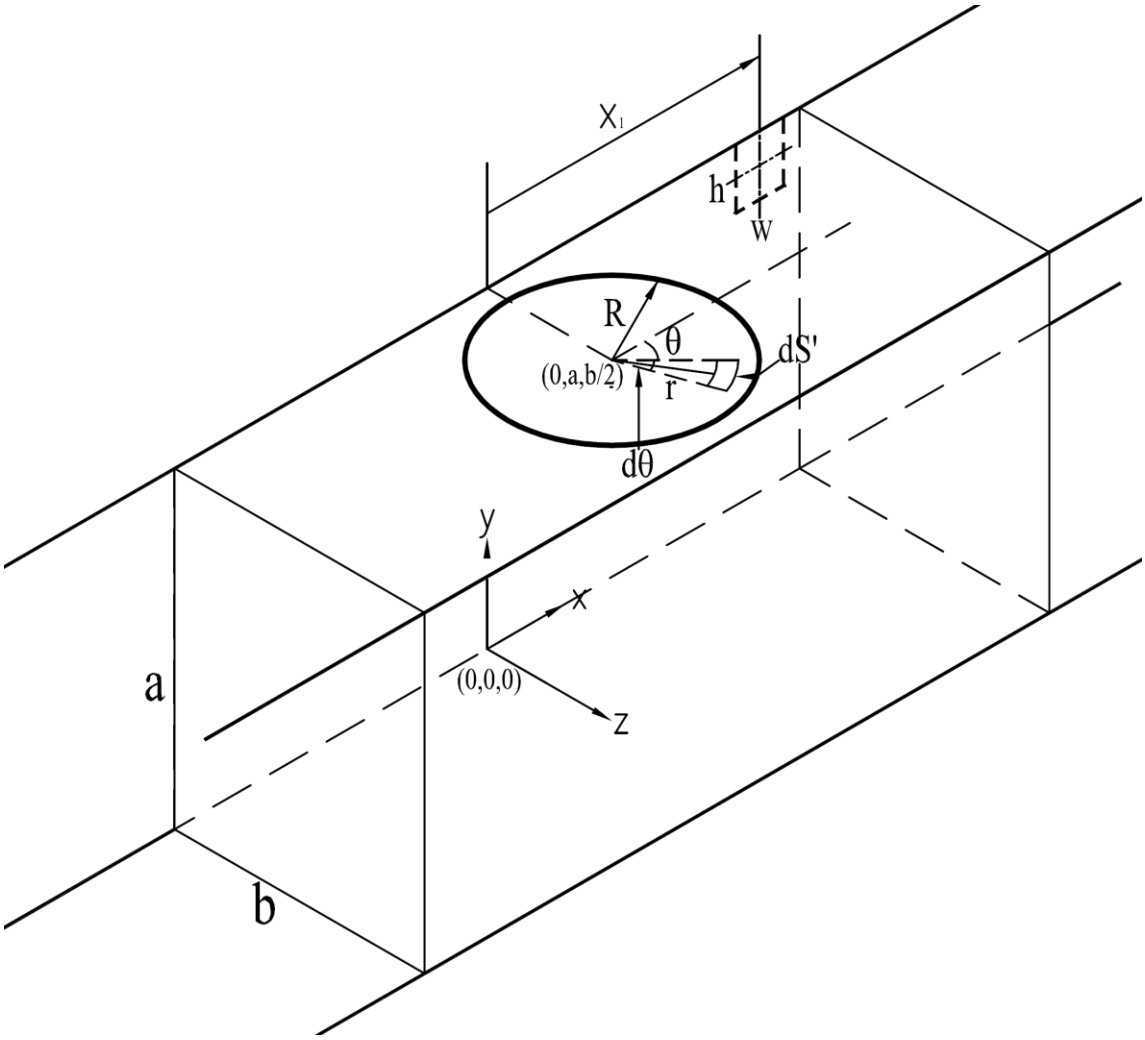

Figure 4.1 - Geometry of the rectangular side wall opening and flush-mounted circular sound source

The average acoustic pressure at the opening contributed by the circular source is:

$$\frac{1}{hw}\iint_{S} p_s(x,y)dS \tag{4.1}$$

where $dS = dxdy$

The self-contribution of a single air piston:

$$\frac{1}{hw}\iint_{S} VF(x,y)dS \tag{4.2}$$

where $F(x,y)$ is a function of a single air piston and this expression is presented in Section 4.4.1.

The average acoustic pressure at the opening of the air piston:

$$\frac{1}{hw}\int_{x_1-w/2}^{x_1+w/2}\int_{a-h}^{a} p_s(x,y|x_1,a-h/2)dxdy+\frac{1}{hw}\int_{-w/2}^{+w/2}\int_{a-h}^{a} VF(x,y)dxdy=\rho_o cVZ_r \tag{4.3}$$

V is the velocity to be solved, Z_r the specific radiation impedance of the air piston and x_1 the centre-to-centre distance from sound source to an opening.

4.2.2 Multiple square openings

This model is set to multiple square openings ($w = h = d$) evenly distributed along a side wall of the duct as shown in Figure 4.2.

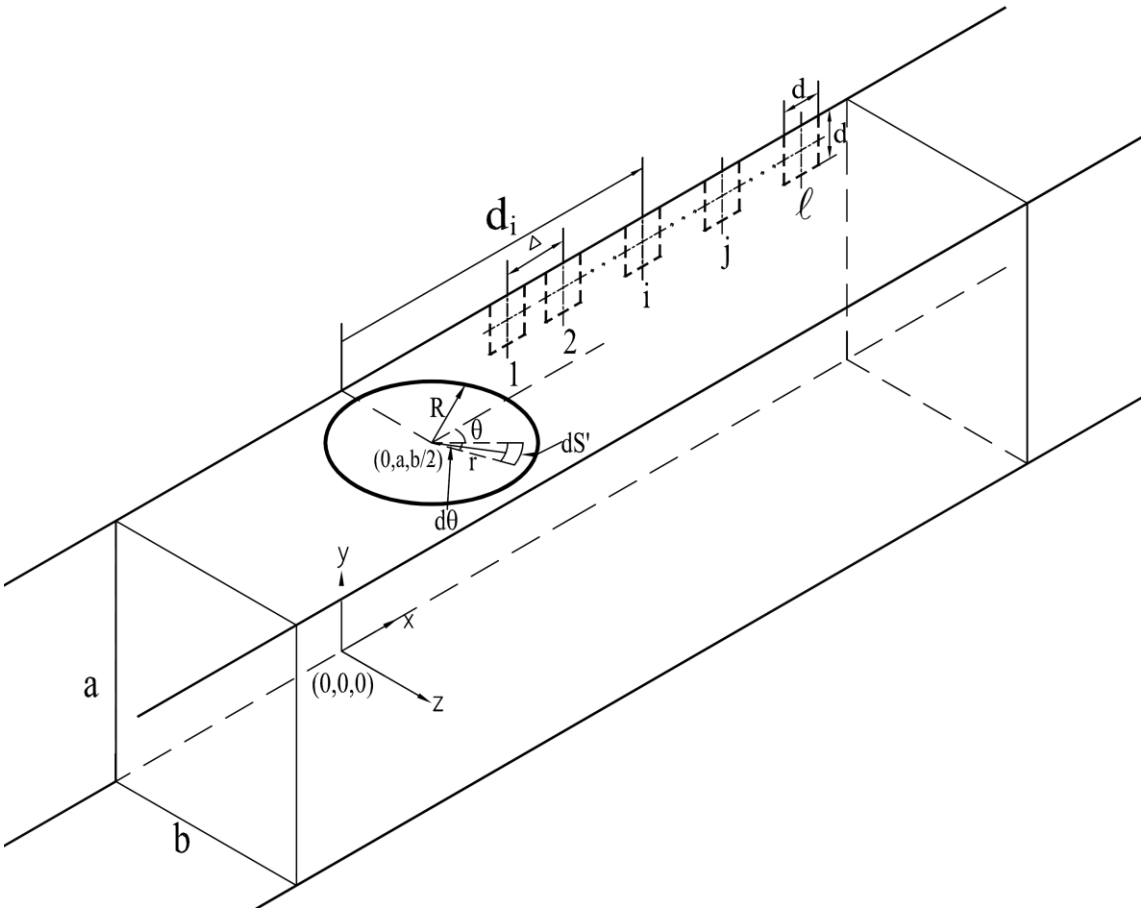

Figure 4.2 - Geometry of the square side wall openings and flush-mounted circular sound source

Consider Eq. (4.1), the average acoustic pressure at the opening contributed by the circular source is:

$$\frac{1}{d^2}\iint_S p_s(x,y)\,dS \tag{4.4}$$

The self-contribution of the *i*th air piston:

$$\frac{1}{d^2}\iint_S V_i F(x,y)\,dS \tag{4.5}$$

The mutual contribution between the *j*th to *i*th air piston:

$$\sum_{\substack{j=1\\ j\neq i}}^{l}\int_{dj-d/2}^{dj+d/2}\int_{a-d}^{a} V_j G(x,y|d_i,a-d/2)\,dxdy \tag{4.6}$$

where $G(x,y|d_i,a-d/2)$ is a function of the *j*th air piston and this expression is presented in Section 4.4.2. Moreover, one can note that:

$$\int_{dj-d/2}^{dj+d/2}\int_{a-d}^{a} G(x,y|d_i,a-d/2)\,dxdy = \int_{di-d/2}^{di+d/2}\int_{a-d}^{a} G\big(x,y|d_j,a-d/2\big)\,dxdy \tag{4.7}$$

The average acoustic pressure at the opening of *i*th air piston:

$$\frac{1}{d^2}\int_{di-d/2}^{di+d/2}\int_{a-d}^{a}\left[p_s(x,y|d_i,a-d/2)+\sum_{\substack{j=1\\ j\neq i}}^{l} V_j G\big(x,y|d_j,a-d/2\big)\right]dxdy + \frac{1}{d^2}\int_{-d/2}^{+d/2}\int_{a-d}^{a} V_i F(x,y)\,dxdy = \rho_o c V_i Z_r \tag{4.8}$$

Then the matrix is set as below and V_i can be calculated by solving the l numbers of simultaneous equations.

$$\begin{pmatrix}\alpha_{1,1} & \alpha_{1,2} & \cdots & \alpha_{1,l}\\ \alpha_{2,1} & \alpha_{2,2} & \cdots & \alpha_{2,l}\\ \vdots & \vdots & \ddots & \vdots\\ \alpha_{l,1} & \alpha_{l,2} & \cdots & \alpha_{l,l}\end{pmatrix}\begin{pmatrix}V_1\\ V_2\\ \vdots\\ V_l\end{pmatrix}=\begin{pmatrix}P_1\\ P_2\\ \vdots\\ P_l\end{pmatrix} \tag{4.9}$$

where

$$P_i = \frac{1}{d^2} \int_{di-d/2}^{di+d/2} \int_{a-d}^{a} p_s(x,y|d_i, a-d/2)dxdy$$

$$\alpha_{i,j} \begin{cases} \rho_o c Z_r - \frac{1}{d^2} \int_{-d/2}^{+d/2} \int_{a-d}^{a} F(x,y)dxdy & \text{for } i = j \\ -\frac{1}{d^2} \int_{dj-d/2}^{dj+d/2} \int_{a-d}^{a} G(x,y|d_i, a-d/2)dxdy & \text{for } i \neq j \end{cases}$$

4.3 General solution for the wave propagation of a wall-mounted air piston

As stipulated in Section 2.2, the general solution for the pressure wave field by a source on the surface *S* can be calculated as below (Huang 2000).

$$p(x,y,z,t) = \frac{\rho_o}{2ab} \sum_{m,n} c_{mn} \psi_{mn}(y,z) \oint \psi^*_{mn}(y',z') V(x',y',z',t) \times \left[H(x-x') e^{\frac{-i\omega(x-x')}{c_{mn}}} + H(x'-x) e^{\frac{i\omega(x-x')}{c_{mn}}} \right] dS' \quad (4.10)$$

where

$$\psi_{mn}(y,z) = \sqrt{(2-\delta_{0m})(2-\delta_{0n})} \cos\left(\frac{m\pi y}{a}\right) \cos\left(\frac{n\pi z}{b}\right)$$

$$\left(\frac{c}{c_{mn}}\right)^2 = 1 - \left(\frac{\omega_{mn}}{\omega}\right)^2; \quad \left(\frac{\omega_{mn}}{c}\right)^2 = \left(\frac{m\pi}{a}\right)^2 + \left(\frac{n\pi}{b}\right)^2$$

$dS' = dx'dy'$ and *V* is a constant. For the air piston is mounted on the top side wall,

$z' = 0,$ centre of $x' = 0$ and $y' = a - \frac{h}{2}$ $(rectangular\ aperture)$

$z' = 0,$ centre of $x' = 0$ and $y' = a - \frac{d}{2}$ $(square\ aperture)$

The integral of Eq. (4.10) is:

$$\sqrt{(2-\delta_{0m})(2-\delta_{0n})}\oint \cos\frac{m\pi y'}{a}\cos\frac{n\pi z'}{b}\left[H(x-x')e^{-i\beta_{mn}(x-x')} + H(x'-x)e^{i\beta_{mn}(x-x')}\right]dS' \tag{4.11}$$

and recall Eq. (2.3),

$$\beta_{mn} = \frac{\omega}{c_{mn}} = \sqrt{\left(\frac{\omega}{c}\right)^2 - \left(\frac{m\pi}{a}\right)^2 - \left(\frac{n\pi}{b}\right)^2}$$

Since the opening is set on the side wall of duct at $z' = 0$, then

$$\cos\frac{n\pi z'}{b} = 1$$

For the rectangular opening region, $(a - h) \le y \le a$, we have

$$\int_{a-h}^{a} \cos\frac{m\pi y'}{a}dy' = \begin{cases} h & ,m = 0 \\ (-1)^m h \sin\left(\frac{m\pi h}{a}\right)/\left(\frac{m\pi h}{a}\right) & ,m \neq 0 \end{cases} (rectangular\ aperture)$$

Similarly, for the square opening region, $(a - d) \le y \le a$, we have

$$\int_{a-d}^{a} \cos\frac{m\pi y'}{a}dy' = \begin{cases} d & ,m = 0 \\ (-1)^m d \sin\left(\frac{m\pi d}{a}\right)/\left(\frac{m\pi d}{a}\right) & ,m \neq 0 \end{cases} (square\ aperture)$$

4.4 Self-contribution of the air piston

The next sub-sections describe the calculations of average pressure on a single rectangular/ square shape air piston. The expressions of $F(x,y)$ in Eqs. (4.2) and (4.5) are also derived here.

4.4.1 A single rectangular air piston

The self-contribution of the air piston at the side opening is derived as below:

for the air piston region, $|x| \leq +w/2$,

$$\int_{-w/2}^{x} e^{-i\beta_{mn}(x-x')}dx' + \int_{x}^{+w/2} e^{i\beta_{mn}(x-x')}dx'$$

$$= \frac{2}{i\beta_{mn}}\left[1 - e^{-i\beta_{mn}w/2}\cos(\beta_{mn}x)\right] \tag{4.12}$$

According to Eq. (4.11), the integral of Eq. (4.10) is, for m = 0:

$$\sqrt{(2-\delta_{0m})(2-\delta_{0n})}\,\frac{2h}{i\beta_{mn}}\left[1 - e^{-i\beta_{mn}w/2}\cos(\beta_{mn}x)\right]$$

for $m \neq 0$,

$$(-1)^m\sqrt{(2-\delta_{0m})(2-\delta_{0n})}\,\frac{2h}{i\beta_{mn}}\left[1 - e^{-i\beta_{mn}w/2}\cos(\beta_{mn}x)\right]\frac{\sin\left(\frac{m\pi h}{a}\right)}{\left(\frac{m\pi h}{a}\right)}$$

The solution, for m = 0:

$$p(x,y,z,t) =$$

$$\omega h \frac{\rho_o V e^{-i\omega t}}{ab} \sum_{m,n} \sqrt{(2-\delta_{0m})(2-\delta_{0n})} \frac{1 - e^{-i(\frac{w}{2})\sqrt{k^2-k_{mn}^2}} \cos(x\sqrt{k^2-k_{mn}^2})}{i(k^2-k_{mn}^2)} \psi_{mn}(y,z) \tag{4.13}$$

for $m \neq 0$,

$$p(x,y,z,t) = \omega h \frac{\rho_o V e^{-i\omega t}}{ab}$$

$$\times \sum_{m,n} \sqrt{(2-\delta_{0m})(2-\delta_{0n})}(-1)^m \frac{\sin\left(\frac{m\pi h}{a}\right)\left[1 - e^{-i(\frac{w}{2})\sqrt{k^2-k_{mn}^2}} \cos(x\sqrt{k^2-k_{mn}^2})\right]}{i\left(\frac{m\pi h}{a}\right)(k^2-k_{mn}^2)} \psi_{mn}(y,z) \tag{4.14}$$

Therefore, the average pressure on the single air piston is:

$$\bar{p} = \frac{V}{hw} \int_{-w/2}^{+w/2} \int_{a-h}^{a} F(x,y)\,dx\,dy$$

In Eq. (4.2), we define $p(x,y) = VF(x,y)$. Comparing Eq. (4.13), for $m = 0$,

$$F(x,y) = \omega h \frac{\rho_o}{ab} \sum_{m,n} (2-\delta_{0m})(2-\delta_{0n}) \cos\frac{m\pi y}{a}$$

$$\times \frac{1 - e^{-i(\frac{w}{2})\sqrt{k^2-k_{mn}^2}} \cos(x\sqrt{k^2-k_{mn}^2})}{i(k^2-k_{mn}^2)} \tag{4.15}$$

Comparing Eq. (4.14), for $m \neq 0$,

$$F(x,y) = \omega h \frac{\rho_o}{ab} \sum_{m,n} (2-\delta_{0m})(2-\delta_{0n})(-1)^m \cos\frac{m\pi y}{a} \times \frac{\sin\left(\frac{m\pi h}{a}\right)\left[1 - e^{-i(\frac{w}{2})\sqrt{k^2-k_{mn}^2}} \cos(x\sqrt{k^2-k_{mn}^2})\right]}{i\left(\frac{m\pi h}{a}\right)(k^2-k_{mn}^2)} \quad (4.16)$$

Consider

$$\int_{-w/2}^{+w/2} \cos(x\sqrt{k^2-k_{mn}^2})\,dx = \frac{2}{\sqrt{k^2-k_{mn}^2}} \sin\left(\frac{w}{2}\sqrt{k^2-k_{mn}^2}\right)$$

$$\int_{a-h}^{a} \cos\frac{m\pi y}{a}\,dy = \begin{cases} h & ,m=0 \\ (-1)^m h \sin\left(\frac{m\pi h}{a}\right)/\left(\frac{m\pi h}{a}\right) & ,m\neq 0 \end{cases}$$

One can note that, for $m = 0$:

$$\bar{p}(x_1, a-h/2, 0) = V\frac{\omega h \rho_o}{abw} \sum_{m,n} \frac{(2-\delta_{0m})(2-\delta_{0n})\left[w - \frac{2e^{-i(\frac{w}{2})\sqrt{k^2-k_{mn}^2}}}{\sqrt{k^2-k_{mn}^2}} \sin\left(\frac{w}{2}\sqrt{k^2-k_{mn}^2}\right)\right]}{i(k^2-k_{mn}^2)} \quad (4.17)$$

for $m \neq 0$,

$$\bar{p}(x_1, a-h/2, 0) = V\frac{\omega h \rho_o}{abw} \sum_{m,n} \frac{(2-\delta_{0m})(2-\delta_{0n})\sin^2\left(\frac{m\pi h}{a}\right)\left[w - \frac{2e^{-i(\frac{w}{2})\sqrt{k^2-k_{mn}^2}}}{\sqrt{k^2-k_{mn}^2}} \sin\left(\frac{w}{2}\sqrt{k^2-k_{mn}^2}\right)\right]}{i\left(\frac{m\pi h}{a}\right)^2(k^2-k_{mn}^2)} \quad (4.18)$$

4.4.2 A square air piston

Similarly, the self-contribution of the air piston at the side square opening is derived as below:

for the square air piston region, $|x| \leq +d/2$,

The solution, for $m = 0$:

$$p(x,y,z,t) = \omega d \frac{\rho_o V e^{-i\omega t}}{ab} \sum_{m,n} \sqrt{(2-\delta_{0m})(2-\delta_{0n})} \frac{1 - e^{-i(\frac{d}{2})\sqrt{k^2-k_{mn}^2}} \cos(x\sqrt{k^2-k_{mn}^2})}{i(k^2-k_{mn}^2)} \psi_{mn}(y,z) \tag{4.19}$$

for $m \neq 0$,

$$p(x,y,z,t) = \omega d \frac{\rho_o V e^{-i\omega t}}{ab} \sum_{m,n} \sqrt{(2-\delta_{0m})(2-\delta_{0n})}(-1)^m \times \frac{\sin\left(\frac{m\pi d}{a}\right)\left[1 - e^{-i(\frac{d}{2})\sqrt{k^2-k_{mn}^2}} \cos(x\sqrt{k^2-k_{mn}^2})\right]}{i\left(\frac{m\pi d}{a}\right)(k^2-k_{mn}^2)} \psi_{mn}(y,z) \tag{4.20}$$

Therefore, the average pressure of the single *i*th air piston:

$$\bar{p} = \frac{V_i}{d^2} \int_{-d/2}^{+d/2} \int_{a-d}^{a} F(x,y)\,dx\,dy \tag{4.21}$$

One can note that, for $m = 0$:

$$\bar{p}(d_i, a-d/2, 0) = V_i \frac{\omega\rho_o}{ab}\sum_{m,n} \frac{(2-\delta_{0m})(2-\delta_{0n})\left[d - \frac{2e^{-i(\frac{d}{2})\sqrt{k^2-k_{mn}^2}}}{\sqrt{k^2-k_{mn}^2}}\sin\left(\frac{d}{2}\sqrt{k^2-k_{mn}^2}\right)\right]}{i(k^2-k_{mn}^2)} \tag{4.22}$$

for $m \neq 0$,

$$\bar{p}(d_i, a-d/2, 0) = V_i \frac{\omega\rho_o}{ab}\sum_{m,n} \frac{(2-\delta_{0m})(2-\delta_{0n})\sin^2\left(\frac{m\pi d}{a}\right)\left[d - \frac{2e^{-i(\frac{d}{2})\sqrt{k^2-k_{mn}^2}}}{\sqrt{k^2-k_{mn}^2}}\sin\left(\frac{d}{2}\sqrt{k^2-k_{mn}^2}\right)\right]}{i\left(\frac{m\pi d}{a}\right)^2(k^2-k_{mn}^2)} \tag{4.23}$$

4.4.3 An open slot model

For a particular slot model, the interval of multiple square openings Δ is set to be equal to d. All square air pistons are packed together as a linear array to form a slot. These air pistons oscillate under the action of the sound excitation. By consideration of a complex wave-number introduced in Chapter 3, an oscillating component of $D = \varepsilon e^{i\emptyset}$ for air pistons at the slot is applied. The modified wave-number $k\sqrt{1-D^2}$ is adopted. Eqs. (4.22) and (4.23) turn out to be:

for $m = 0$:

$$\bar{p}(d_i, a-d/2, 0) = V_i \frac{\rho_o ck\sqrt{1-D^2}}{ab}\sum_{m,n}(2-\delta_{0m})(2-\delta_{0n})$$

$$\times \frac{\left[d - \frac{2e^{-i\left(\frac{d}{2}\right)}\sqrt{(1-D^2)k^2 - k_{mn}^2}}{\sqrt{(1-D^2)k^2 - k_{mn}^2}} \sin\left(\frac{d}{2}\sqrt{(1-D^2)k^2 - k_{mn}^2}\right)\right]}{i[(1-D^2)k^2 - k_{mn}^2]} \tag{4.24}$$

for $m \neq 0$,

$$\bar{p}(d_i, a - d/2, 0) = V_i \frac{\rho_o ck\sqrt{1-D^2}}{ab} \sum_{m,n} (2 - \delta_{0m})(2 - \delta_{0n})$$

$$\times \frac{\sin^2\left(\frac{m\pi d}{a}\right)\left[d - \frac{2e^{-i\left(\frac{d}{2}\right)}\sqrt{(1-D^2)k^2 - k_{mn}^2}}{\sqrt{(1-D^2)k^2 - k_{mn}^2}} \sin\left(\frac{d}{2}\sqrt{(1-D^2)k^2 - k_{mn}^2}\right)\right]}{i\left(\frac{m\pi d}{a}\right)^2 [(1-D^2)k^2 - k_{mn}^2]} \tag{4.25}$$

4.5 Mutual contribution between multiple air pistons

This section describes the calculations of average pressure on each square shape air pistons due to their mutual contribution. The expressions of $G(x,y)$ in Eq. (4.6) are also derived here. By consideration of the contribution of the *j*th to *i*th air piston and $i \neq j$, for the region $x > +d/2$,

$$\int_{-d/2}^{+d/2} e^{-i\beta_{mn}(x-x')} dx' = \frac{2e^{-i\beta_{mn}x}}{\beta_{mn}} \sin\left(\frac{\beta_{mn}d}{2}\right)$$

For the region, $x < -d/2$,

$$\int_{-d/2}^{+d/2} e^{i\beta_{mn}(x-x')} dx' = \frac{2e^{i\beta_{mn}x}}{\beta_{mn}} \sin\left(\frac{\beta_{mn}d}{2}\right)$$

Therefore, $|x| > +d/2$,

$$\frac{2e^{-i\beta_{mn}|x|}}{\beta_{mn}}\sin\left(\frac{\beta_{mn}d}{2}\right)\begin{cases}\int_{-d/2}^{+d/2} e^{-i\beta_{mn}(x-x')}dx', & x > +d/2\\ \int_{-d/2}^{+d/2} e^{i\beta_{mn}(x-x')}dx', & x < -d/2\end{cases} \tag{4.26}$$

The solution of Eq. (4.10) due to mutual contribution, for $m = 0$:

$$p(x,y,z,t) = \omega d\frac{\rho_o V e^{-i\omega t}}{ab}\sum_{m,n}\sqrt{(2-\delta_{0m})(2-\delta_{0n})}\frac{\sin\left(\frac{d}{2}\sqrt{k^2-k_{mn}^2}\right)}{(k^2-k_{mn}^2)}\psi_{mn}(y,z)\,e^{-i|x|\sqrt{k^2-k_{mn}^2}} \tag{4.27}$$

for $m \neq 0$,

$$p(x,y,z,t) = \omega d\frac{\rho_o V e^{-i\omega t}}{ab}\sum_{m,n}\sqrt{(2-\delta_{0m})(2-\delta_{0n})}(-1)^m \times\frac{\sin\left(\frac{m\pi d}{a}\right)\sin\left(\frac{d}{2}\sqrt{k^2-k_{mn}^2}\right)}{\left(\frac{m\pi d}{a}\right)(k^2-k_{mn}^2)}\psi_{mn}(y,z)\,e^{-i|x|\sqrt{k^2-k_{mn}^2}} \tag{4.28}$$

Therefore, the average pressure of the mutual contribution between the jth to ith air piston:

$$\bar{p} = \frac{V_j}{d^2}\int_{dj-d/2}^{dj+d/2}\int_{a-d}^{a} G(x,y|d_i,a-d/2)dxdy \tag{4.29}$$

In Eq. (4.6), we define $p(x,y) = V_j G(x,y|d_i,a-d/2)$. Comparing Eq. (4.27), for $m =$ 0,

$$G(x,y|d_i,a-d/2)$$
$$=\omega d\frac{\rho_o}{ab}\sum_{m,n}\frac{(2-\delta_{0m})(2-\delta_{0n})\sin\left(\frac{d}{2}\sqrt{k^2-k_{mn}^2}\right)\cos\frac{m\pi y}{a}}{(k^2-k_{mn}^2)}e^{-i|x|\sqrt{k^2-k_{mn}^2}}$$

Comparing Eq. (4.28), for $m\neq 0$,

$$G(x,y|d_i,a-d/2)$$
$$=\omega d\frac{\rho_o}{ab}\sum_{m,n}\frac{(2-\delta_{0m})(2-\delta_{0n})(-1)^m\sin\left(\frac{m\pi d}{a}\right)\sin\left(\frac{d}{2}\sqrt{k^2-k_{mn}^2}\right)\cos\frac{m\pi y}{a}}{\left(\frac{m\pi d}{a}\right)(k^2-k_{mn}^2)}e^{-i|x|\sqrt{k^2-k_{mn}^2}}$$

(4.30)

Recall Eq. (4.7),

$$\int_{dj-d/2}^{dj+d/2}\int_{a-d}^{a}G(x,y|d_i,a-d/2)dxdy=\int_{di-d/2}^{di+d/2}\int_{a-d}^{a}G\left(x,y|d_j,a-d/2\right)dxdy$$

Then

$$\int_{dj-d/2}^{dj+d/2}e^{-i|x-di|\sqrt{k^2-k_{mn}^2}}dx=\frac{2\sin\left(\frac{d}{2}\sqrt{k^2-k_{mn}^2}\right)}{\sqrt{k^2-k_{mn}^2}}e^{-i|dj-di|\sqrt{k^2-k_{mn}^2}}$$

$$\int_{a-d}^{a}\cos\frac{m\pi y}{a}dy=\begin{cases}d & ,m=0\\(-1)^m d\sin\left(\frac{m\pi d}{a}\right)/\left(\frac{m\pi d}{a}\right) & ,m\neq 0\end{cases}$$

One can note that, for m = 0:

$$\bar{p}(d_i,a-d/2,0)$$
$$=V_j\frac{2\omega\rho_o}{ab}\sum_{m,n}\frac{(2-\delta_{0m})(2-\delta_{0n})\sin^2\left(\frac{d}{2}\sqrt{k^2-k_{mn}^2}\right)}{(k^2-k_{mn}^2)^{3/2}}e^{-i|dj-di|\sqrt{k^2-k_{mn}^2}}$$

(4.31)

for $m\neq 0$,

$$\bar{p}(d_i, a-d/2,0) = V_j \frac{2\omega\rho_o}{ab} \sum_{m,n} \frac{(2-\delta_{0m})(2-\delta_{0n})\sin^2\left(\frac{m\pi d}{a}\right)\sin^2\left(\frac{d}{2}\sqrt{k^2-k_{mn}^2}\right)}{\left(\frac{m\pi d}{a}\right)^2 (k^2-k_{mn}^2)^{3/2}} e^{-i|dj-di|\sqrt{k^2-k_{mn}^2}} \quad (4.32)$$

4.5.1 Open slot model

For the slot model, an oscillating component of $D = \varepsilon e^{i\emptyset}$ for air pistons at the slot is applied. The modified wave-number $k\sqrt{1-D^2}$ is adopted. Eqs. (4.31) and (4.32) turn out to be:

for $m = 0$:

$$\bar{p}(d_i, a-d/2,0) = V_j \frac{2\rho_o ck\sqrt{1-D^2}}{ab} \times \sum_{m,n} \frac{(2-\delta_{0m})(2-\delta_{0n})\sin^2\left(\frac{d}{2}\sqrt{(1-D^2)k^2-k_{mn}^2}\right)}{[(1-D^2)k^2-k_{mn}^2]^{3/2}} e^{-i|dj-di|\sqrt{(1-D^2)k^2-k_{mn}^2}} \quad (4.33)$$

for $m \neq 0$,

$$\bar{p}(d_i, a-d/2, 0) = V_j \frac{2\rho_o ck\sqrt{1-D^2}}{ab} \times \sum_{m,n} \frac{(2-\delta_{0m})(2-\delta_{0n})\sin^2\left(\frac{m\pi d}{a}\right)\sin^2\left(\frac{d}{2}\sqrt{(1-D^2)k^2-k_{mn}^2}\right)}{\left(\frac{m\pi d}{a}\right)^2 [(1-D^2)k^2-k_{mn}^2]^{3/2}} e^{-i|dj-di|\sqrt{(1-D^2)k^2-k_{mn}^2}} \quad (4.34)$$

4.6 Average acoustic pressure at the opening contributed by a circular source

According to Eq. (2.6), for even n, the wave field generated by a flush-mounted circular piston upstream and downstream of the piston in a rigid duct is:

$$p_s(x,y,z,t) = \pi\omega R\frac{\rho_o V_s e^{-i\omega t}}{ab}\times$$

$$\sum_{m,n}\sqrt{(2-\delta_{0m})(2-\delta_{0n})}(-1)^{m+\frac{n}{2}}\frac{J_1\left(R\sqrt{k^2-k_{m0}^2}\right)}{\sqrt{k^2-k_{mn}^2}\sqrt{k^2-k_{m0}^2}}\psi_{mn}(y,z)e^{-i|x|\sqrt{k^2-k_{mn}^2}} \tag{4.35}$$

4.6.1 A single rectangular opening

The average pressure of source contribution to the side rectangular opening is as below.

$$\overline{p_s} = \frac{1}{hw}\int_{x_1-w/2}^{x_1+w/2}\int_{a-h}^{a} p_s(x,y|x_1,a-h/2)dxdy \tag{4.36}$$

Consider

$$\int_{x_1-w/2}^{x_1+w/2} e^{-i|x|\sqrt{k^2-k_{mn}^2}}dx = \frac{2\sin\left(\frac{w}{2}\sqrt{k^2-k_{mn}^2}\right)}{\sqrt{k^2-k_{mn}^2}}e^{-i|x_1|\sqrt{k^2-k_{mn}^2}}$$

$$\int_{a-h}^{a}\cos\frac{m\pi y}{a}dy = \begin{cases} h & ,m=0 \\ (-1)^m h\sin\left(\frac{m\pi h}{a}\right)/\left(\frac{m\pi h}{a}\right) & ,m\neq 0\end{cases}$$

One can note that, for $m = 0$:

$$\overline{p_s}(x_1, a - h/2, 0) = 2\pi\omega R\frac{\rho_o V_s}{abw} \times \sum_{m,n}(-1)^{\frac{n}{2}}\frac{(2-\delta_{0m})(2-\delta_{0n})J_1\left(R\sqrt{k^2-k_{m0}^2}\right)}{(k^2-k_{mn}^2)\sqrt{k^2-k_{m0}^2}}\sin\left(\frac{w}{2}\sqrt{k^2-k_{mn}^2}\right)e^{-i|x_1|\sqrt{k^2-k_{mn}^2}} \quad (4.37)$$

for $m \neq 0$,

$$\overline{p_s}(x_1, a - h/2, 0) = 2\pi\omega R\frac{\rho_o V_s}{abw}\sum_{m,n}(-1)^{2m+\frac{n}{2}}\frac{(2-\delta_{0m})(2-\delta_{0n})\sin\left(\frac{m\pi h}{a}\right)J_1\left(R\sqrt{k^2-k_{m0}^2}\right)}{\left(\frac{m\pi h}{a}\right)(k^2-k_{mn}^2)\sqrt{k^2-k_{m0}^2}} \times \sin\left(\frac{w}{2}\sqrt{k^2-k_{mn}^2}\right)e^{-i|x_1|\sqrt{k^2-k_{mn}^2}} \quad (4.38)$$

4.6.2 A square opening

The average pressure of the source contribution to *i*th air piston:

$$P_i = \overline{p_s} = \frac{1}{d^2}\int_{di-d/2}^{di+d/2}\int_{a-d}^{a} p_s(x, y|di, a - d/2)dxdy \quad (4.39)$$

One can note that, for $m = 0$:

$$\overline{p_s}(d_i, a - d/2, 0) = 2\pi\omega R\frac{\rho_o V_s}{abd}\sum_{m,n}(-1)^{\frac{n}{2}}\frac{(2-\delta_{0m})(2-\delta_{0n})J_1\left(R\sqrt{k^2-k_{m0}^2}\right)}{(k^2-k_{mn}^2)\sqrt{k^2-k_{m0}^2}} \times \sin\left(\frac{d}{2}\sqrt{k^2-k_{mn}^2}\right)e^{-i|di|\sqrt{k^2-k_{mn}^2}} \quad (4.40)$$

for $m \neq 0$,

$$\overline{p_s}(d_i, a - d/2, 0)$$
$$= 2\pi\omega R \frac{\rho_o V_s}{abd} \sum_{m,n} (-1)^{2m+\frac{n}{2}} \frac{(2-\delta_{0m})(2-\delta_{0n}) \sin\left(\frac{m\pi d}{a}\right) J_1\left(R\sqrt{k^2 - k_{m0}^2}\right)}{\left(\frac{m\pi d}{a}\right)(k^2 - k_{mn}^2)\sqrt{k^2 - k_{m0}^2}}$$
$$\times \sin\left(\frac{d}{2}\sqrt{k^2 - k_{mn}^2}\right) e^{-i|di|\sqrt{k^2 - k_{mn}^2}}$$

(4.41)

4.7 Concluding remarks

A mathematical model of sound field of the following configurations is derived in this chapter:

(1) A single rectangular opening on the side wall of an infinitely long duct

(2) Multiple square openings or open slot on the side wall of an infinitely long duct

This study develops the mathematical models in details for the prediction of leaky sound behaviour of such partial enclosures. Sound pressures of discrete propagating modes can be determined.

Chapter 5

Validation of the three-dimensional numerical modelling

5.1 Introduction

Mathematical models for the internal sound field in an infinitely long rectangular duct with finite side opening(s) or open slot are derived in the previous chapters. In order to examine the theories, finite element numerical modelling is adopted. Three-dimensional (3-D) finite element model is set up to deal with the in-duct sound behaviour. It is essential to verify the reliability and the capability of the 3-D modelling in simulating the duct sound principle. This chapter is to validate the 3-D numerical models with the assessments of benchmark cases as follows:

1. Comparing the in-duct sound theory of an infinitely long rectangular duct
2. Grid sensitivity test for two-aperture on the side wall of a long duct

Subsequent to the validation of the numerical models, comparisons between the mathematical predictions and numerical results of the single aperture and two-aperture on the side wall of long duct are presented.

5.2 The finite element computational model

The geometry of the finite element computational models of infinitely long duct and two-aperture case are illustrated in Figures 5.1 and 5.2 respectively. The acoustic model of interest in this section is an infinitely long duct of constant uniform cross-section area of height a and width b. The thickness of duct wall is δ.

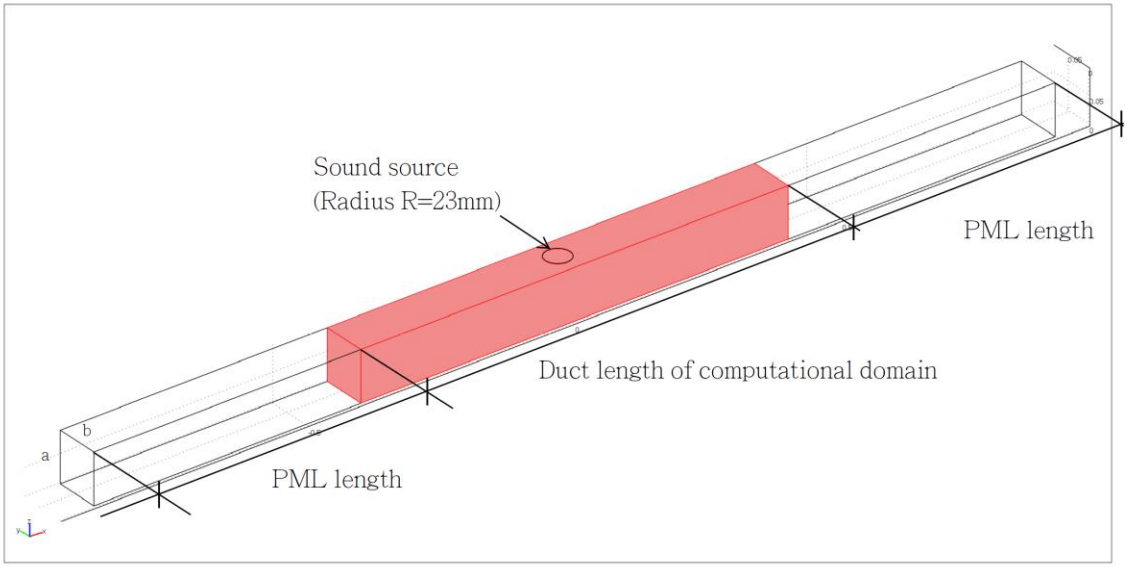

Figure 5.1 – PML at two ends of the model

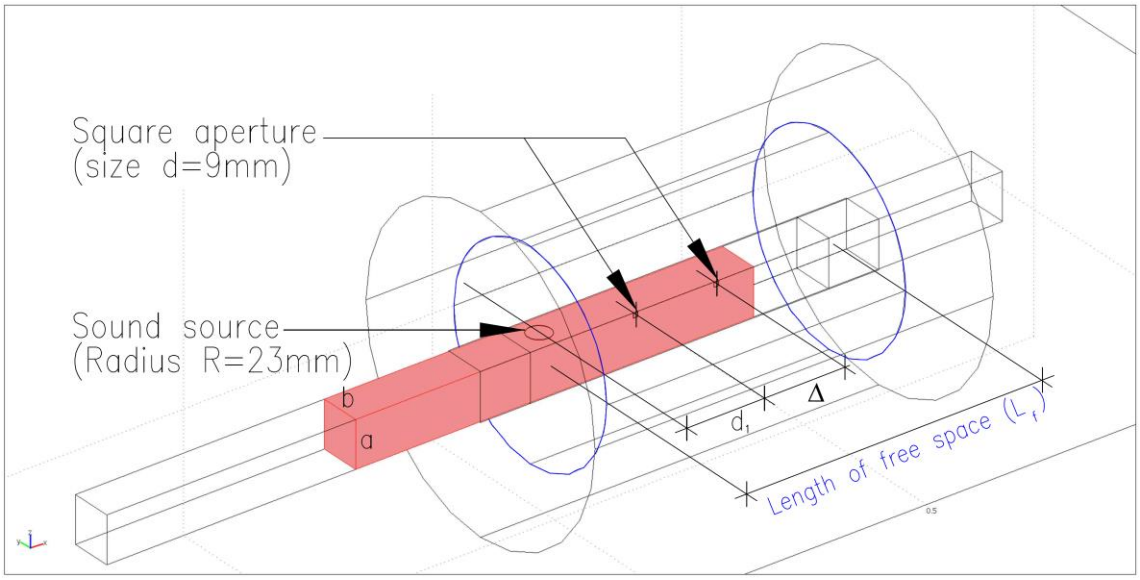

Figure 5.2 – An isometric view of the computational model for an infinitely long duct with two-aperture

The Helmholtz equation, which describes harmonic wave propagation in medium, is represented as follow:

$$\nabla^2 p + k^2 p = 0 \tag{5.1}$$

where p and k denote the acoustic pressure and the wave-number.

The boundary condition associated with all surfaces of the partial enclosure follows that of a rigid wall of vanishing normal acoustic particle velocity. The absorption property of boundary is ignored (Pan *et al.* 1999 and, Pritz 2004).

$$\left.\frac{\partial p}{\partial n}\right|_{\text{wall}} = 0 \tag{5.2}$$

where n represents the outward normal direction of a boundary.

The interactions between sound in the air and the 3-D solid partial enclosure are modelled by using the finite element software COMSOL Multiphysics. The

inhomogeneous wave equation as shown in Eq. (5.3) is implemented in the numerical model (Floody *et al.* 2010, COMSOL 2012). The Cartesian coordinates are pre-set in accordance with the software.

$$\nabla \cdot (\frac{1}{\rho_0}(\nabla p - q)) - \frac{\omega^2 p}{\rho_0 c^2} = Q \tag{5.3}$$

where the dipole source q and monopole source Q are set to be zero, ρ_0 is the fluid density, c is the speed of sound.

The boundary conditions of wall, sound source and the free field environment are introduced. The sound-hard boundary is:

$$\mathrm{n} \cdot (\frac{1}{\rho_0}(\nabla p - q)) = 0 \tag{5.4}$$

This turns out to be Eq. (5.2) for zero dipole source. The circular sound source is set to be the normal acceleration boundary condition. A unity inward acceleration enters at the circular boundary.

To eliminate the effect of reflections at the duct ends of the computational domain, a perfectly matched layer (PML) is added to each end as the buffer zone. PML can provide great performance for waveguide-modelling problems (Richards *et al.* 2004, COMSOL 2012). It is a domain which has damping effect and can be treated as a non-reflecting boundary. Such extra damping region is adjacent to the computational domains. The formulation of the equations in the PML is such that in theory the outgoing waves from the computational domains will not create any reflection, no matter its frequency and propagating direction, when entering the PML domain.

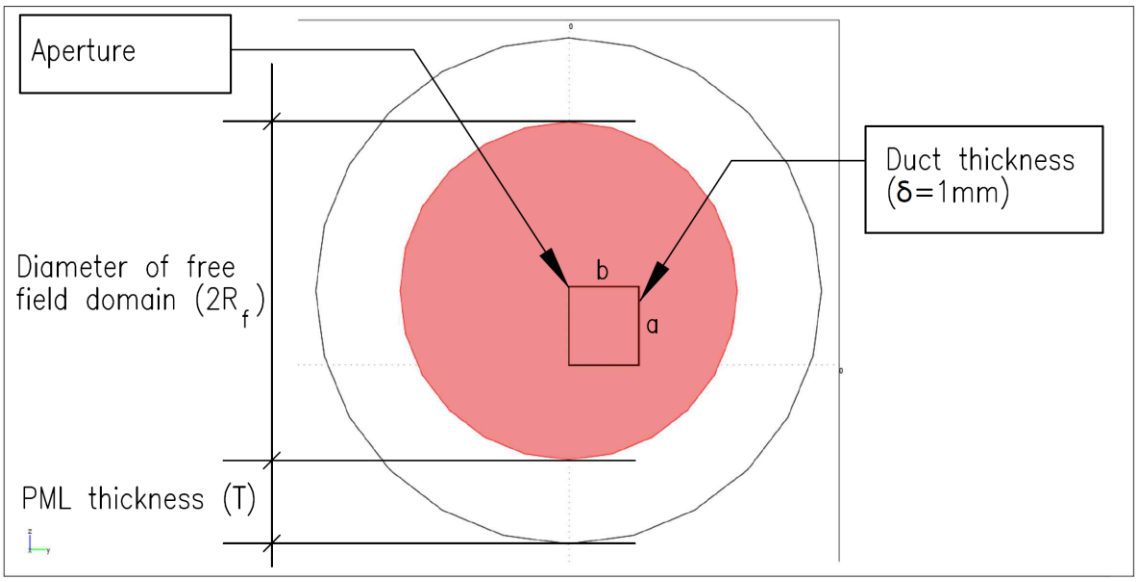

Figure 5.3 – A section of the computational model for an infinitely long duct with two-aperture

The aperture(s) are connected to the free field environment. PML in cylindrical type is added (Figures 5.2 and 5.3). Validation of three-dimensional PML technique was presented for electromagnetic waves in finite elements method in Katz *et al.* (1994) and Berenger (1996). They reported the effectiveness of the PML with discretization error by varying PML thickness. The PML technique also is applicable for acoustical wave field (Hastings 1996). The PML absorption can produce negligible reflections for a PML layer of only half a wavelength (0.5λ) (Johnson 2007 and Taflove & Hagness 2000). In view of the above and COMSOL 2012a, the air of free space around the apertures of the present model is fixed to be minimum of one wavelength (λ) for the sound radiation while the setting of PML domain thickness outside the free space is a half-wavelength.

5.3 Infinitely long rectangular duct model

The acoustic model of interest is set to be a 0.8-metre long duct of internal uniform cross-section area of 82mm in width and 92mm in height. The aspect ratio of the cross-section is around 1.12 which can reduce the opportunity of modal overlapping occurred. The sound source has a diameter of 46mm. The duct thickness is fixed at 1mm. The base setting of the PMLs at two ends is 0.5m (2.7λ at 1850Hz) in length with the same uniform cross-section of the duct. The maximum element size of numerical model is described in the next section.

An attempt is made to seek for the modal frequencies of the finite element simulation. Numerical results shall be compared with the theory. A plot of the integral of acoustic pressure (absolute value) in frequency variations is shown in Figure 5.4. It is the volume integration evaluated over a computational domain in the 3D numerical model (COMSOL 2012) as Eq. (5.5) as follow:

$$\iiint_V |p| dV \tag{5.5}$$

where V is the volume of the computational domain and p the sound pressure in the domain.

Although such result of volume integral may not have a clearly term in acoustical definition, it is useful to recognize the peaks of sound pressure magnitude in the computational domain.

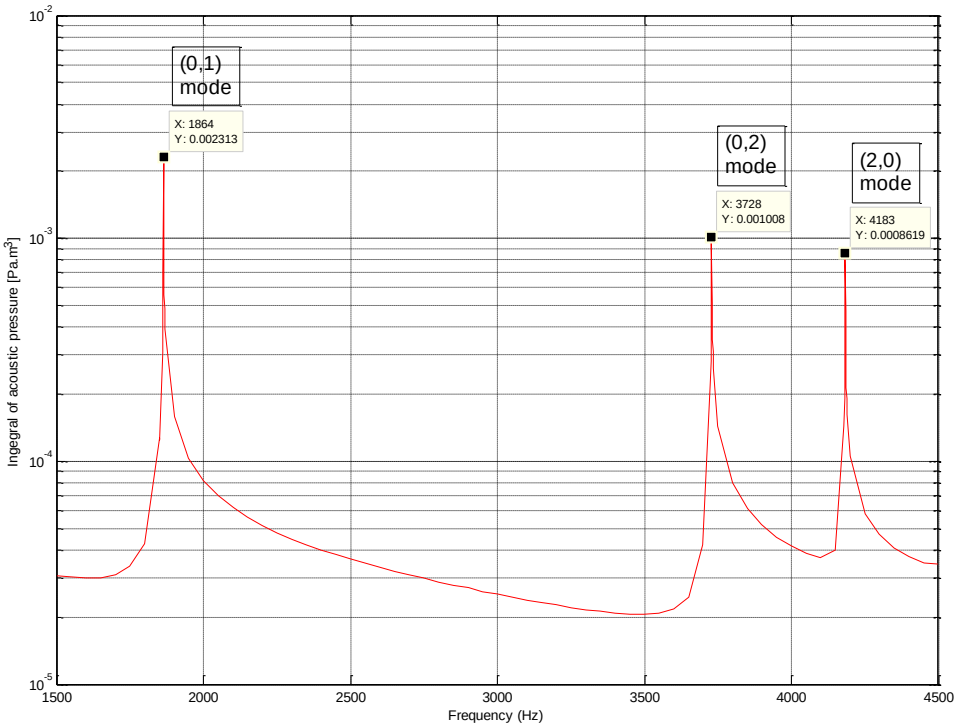

Figure 5.4 – Plot of the integral of acoustic pressure against frequency variations for the infinitely long duct model

Results are obtained with frequency increment interval of 1Hz at the regions approaching resonance frequencies and of 50Hz for the rest of the frequencies. The resonant effects of duct eigen-frequency at (0,1), (0,2) and (2,0) modes (1864Hz, 3728Hz and 4183Hz respectively) are observed. As the circular sound source is at the centre of the top duct wall, odd spanwise modes are not excited as illustrated in Chapter 2. Sound field patterns at the eigen-frequencies of the (0,1), (0,2) and (2,0) modes obtained from the finite element simulation is captured at $x = 0.2$m arbitrarily (Figure 5.5).

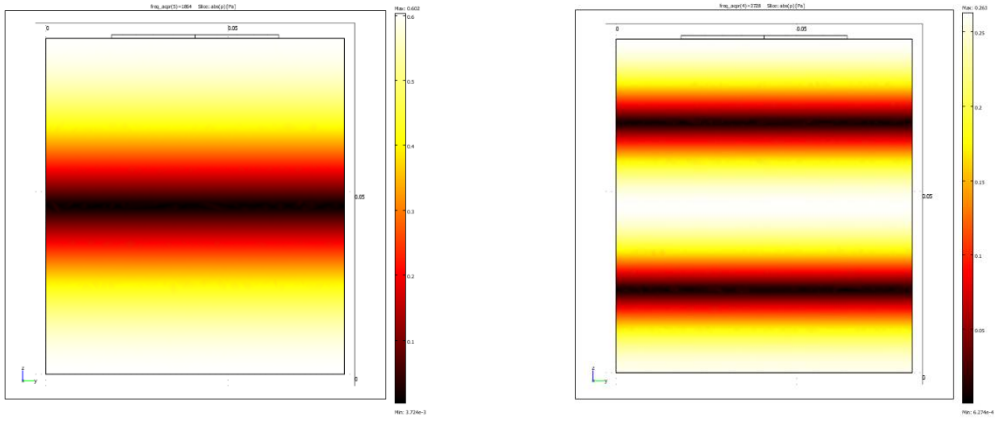

(a) (b)

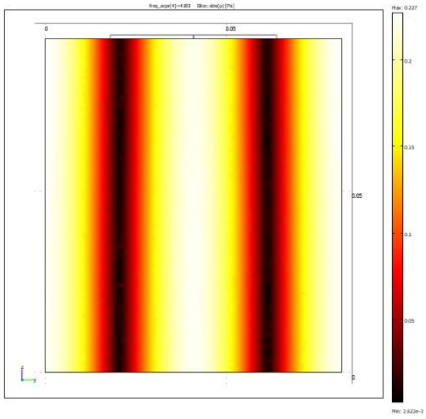

(c)

Figure 5.5 – Sound field patterns at the eigen-frequencies of infinitely long duct models. (a) (0,1) mode; (b) (0,2) mode; (c) (2,0) mode.

Subsequently, PML length at the ends of duct is accessed by the test cases presented in Table 5.1. In-duct modal decomposition technique as per Section 2.4 is adopted to analyse the computed sound pressures. A rectangular grid with $\Delta y = 2$mm and $\Delta z = 2$mm across the duct cross-section is used. A 41 by 46 grid point array is formed.

Table 5.1 – Test cases for infinitely long duct model

	Frequency range		
Description	1850-1950Hz	3700-3800Hz	4170-4270Hz
PML 0.5m (base)	Case A1	Case A2	Case A3
PML 0.75m	-	-	Case A4

The amplitude of an acoustic mode across a duct cross-section can be obtained from the abovementioned 41×46 point arrays. The interval of cross-section along the x direction is 9mm and the frequency resolution is 10Hz. Data from 75 duct sections and 11 frequencies (total 825 numbers of data) are gathered for each test case. Results are taken for comparison with the theoretical prediction where R=23mm, ρ_0=1.25kg/m^3, c=343m/s, a=92mm and b=82mm. The source normal acceleration is unity and $\dot{V}_s = -i\omega V_s$, V_s is (i/kc).

Figure 5.6 illustrates the findings of Case A1 for PML length of 0.5m. One can note that exponential decaying sound pressure magnitude is happened at 1850Hz and 1860Hz which are just below the (0,1) eigen-frequency (1864Hz). Meanwhile, at frequencies above 1864Hz, there are constant sound propagation along the duct. Results from numerical models show excellent agreement with the fundamental duct sound theory at frequencies near the resonance.

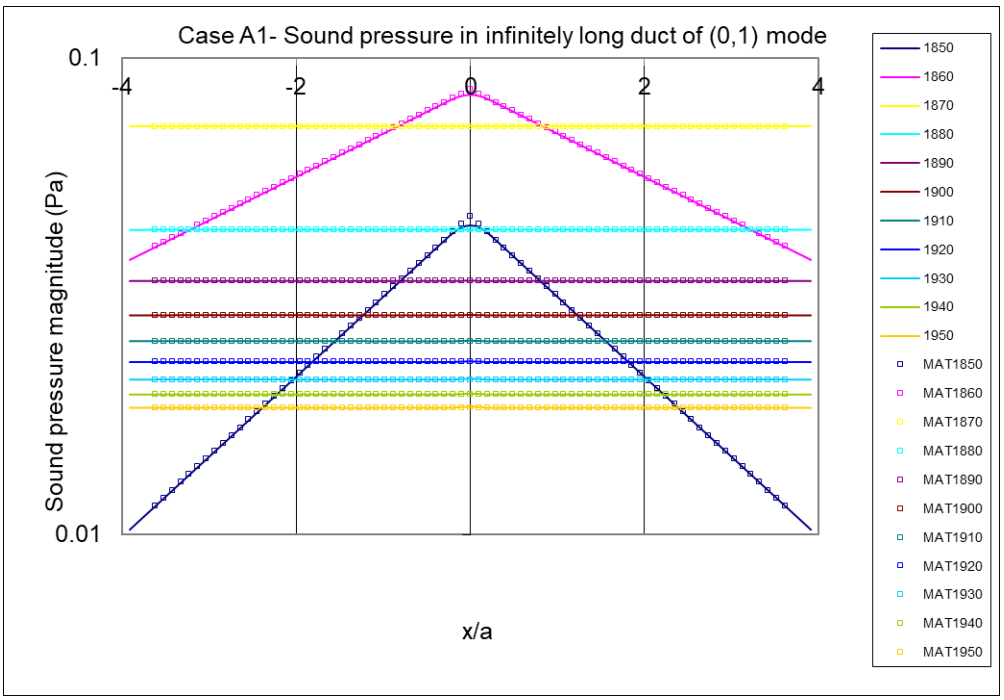

Figure 5.6 – Validation by infinitely long duct model (Case A1)

As far as the accuracy of sound pressure magnitude is concerned, the percentage deviation (%) between numerical model and theoretical prediction, Eq. (5.6) is applied as measure of goodness of a validation.

$$\text{Percentage deviation} = 100\% \times \frac{|V_C| - |V_M|}{|V_C|} \tag{5.6}$$

where

V_C are the values obtained from COMSOL 3-D numerical model and

V_M are the prediction values calculated by mathematical model (MATLAB)

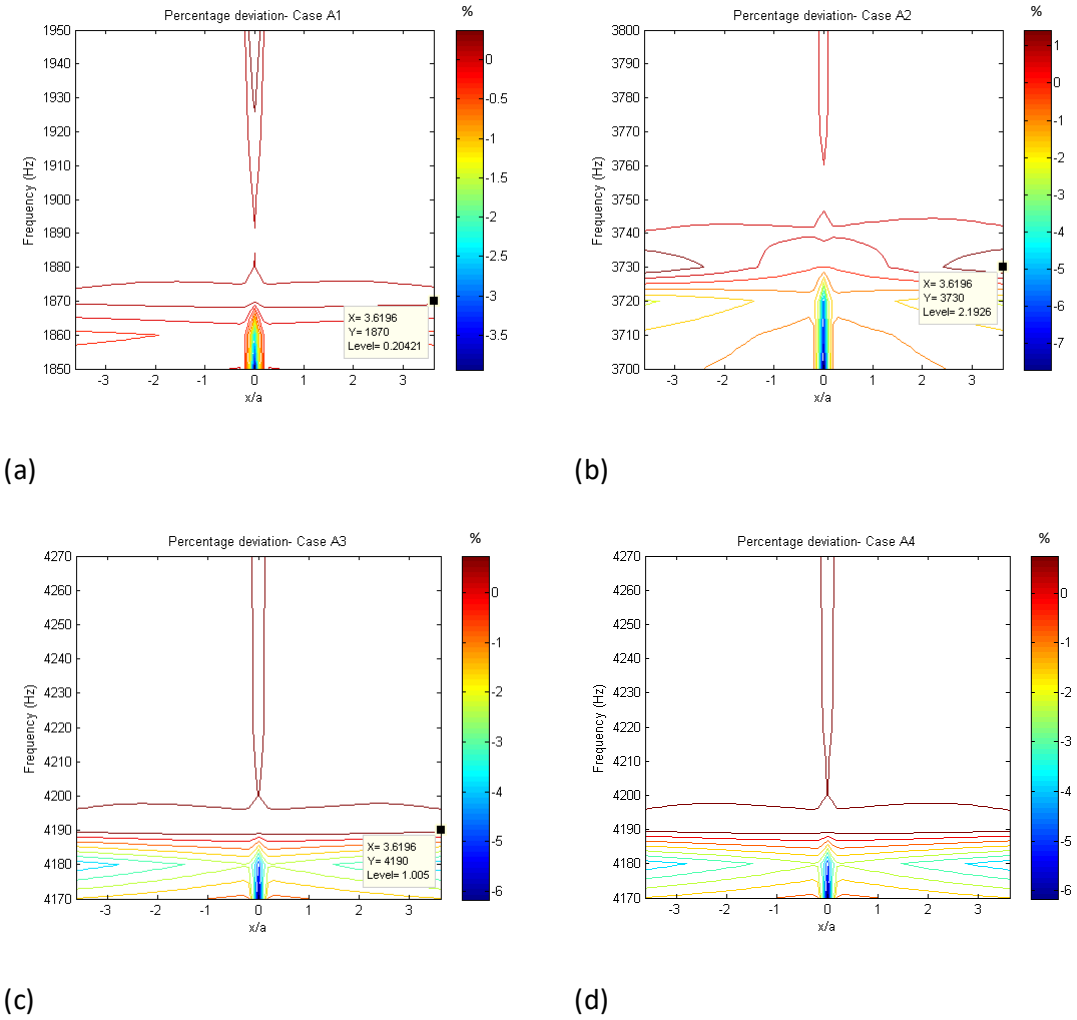

Figure 5.7 – Contour of percentage deviation of results from COMSOL against MATLAB. (a) Case A1; (b) Case A2; (c) Case A3; (d) Case A4: PML length 0.75m.

Figure 5.7(a) is the contour of the percentage deviation for the frequency against *x/a* (Case A1). One can observe that the majority of the results are well under ±0.3% except some deviations at the narrow zone around the sound source (*x/a* = 0) and/or at below the eigen-frequency (1864Hz). Such results within the sound source region and at non-propagating modes are not our major concerns.

The findings of Case A2 (0,2) mode and Case A3 (2,0) mode are shown in Figures 5.8 and 5.9 respectively. The corresponding percentage deviations in form of contour are shown in Figures 5.7(b) and 5.7(c). The majority of the results are under ±2.2%. Numerical results also show excellent agreement with the theory.

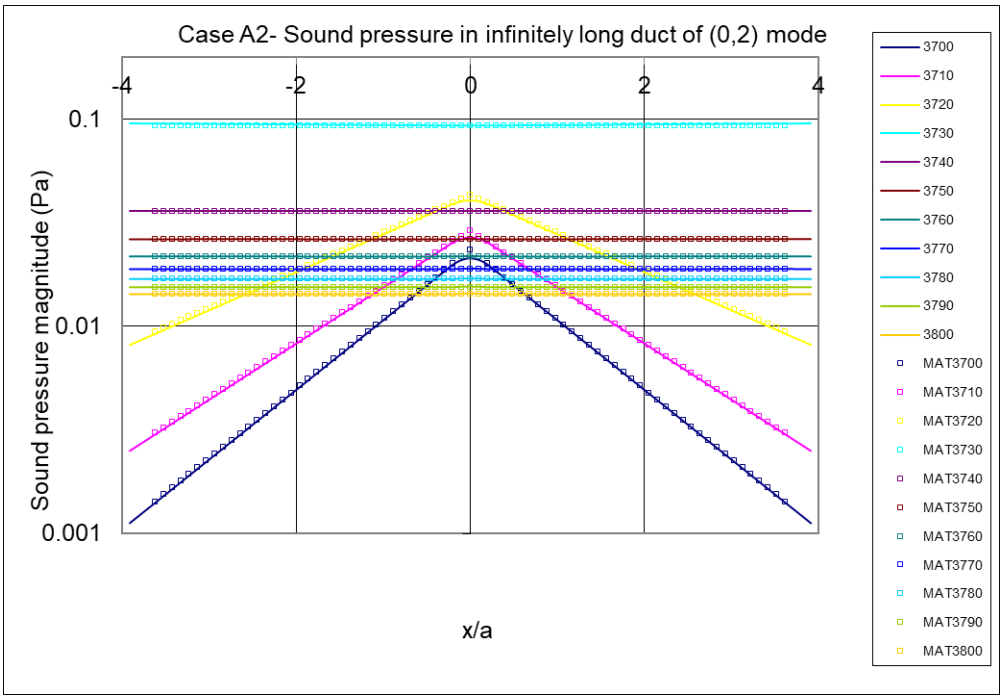

Figure 5.8 – Validation by infinitely long duct model (Case A2)

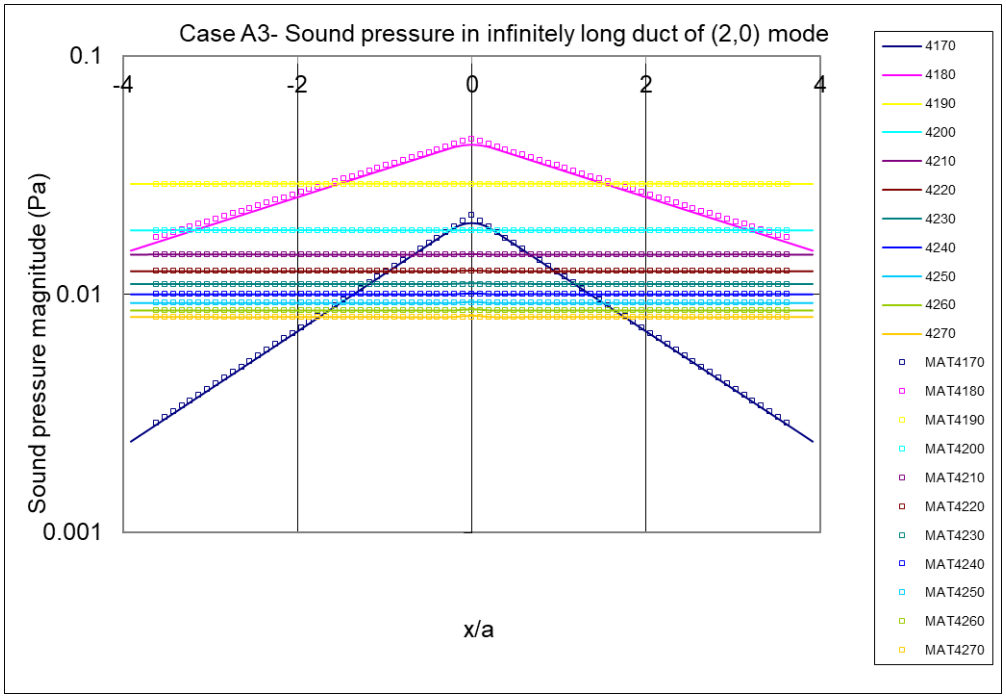

Figure 5.9 – Validation by infinitely long duct model (Case A3)

In order to summarize the overall percentage deviation for each test case, the root mean square (RMS) percentage deviation, Eq. (5.7), is adopted (Pelat *et al.* 2009). Results of various cases are shown in Table 5.2.

$$\text{RMS percentage deviation} = 100\% \sqrt{\frac{1}{s}\sum_{t=1}^{s}\left(\frac{|V_C|-|V_M|}{|V_C|}\right)_t^2} \qquad (5.7)$$

where s is number of fitted points,

V_C are the values obtained from COMSOL 3-D numerical model and

V_M are the prediction values calculated by mathematical model (MATLAB)

Table 5.2 – RMS percentage deviation of results from COMSOL against MATLAB (infinitely long duct)

Case	PML length (m)	Frequency range (Hz)	Sound propagating mode	RMS percentage deviation
A1	0.5	1850-1950	(0,1)	0.229%
A2	0.5	3700-3800	(0,2)	0.808%
A3	0.5	4170-4270	(2,0)	1.213%
A4	0.75	4170-4270	(2,0)	1.211%

In the meantime, no significant difference of RMS percentage deviation is obtained for an increase of PML length to 0.75m for Case A4. Moreover, the contour of percentage deviation of Case A4 in Figure 5.7(d) is very similar to that of Case A3 in Figure 5.7(c). Thus, the plot of comparisons between theoretical and numerical results for Case A4 are not shown here. The above suggests that the base setting of PML length of 0.5m at the duct ends is effective and sufficient for the present study.

5.4 Grid sensitivity test

The two-aperture on side wall case is examined in this section. The centre of the two apertures are allocated along x-axis arbitrarily at 0.162m ($d_1 = 9\text{mm} \times 18, d_1/a = 1.76$) and 0.324m ($d_2 = 9\text{mm} \times 36, d_2/a = 3.52$). Each aperture is a 9mm square (approximate a/10). The frequencies near to the (0,1), (0,2) and (2,0) mode cut-on frequencies are considered since higher order modes are focused in the current study. The physical sizes of free field PML thickness and free space are shown in Table 5.3.

Table 5.3 – Physical sizes of free field PML thickness and free space

Description	(0,1) 1850-1950Hz	(0,2) 3700-3800Hz; (2,0) 4170-4270Hz
Free field PML thickness (T)	100mm ($T/\lambda = 0.54$ at 1850Hz)	50mm ($T/\lambda = 0.54$ at 3700Hz)
Radius of free space (R_f)	200mm ($R_f/\lambda = 1.08$ at 1850Hz)	100mm ($R_f/\lambda = 1.08$ at 3700Hz)
Length of free space (L_f)	0.6m ($L_f/\lambda = 3.24$ at 1850Hz)	0.5m ($L_f/\lambda = 5.39$ at 3700Hz)

Remark: λ denotes the wavelength.

According to COMSOL 2012 tutorial and reference guide, the default element type of Acoustics Module is second order Lagrange elements (Lagrange-Quadratic). The 3-D tetrahedral element is adopted. The rule of maximum element size is 0.2λ of the sound waves in the acoustical domain. Special care is made to investigate the grid sensitivity of these numerical models. The grid sensitivity test is carried out with 6 to 8 elements per wavelength (E/λ). The outcomes with respect to E/λ being used to solve the same numerical model for (0,1) 1850-1950Hz are shown in Table 5.4. Figure 5.10 illustrates the RMS percentage deviations against E/λ at 1950Hz which has the shortest wavelength in the frequency range. All deviations are under 0.9%. One can observed that the decreasing rate of deviation reduces as E/λ increases. The above suggests that further refinement of the grids should not produce significant variations in results. The grid size of current numerical model setting is small enough to minimize error and the solver of the model can show good performance. $E/\lambda = 8.0$ (1950Hz) is adopted for the simulation near (0,1) mode frequencies in this study.

Table 5.4 – Results of grid sensitivity test of (0,1) mode

Maximum element size (m)	E/λ at 1950 Hz	RMS percentage deviation
0.021	8.38	-
0.022	8.00	0.146%
0.023	7.65	0.209%
0.024	7.33	0.328%
0.025	7.04	0.458%
0.026	6.77	0.577%
0.027	6.51	0.720%
0.028	6.28	0.877%

Remarks:

1. E/λ denotes the element per wavelength.
2. RMS percentage deviations are estimated with reference to the results of $E/\lambda = 8.38$ at 1950Hz.

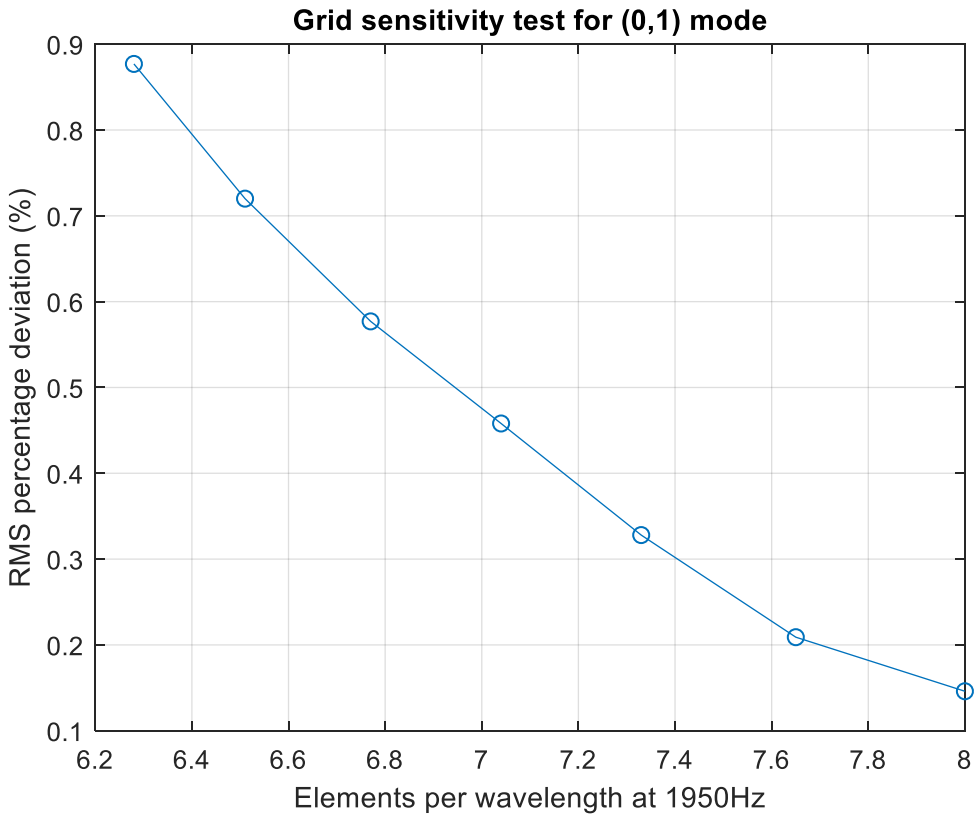

Figure 5.10 – Grid sensitivity test for (0,1) mode

Results in term of E/λ for (2,0) 4170-4270Hz are shown in Table 5.5. Figure 5.11 shows the RMS percentage deviations against E/λ at 4270Hz accordingly. All deviations are under 3%. It is also noted that the decreasing rate of deviation reduces as E/λ increases. The deviation of $E/\lambda = 8.03$ (4270Hz) is approximate 0.3%. The above suggests that the grid size of current numerical model setting is small enough to minimize error and considered appropriate for the present study. $E/\lambda = 8.03$ is applied for (1,0) and (2,0) mode of this study.

Table 5.5 – Results of grid sensitivity test of (2,0) mode

Maximum element size (m)	E/λ at 4270 Hz	RMS percentage deviation
0.0095	8.46	-
0.01	8.03	0.301%
0.0105	7.65	0.632%
0.011	7.30	0.989%
0.0115	6.99	1.420%
0.012	6.69	1.814%
0.0125	6.43	2.263%
0.013	6.18	2.932%

Remarks:

1. E/λ denotes the element per wavelength.
2. RMS percentage deviations are estimated with reference to the results of $E/\lambda = 8.46$ at 4270Hz.

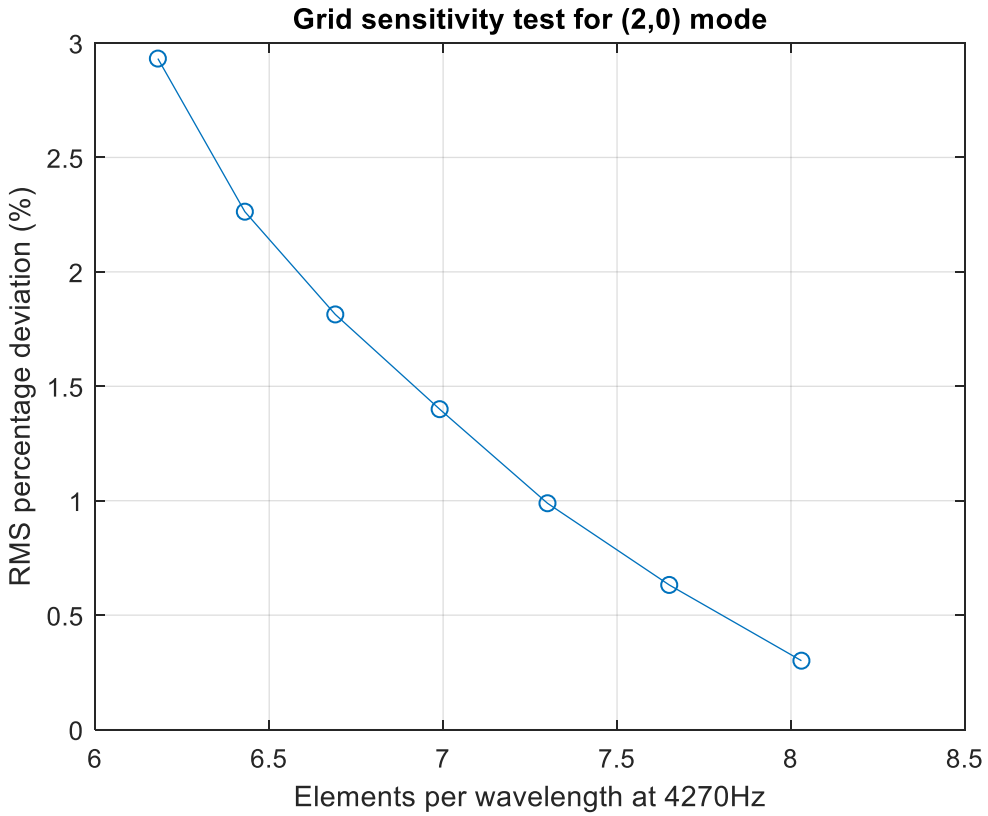

Figure 5.11 – Grid sensitivity test for (2,0) mode

5.5 Comparisons of results from the validated numerical models against the mathematical models

In Chapters 3 and 4, the mathematical model has been derived to predict the sound field inside the duct with side opening(s). The next sub-sections discuss the comparisons of mathematical predications against results from numerical models validated in the aforesaid sections. A single and two-aperture on the side wall of a long duct cases are evaluated.

5.5.1 A single aperture on the side wall of a long duct model

The centre of an opening is allocated along x-axis arbitrarily at 0.162m ($x_1 = 9\text{mm} \times 18, x_1/a = 1.76$). The size of the opening is 9mm (approximate a/10) in height and 8mm in width. Table 5.6 shows the cases for comparisons of mathematical predictions against numerical results. The frequency range below the first cut-on frequency are concerned as well. The inclusion of aperture thickness in mathematical model is reviewed.

Table 5.6 – Cases for duct model with single aperture

Frequency range (Hz)	Exclusion of aperture thickness (mathematical model)	Inclusion of aperture thickness (mathematical model)
50-600	Case B1	Case B2
1850-1950	Case B3	Case B4
3700-3800	Case B4	Case B6
4170-4270	Case B7	Case B8

Acoustic mode shapes across the cross-section of the duct at various frequencies are generated. The sound field patterns at 50Hz plane mode, 1870Hz (0,1) mode, 3730Hz (0,2) mode and 4190Hz (2,0) mode, obtained from the finite element simulation, are captured at the centre of opening and presented in Figure 5.12. Acoustic modes with pattern similar to those of the rigid-wall duct can be observed. However, the nodal line of (0,1) mode is biased. The nodal line nearer the opening is found distorted at (0,2) and (2,0) modes. The sound leakage at the aperture results in asymmetrical mode shape. The form of spherical sound radiation at the aperture is observed.

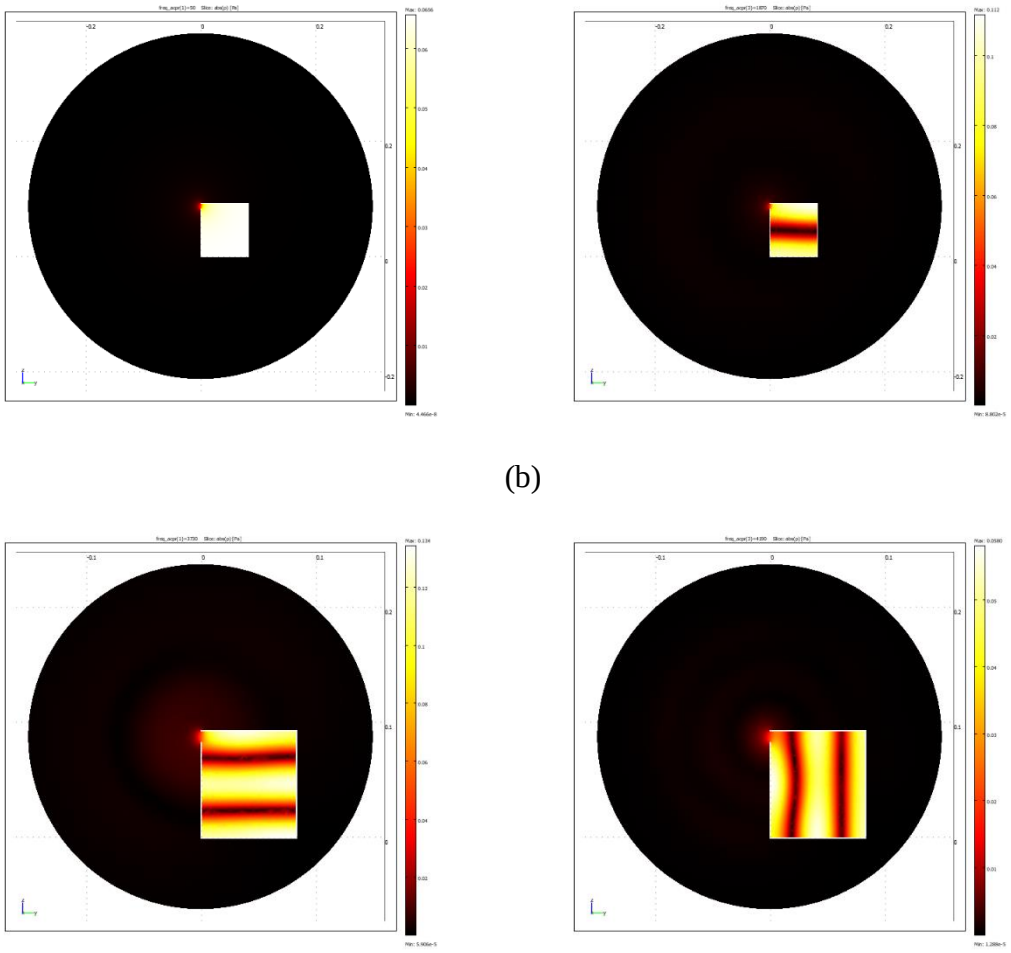

(a) (b)

(c) (d)

Figure 5.12 – Sound field pattern for Case B. (a) 50Hz (0,0) mode; (b) 1870Hz (0,1) mode; (c) 3730Hz (0,2) mode; (d) 4190Hz (2,0) mode.

The same procedures as the Section 5.3 is adopted to analyse the computational data of sound pressure over the concerned internal cross-sections. The interval of cross-section along the *x* direction is 9mm and the frequency resolution is 50Hz for Cases B1 and B2. Numerical results from 37 sections and 12 frequencies are collected. For the mathematical model, the acoustic velocity *V* normal to the single opening (Eq. 4.3) can be solved mathematically. Thus, the predicted sound field along the duct can be calculated by using Eqs. (4.13), (4.14) and the force from source Eq. (4.35).

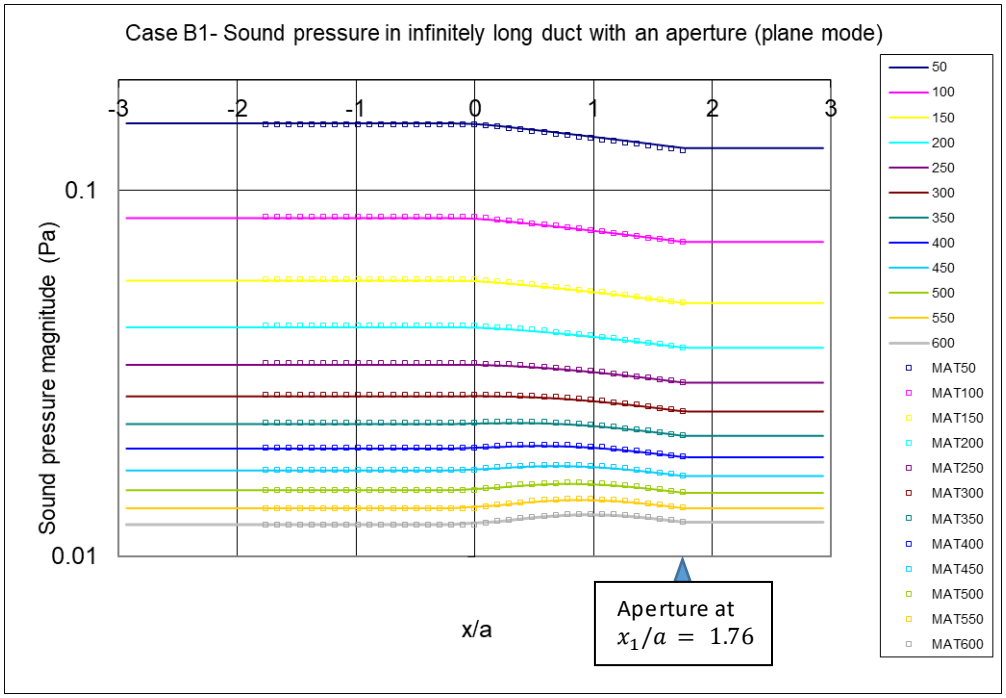

Figure 5.13 – Validation by single aperture model (Case B1, exclusion of aperture thickness)

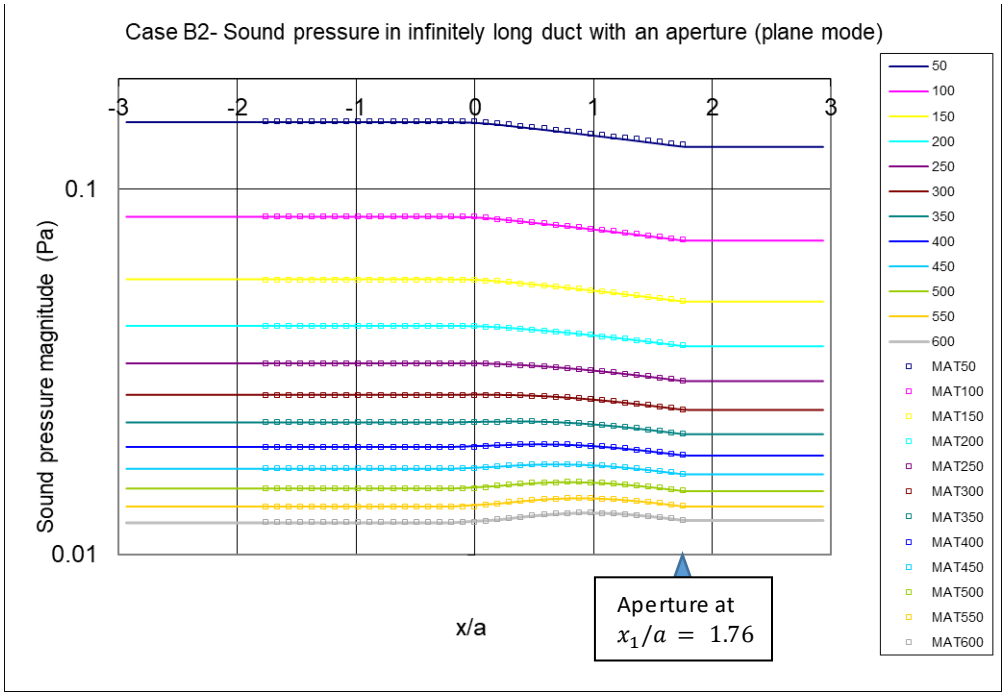

Figure 5.14 – Validation by single aperture model (Case B2)

Figures 5.13 and 5.14 illustrate the findings of Cases B1 and B2 at frequency range of 50-600Hz (plane mode). A resonant effect is noted in the plane mode. The mode magnitude decreases with increasing frequency. Further discussions on such effect and the modal frequency are provided in Section 6.2. Results of the numerical models show excellent agreement with mathematical predictions. The contours of percentage deviation of Cases B1 and B2 are shown in Figure 5.15. The inclusion of aperture thickness effect on the radiation impedance of aperture gives better accuracy of the mathematical model.

One can observe that the percentage deviations are well under ±1% at the plane mode (Case B2).

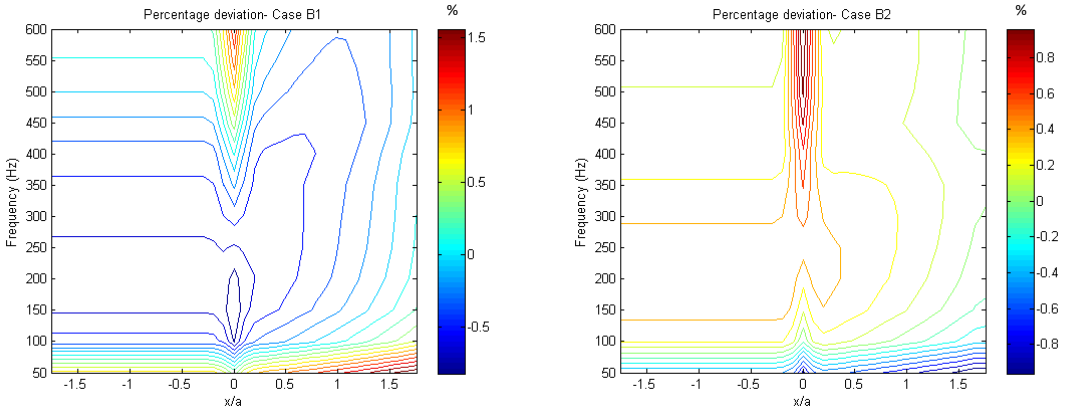

(a) (b)

Figure 5.15 – Contour of percentage deviation of results from COMSOL against MATLAB, 50-600Hz, (0,0) mode. (a) Case B1; (b) Case B2

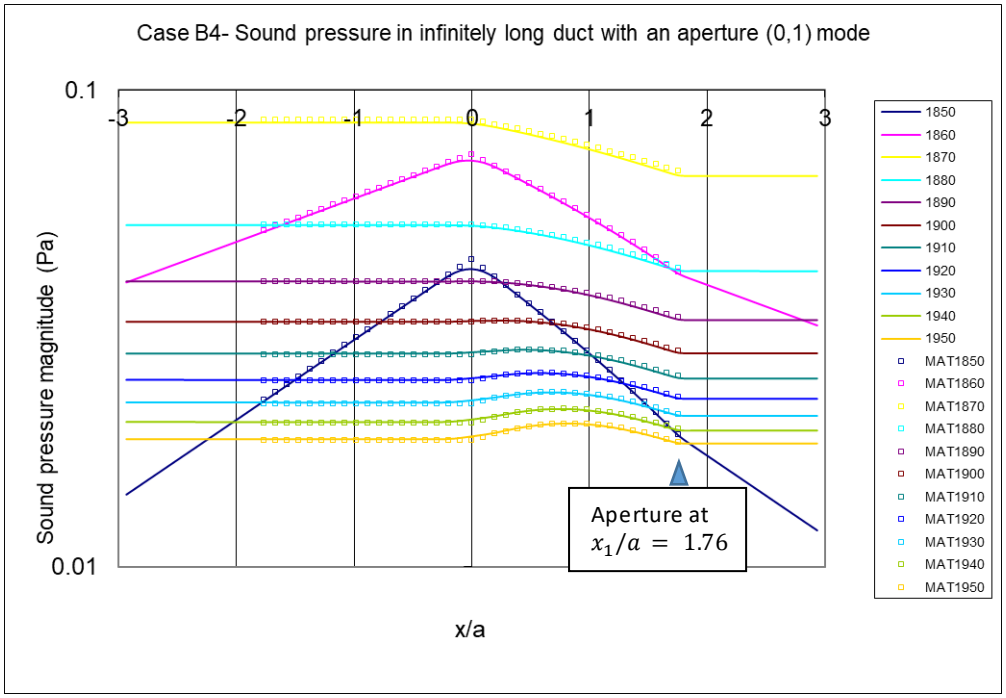

Figure 5.16 – Validation by single aperture model (Case B4 at 1850-1950Hz)

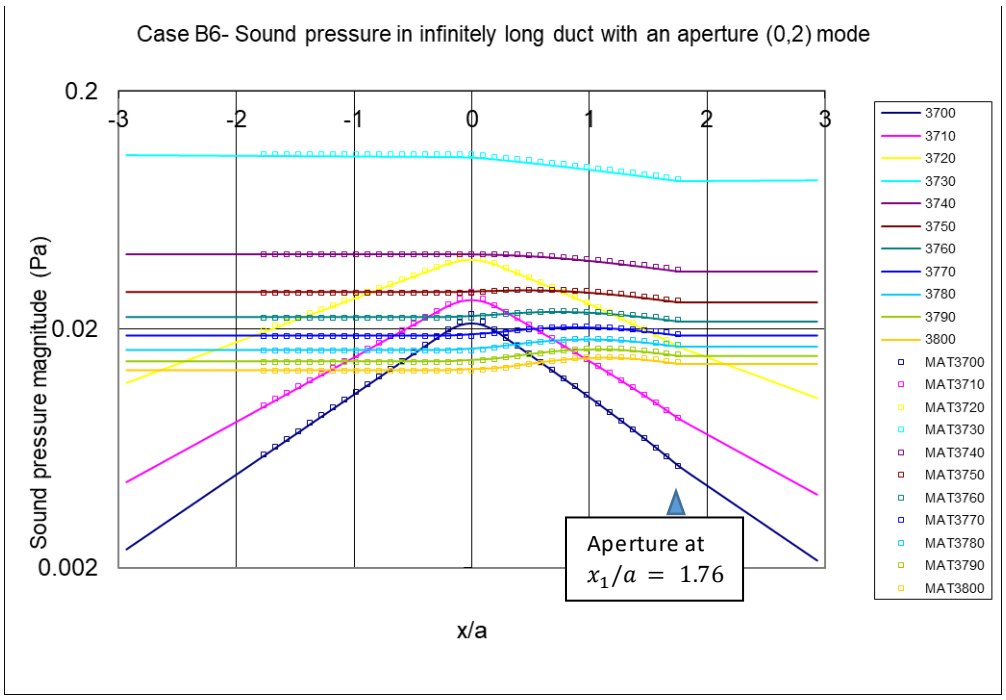

Figure 5.17 – Validation by single aperture model (Case B6 at 3700-3800Hz)

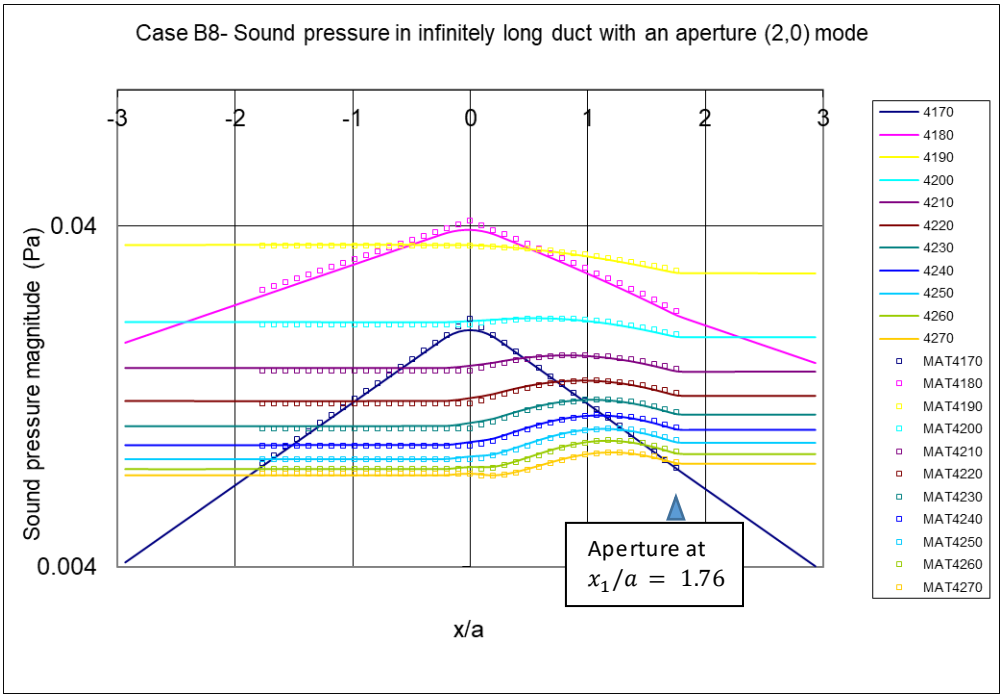

Figure 5.18 – Validation by single aperture model (Case B8 at 4170-4270Hz)

For Cases B3 to B8, the frequency resolution is 10Hz. Numerical results from 37 duct sections and 11 frequencies are gathered. Figures 5.16, 5.17 and 5.18 illustrate the findings of Cases B4, B6 and B8 (aperture thickness effect is included in the mathematical prediction) at frequency ranges near propagation modes (0,1), (0,2) and (2,0) respectively. In Figure 5.19, the contours of percentage deviation of Cases B4 to B8 are presented. Except some deviations at the zone around $x/a = 0$ and at below the eigen-frequency (4187Hz) which are not our major concerned, the majority are well under ±2.2%.

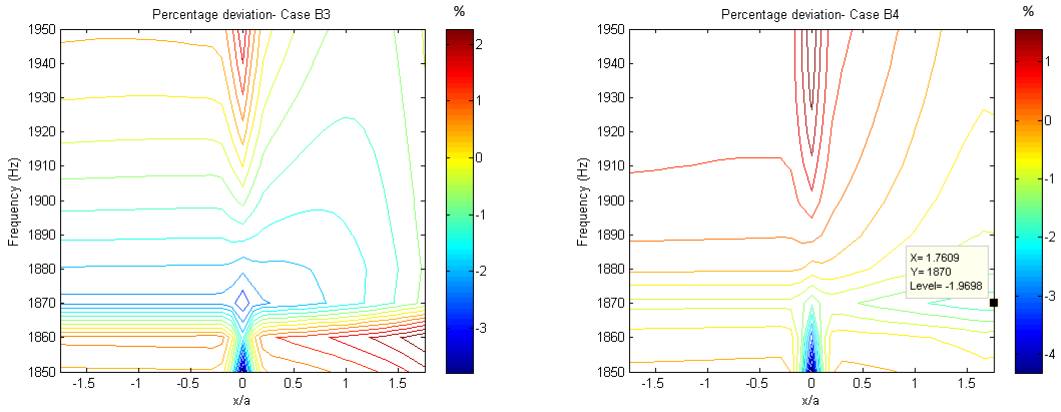

(a)

(b)

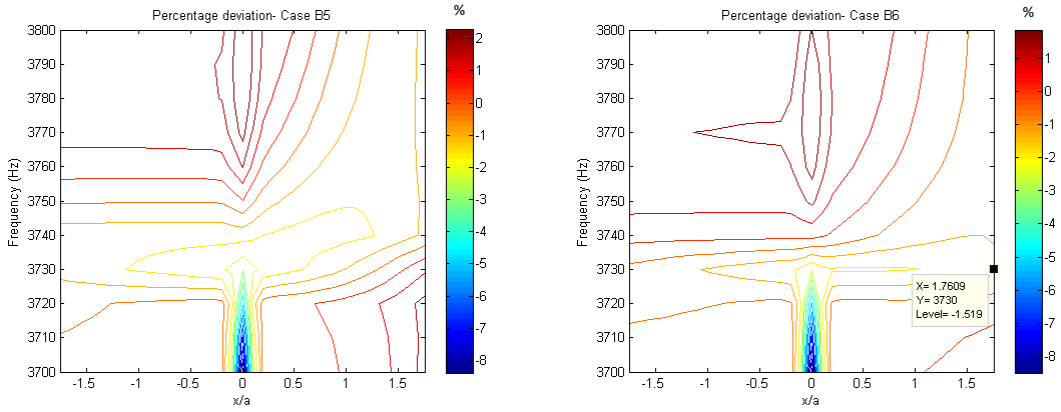

(c)

(d)

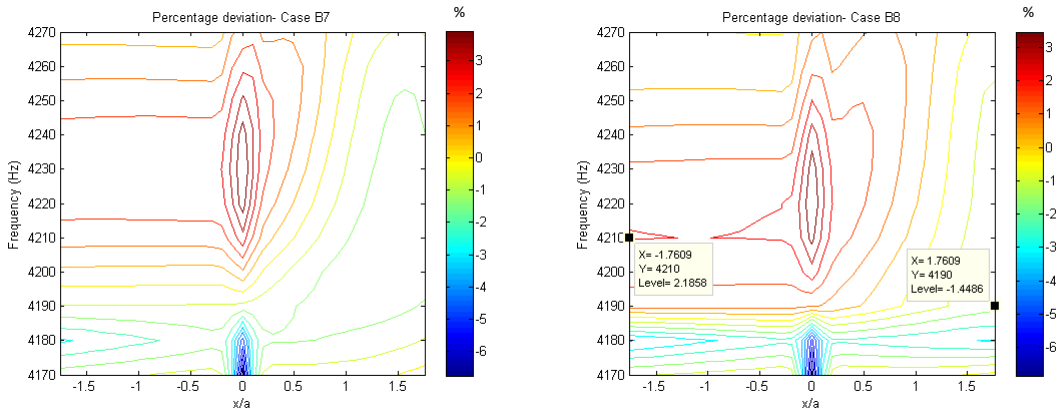

(e)

(f)

Figure 5.19 – Contour of percentage deviation of results from COMSOL against MATLAB. (a) Case B3; (b) Case B4; (c) Case B5; (d) Case B6; (e) Case B7; (f) Case B8.

Table 5.7 – RMS percentage deviation of results from COMSOL against MATLAB (Case B)

Case	Inclusion of Aperture thickness	Frequency range (Hz)	Sound propagating mode	RMS percentage deviation
B1	No	50-600	(0,0)	0.52%
B2	Yes	50-600	(0,0)	0.32%
B3	No	1850-1950	(0,1)	1.22%
B4	Yes	1850-1950	(0,1)	0.74%
B5	No	3700-3800	(0,2)	1.38%
B6	Yes	3700-3800	(0,2)	1.19%
B7	No	4170-4270	(2,0)	1.63%
B8	Yes	4170-4270	(2,0)	1.61%

In Table 5.7, the RMS percentage deviations are also improved for Cases B4, B6 and B8 when the aperture thickness effect is included in the mathematical prediction. Results of the numerical models show excellent agreement with mathematical predictions as well. The small deviations may be due to the existence of uneven acoustic velocity and sound diffraction at the opening in numerical modelling. As mentioned in the mathematical model for the open slot case in Chapter 3, the x-component wave propagation at the aperture could be happened.

5.5.2 Two-aperture on the side wall of a long duct model

The two-aperture on side wall case is examined in this section. The same geometry settings as Section 5.4 are adopted. Table 5.8 summarizes the cases for comparisons between mathematical predictions and numerical results.

Table 5.8 – Cases for duct model with two-aperture

Frequency range (Hz)	Cases for two-aperture
1850-1950	Case C1
3700-3800	Case C2
4170-4270	Case C3

Sound field patterns at 1870Hz (0,1) mode, 3730Hz (0,2) mode and 4190Hz (2,0) mode, obtained from the finite element simulation, are captured at the centre of the two apertures (an isometric view with 2 slices) as shown in Figures 5.20(a), (b) and (c) respectively. Owing to the leaky sound at the apertures, the asymmetric mode shapes can be found. Also, it is noted that both nodal lines of Case C3 (Figure 5.20(c)) are distorted at $d_2/a = 3.52$. The observations identify that the mode amplitude at $d_1/a = 1.76$ is higher than the amplitude at $d_2/a = 3.52$ in these cases.

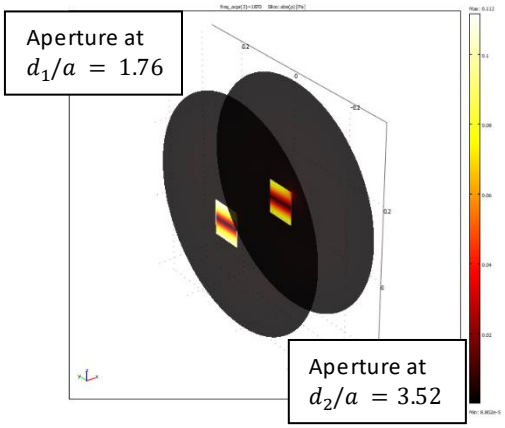

(a)

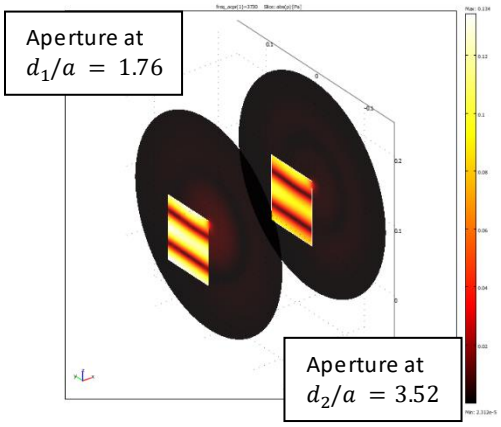

(b)

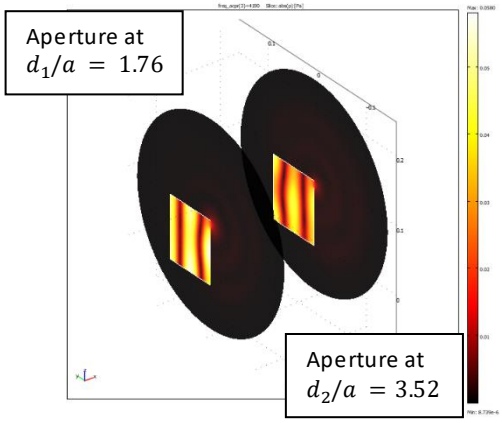

(c)

Figure 5.20 – Sound field patterns near the eigen-frequency. (a) (0,1) mode for Case C1; (b) (0,2) mode for Case C2; (c) (2,0) mode for Case C3.

The in-duct computed sound pressures are analysed. Data from 75 duct sections and 11 frequencies are collected for Case C. Results are obtained for comparison with the mathematical prediction. The acoustic velocity V_i normal to the openings (Eq. 4.8) can be solved mathematically. Thus, the predicted sound field along the duct can be calculated by using Eqs. (4.27), (4.28) and the force from source Eq. (4.35).

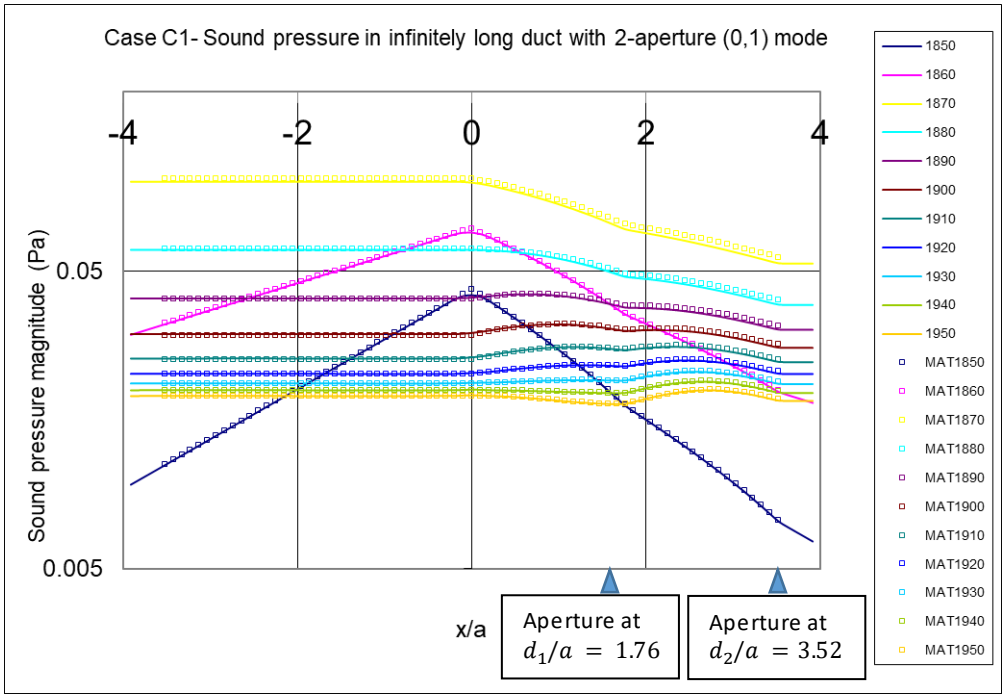

Figure 5.21 – Validation by two-aperture model (Case C1)

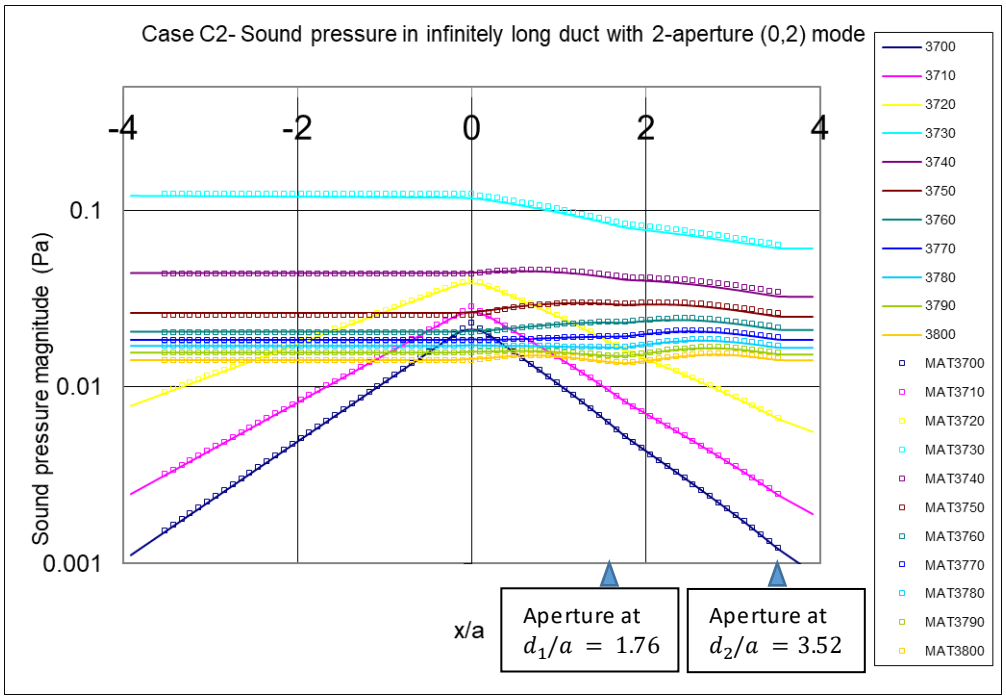

Figure 5.22 – Validation by two-aperture model (Case C2)

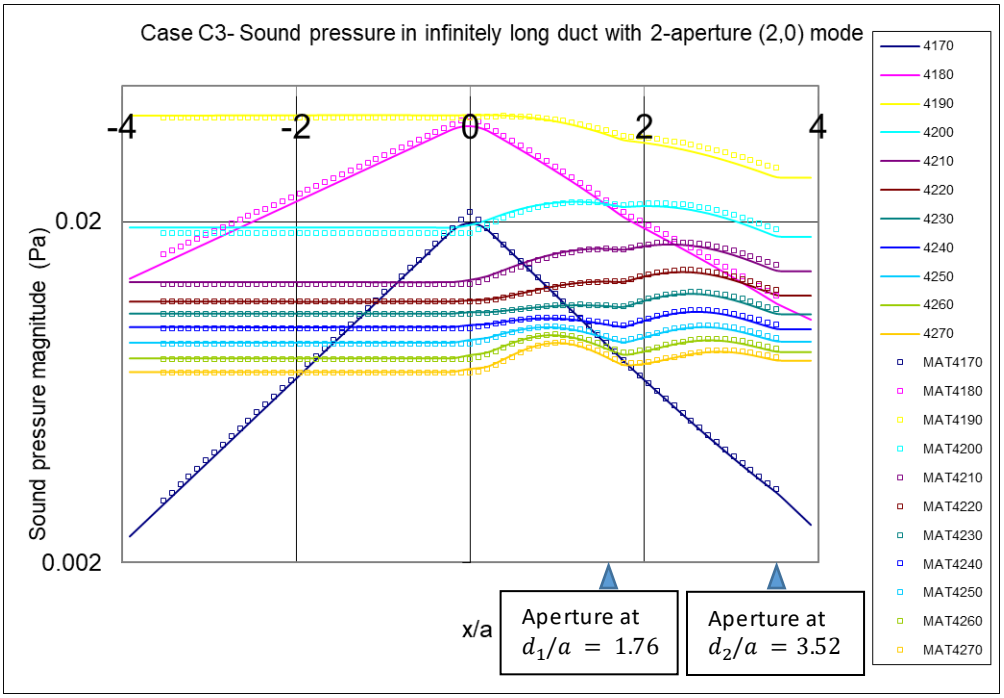

Figure 5.23 – Validation by two-aperture model (Case C3)

Figures 5.21, 5.22 and 5.23 illustrate the findings of Cases C1, C2 and C3 at various frequency ranges. The contours of percentage deviations are presented in Figures 5.24(a), (b) and (c). One can note that the concerned deviations are under ±5.7%. Results from numerical models show very good agreement with mathematical predictions.

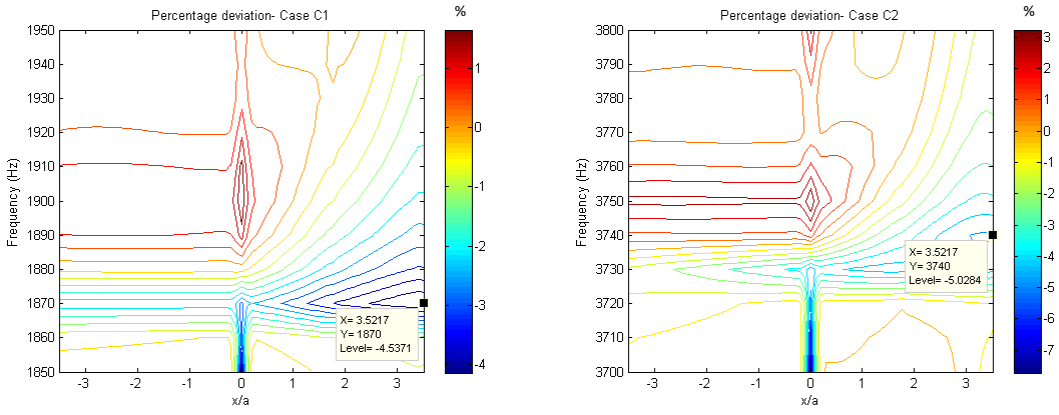

(a) (b)

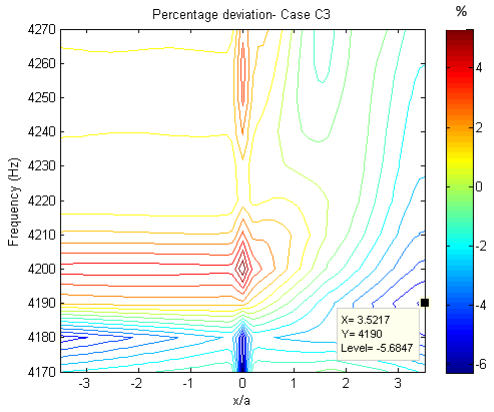

(c)

Figure 5.24 – Contour of percentage deviation of results from COMSOL against MATLAB. (a) Case C1; (b) Case C2; (c) Case C3.

The RMS percentage deviations of the various cases are listed in Table 5.9.

Table 5.9 – Percentage deviation of results from COMSOL against MATLAB (Case C)

Case	Frequency range (Hz)	Sound propagating mode	RMS Percentage deviation
C1	1850-1950	(0,1)	1.29%
C2	3700-3800	(0,2)	1.82%
C3	4170-4270	(2,0)	2.09%

5.7 Concluding remarks

The validation is made by comparing three-dimensional (3-D) numerical results of the infinitely long rectangular duct with those predicted by theory. The exact resonance frequencies are found in the numerical computation. The mode amplitude for various frequencies in a long rectangular duct in the presence of a circular sound source is

illustrated graphically. Values calculated from numerical model show excellent agreement with those predicted by mathematical model. Grid sensitivity test by two-aperture on the duct wall were implemented. Findings of this study are convinced that the present set-up of 3-D finite element modelling is appropriate for the research.

Subsequently, the analytical results of the single aperture and two-aperture cases show consistent acoustical behaviour with those computed by the numerical model. Observations of acoustic modes shape and leaky sound pressure from aperture(s) of numerical models are discussed. During the sound excitation, the acoustic modes with pattern is similar to those of the rigid-wall duct but sound leakage results in the asymmetrical mode shapes. Moreover, the precision of the radiation impedance of aperture is important to the accuracy of mathematical prediction.

Chapter 6

Prediction of the complex wave-number for the open slot cases

6.1 Introduction

A complex wave-number is introduced to model the sound propagation inside the leaky duct in Chapter 3. This section is an attempt to develop a method for predicting the complex wave-numbers for different slot dimensions. The finite element modelling is used. Section 6.2 and 6.3 describe some criterions, including setting the frequency ranges, for the prediction.

6.2 Modal frequencies of a duct with an infinitely long gap

Geometrically, one interesting case is a duct with an infinitely long slot, so called an infinite gap. Figure 6.1 illustrates the configuration and a cross-section of a rectangular duct with an infinite gap. The model of interest in this section is a duct of uniform internal cross-section area of height a and width b. The gap is on the side wall of the duct. The opening size is named as the gap width (gth).

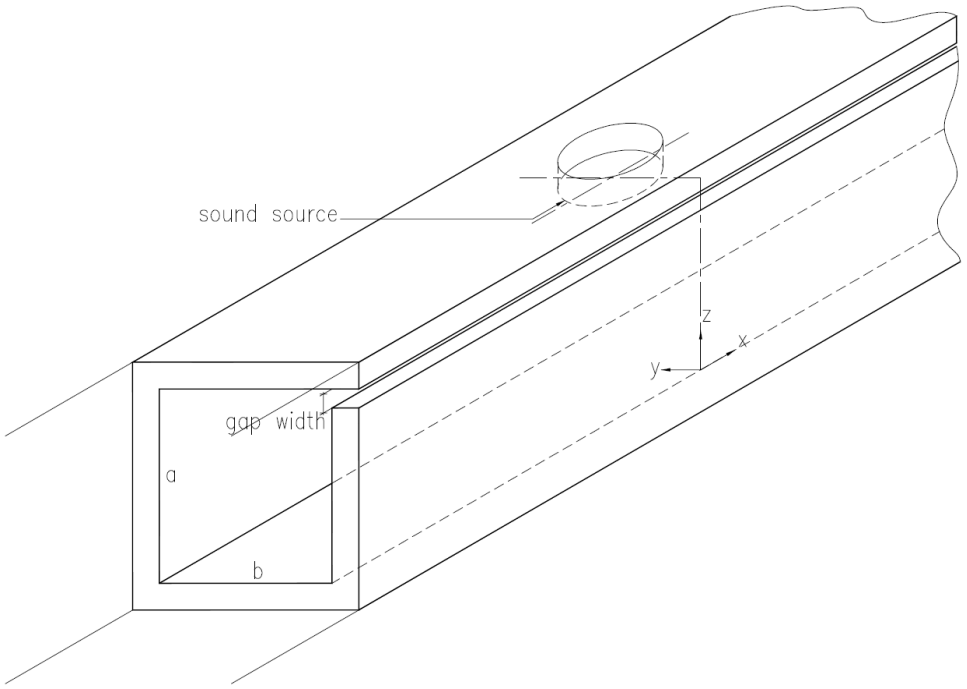

Figure 6.1 – A rectangular duct with an infinitely long gap

Obviously, it is not practical to adopt the theoretical slot model by using an infinite array of square air pistons. It is considered an effective way to set up a 3-D COMSOL model with an infinite gap along the duct for the analysis. The numerical model is established in a way similar as the one in Chapter 5 except that the PML of the free field which has the same length of the duct domain (0.8m) and *gth* is 4.5mm (see Figure 6.2).

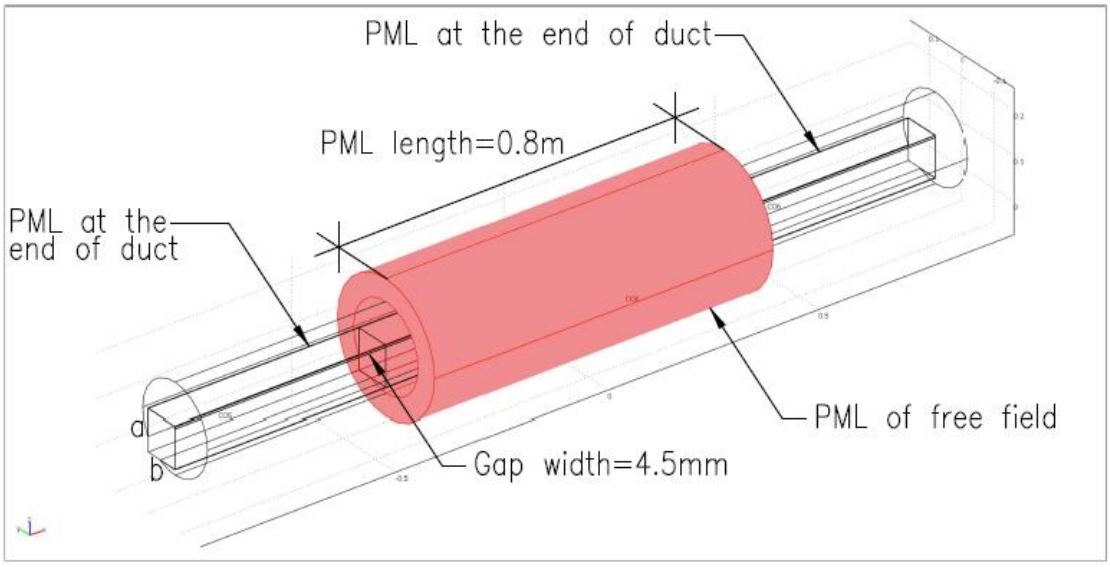

Figure 6.2 – The COMSOL model of a rectangular duct with an infinitely long gap

The frequency variation of the volume integral of acoustic pressure (absolute value) is shown in Figure 6.3. The same technique as stipulated in Section 5.3 is adopted. It is taken by the numerical model from 100Hz up to 4300Hz with frequency interval of 1Hz at the regions near to the resonance frequencies and 50Hz otherwise.

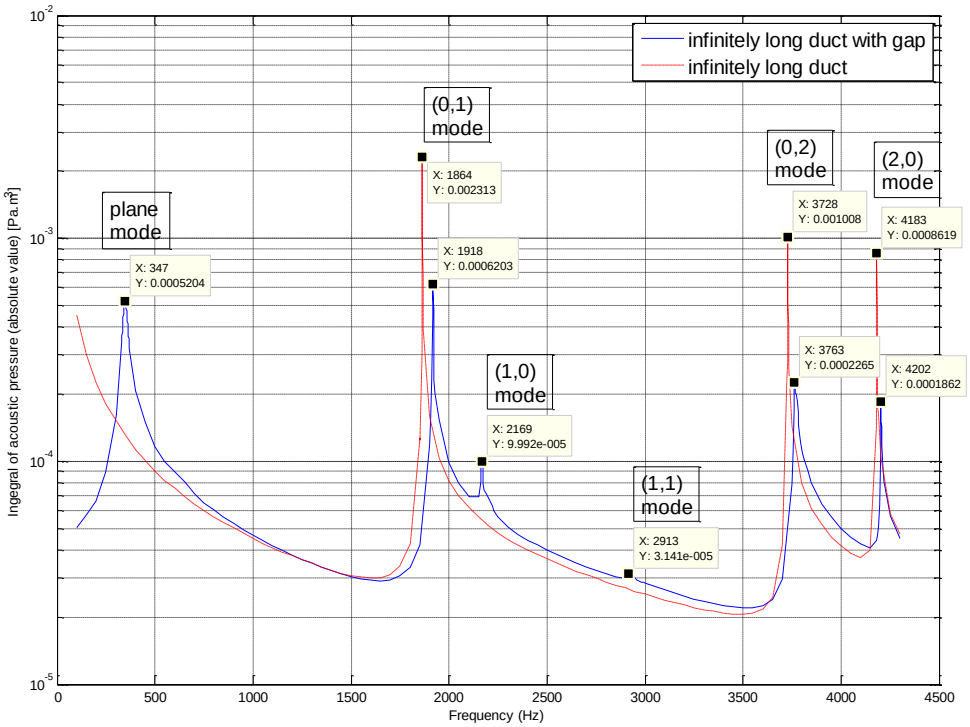

Figure 6.3 – Frequency variation of the volume integral of acoustic pressure (absolute value) for 4.5mm infinite gap model and infinitely long duct model

Similar data obtained with an infinitely long duct without gap is superimposed into the plot. One can note that there are peaks above and near to the eigen-frequencies of the infinitely long duct. We call the corresponding frequencies of the peaks "modal frequencies" (f_{mn}) of the infinite gap case. These modal frequencies are 1918Hz, 3763Hz and 4202Hz for the (0,1), (0,2) and (2,0) mode respectively. In addition, relatively weak resonant effects in the vicinity of duct eigen-frequencies at (1,0) and (1,1) modes are observed. The corresponding modal frequencies are 2169Hz and 2913Hz respectively. Since the circular sound source is at the centre of top wall, the odd modes in the duct

spanwise direction will not be excited as mentioned in Chapter 2. However, owing to sound leakage at the gap to the surroundings, an addition of sound source contribution from air piston(s) in the gap are involved in the duct. The resulting sound source position is no longer at the nodal line exactly.

Besides, a resonant effect is found at 347Hz (plane mode) for the duct with gap and it is below the first eigen-frequency of duct. Such effect can be associated with that of the Helmholtz resonator. Similar to the open slot model discussed in Chapters 3 and 4, the moving air in the gap radiates sound into the exterior. One can consider that the duct interior cavity is large in compare with the air pistons volume in the gap. This can be treated as a cavity resonator. Section 5.5.1 also describes the sound field for the infinitely long duct with an aperture in plane wave mode. In this chapter, we focus on the above-observed resonant cases near to and above the eigen-frequencies (0,1), (0,2) and (2,0) of the duct modes.

6.3 Evaluation of the sound behaviour of the single aperture cases in frequency domain

The above section discusses the modal frequencies of the infinite gap case. It is tried to further figure out the modal frequencies inside the infinitely long duct with an aperture. Special efforts are made in examining the influence of aperture sizes on the duct sound behaviour in frequency domain. The mathematical model derived in Chapter 4 is adopted for evaluation.

According to the validation of COMSOL model of single aperture cases in Chapter 5, an aperture is located at the right side of an infinitely long duct at $x_1/a = 1.76$ while the sound source is at the centre. Constant duct mode magnitudes can be found on both the left side of sound source and the right side of the opening (see Figures 5.18, 5.19 & 5.20). Sound should leak out from the opening, resulting in subsequent pressure drop at the downstream normally. However, one can note that the internal duct pressure difference between both sides varies with frequency. It is observed that the downstream pressure could be even higher than that of left side at certain higher frequencies. The question here is what the physical reason is? It can be explained by the previous finding of the modal frequency of the duct and it is further discussed in the followings.

To follow the validation procedure in Chapter 5, same sets of equations derived in Chapter 4 are solved to calculate the sound pressures for analysis.

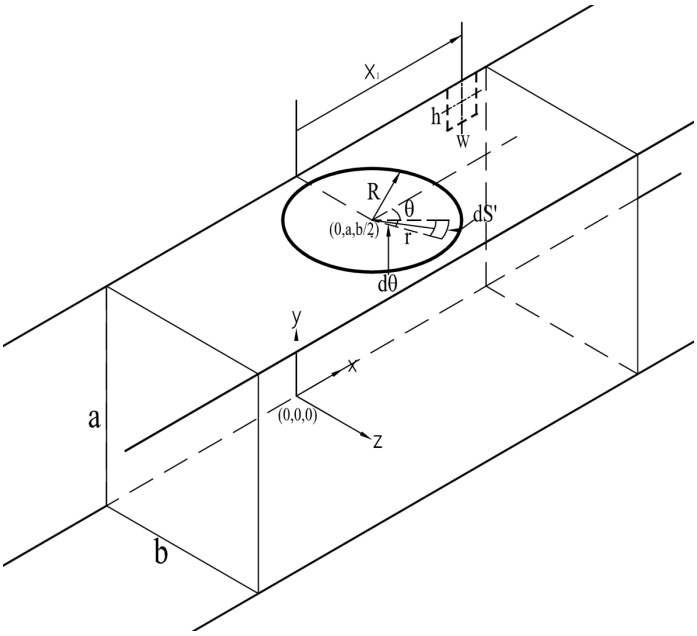

Figure 6.4 - Geometry of the square side wall opening and flush-mounted circular sound source

Figure 6.4 is retrieved from Figure 4.1. It shows the configuration of the infinitely long duct with a single side opening. In the present analysis, an aperture is set as a square. That is,

$$w = h = d$$

It is meaningful to analyse various cases in terms of aperture size and duct mode. The combinations are shown in Table 6.1:

Table 6.1 – Selected cases for duct model with single square aperture

Aperture size	Frequency range		
(square)	*1850-2000Hz*	*3710-3850Hz*	*4170-4300Hz*
d=4.5mm	Case 1(a)	Case 1(b)	Case 1(c)
d=9mm	Case 2(a)	Case 2(b)	Case 2(c)

Remark: a, b, c denote the (0,1), (0,2) and (2,0) mode respectively.

Duct acoustic pressure magnitude for various frequencies of Case 1(a) at (0,1) mode are plotted in Figure 6.5. In this research, acoustical behaviours near resonance with leaky sound characteristic at an aperture are the foci. Along the duct, the internal sound pressure is expected to be reduced on the side with opening ($x_1/a = 1.76$). Nevertheless, there are some data (around 1950Hz and frequencies above) showing rebound of mode magnitude inside the duct downstream of the opening. However, the pressure magnitudes

are relatively low and thus insignificant. One can note that there is transitional frequency, so-called "turning-point" frequency, at which the pressure difference between both sides are close to zero. Around the turning-point frequency, the mode magnitude differences between the left and right sides of the duct change sign.

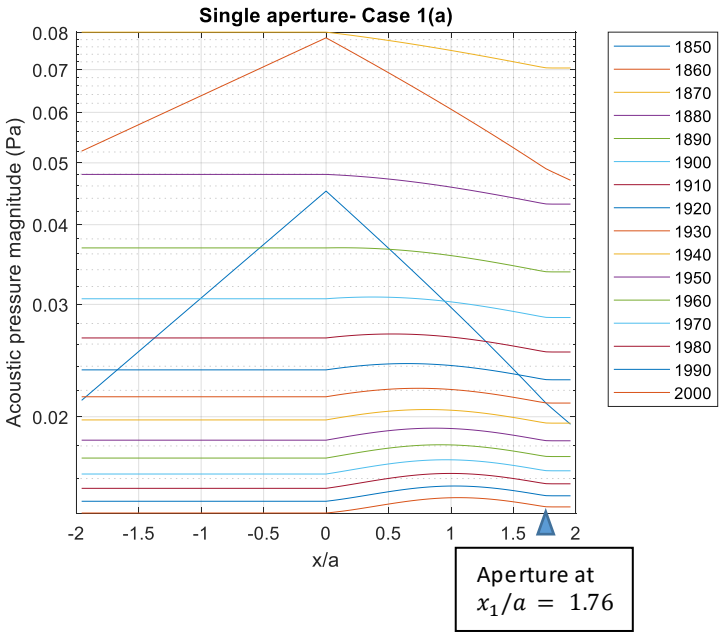

Figure 6.5 – Plots of acoustic pressure magnitude against *x/a* for Case 1(a).

Figure 6.6 shows the turning-point with frequency resolution of 1Hz. As there are constant mode magnitudes in the left side of duct (without side opening) at each frequency, these magnitudes are plotted against the frequency as a reference.

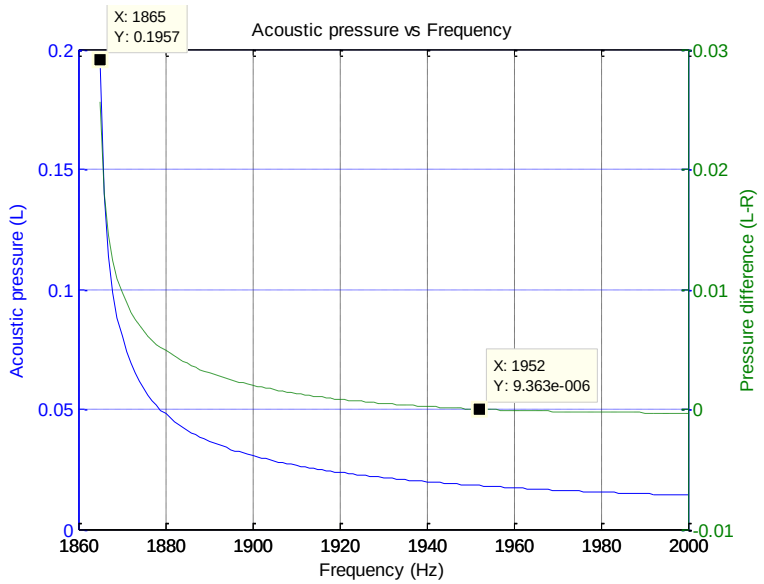

Figure 6.6 – Plots of acoustic pressure magnitude at the infinite duct side (left side) and pressure difference between left and right sides of duct in frequency domain for Case 1(a).

For the Case 1(b), the in-duct sound field of (0,2) mode is shown in Figure 6.7. The turning-point frequency of such case is 3762Hz (see Figure 6.8).

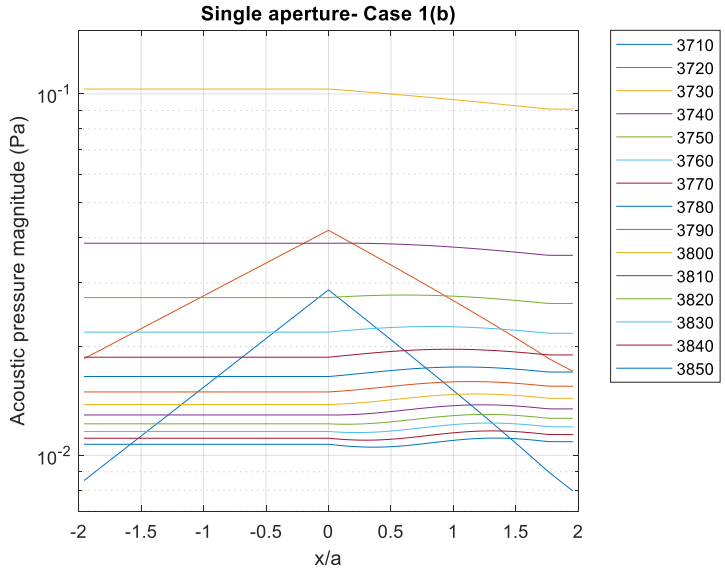

Figure 6.7 – Plots of acoustic pressure magnitude against *x/a* for Case 1(b).

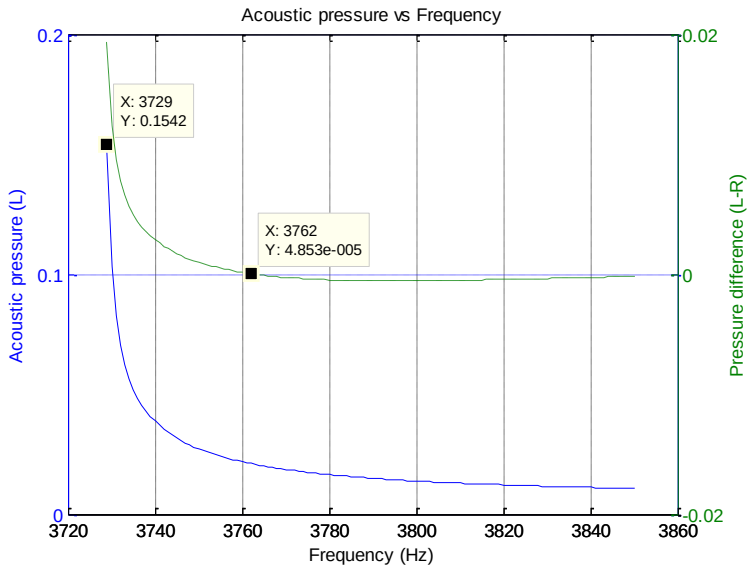

Figure 6.8 – Plots of acoustic pressure magnitude at infinite duct side (left side) and pressure difference between left and right sides of duct in frequency domain for Case 1(b).

For the Case 1(c), the in-duct sound field of (2,0) mode is shown in Figure 6.9. The turning-point frequency of such case is 4205Hz (see Figure 6.10).

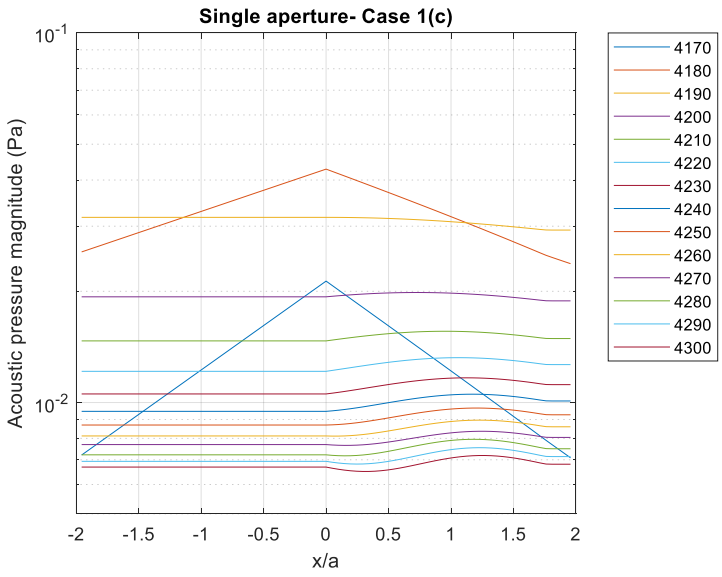

Figure 6.9 – Plots of acoustic pressure magnitude against *x/a* for Case 1(c).

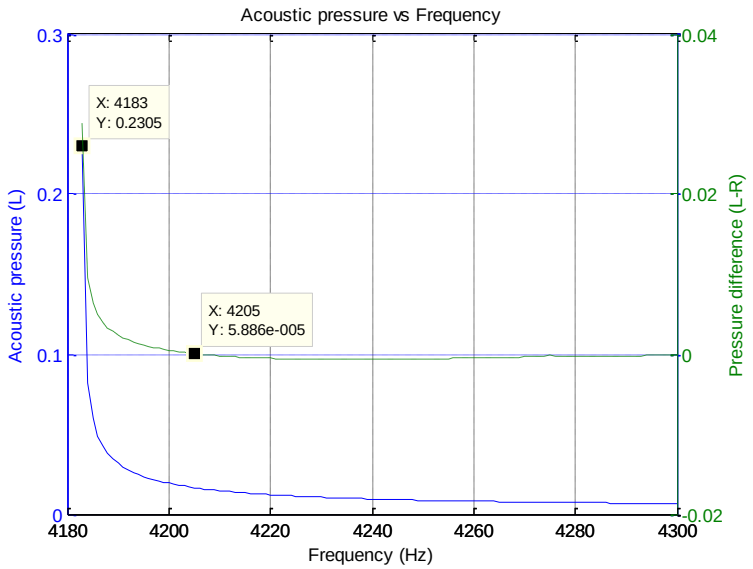

Figure 6.10 – Plots of acoustic pressure magnitude at infinite duct side (left side) and pressure difference between left and right sides of duct in frequency domain for Case 1(c).

Although the acoustic pressures at frequencies higher than the turning-point are rather low, it is interesting to discuss the phenomenon of pressure rebound in the single side opening model. According to Section 6.2, modal frequency (f_{mn}) of duct is introduced in the infinite gap model and f_{mn} is above and near to the duct eigen-frequency. Similarly, one can expect that there is a modal frequency or wave-number of duct with single side opening ($k_{n,o}$) which should be higher than that of the infinitely long duct without side opening ($k_{n,c}$). That is,

$$k_{n,o} > k_{n,c} \tag{6.1}$$

With reference to the Eq. (2.9), the argument $\frac{1}{\sqrt{k^2 - {k_{mn}}^2}}$ has a singularity at $k = k_{mn}$ and this is the indication of resonance. In the current geometry where there is a single side opening at the long duct, resonant behaviour can be observed as well.

For k above and close to $k_{n,o}$,

$$k^2 - {k_{n,c}}^2 > k^2 - {k_{n,o}}^2$$

$$\frac{1}{k^2 - {k_{n,c}}^2} < \frac{1}{k^2 - {k_{n,o}}^2} \tag{6.2}$$

This explains that the pressure amplitude of infinitely long duct side could be less than that downstream of the opening when the sound wave is excited above the modal frequency of duct with side opening.

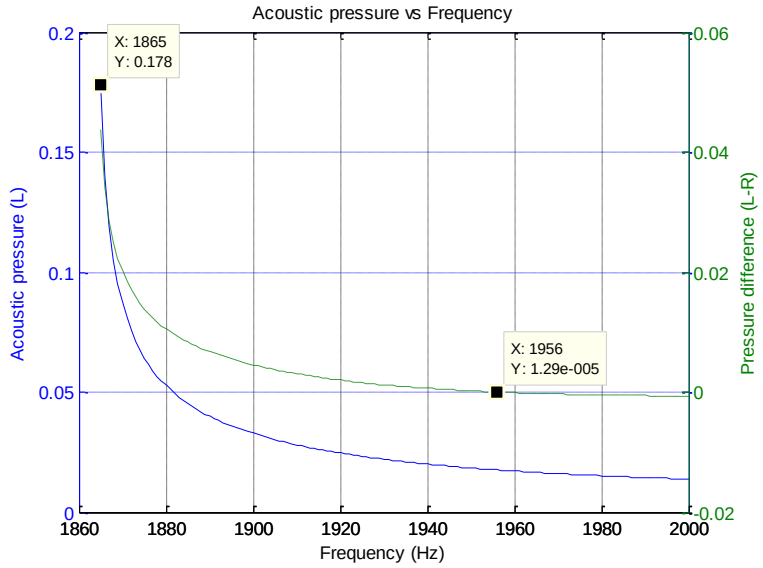

Figure 6.11 – Plots of acoustic pressure magnitude at infinite duct side (left side) and pressure difference between left and right sides of duct in frequency domain for Case 2(a).

Moreover, for the Case 2(a) as shown in Figure 6.11, the turning-point frequency of duct with side opening increases as the opening size is enlarged from 4.5mm to 9mm square (1952Hz and 1956Hz respectively). Such finding shows similar phenomenon as

the Helmholtz resonator whose resonance frequency increases with increasing opening size.

Figures 6.12 and 6.13 show the finding of turning-point frequency of (0,2) and (2,0) mode respectively.

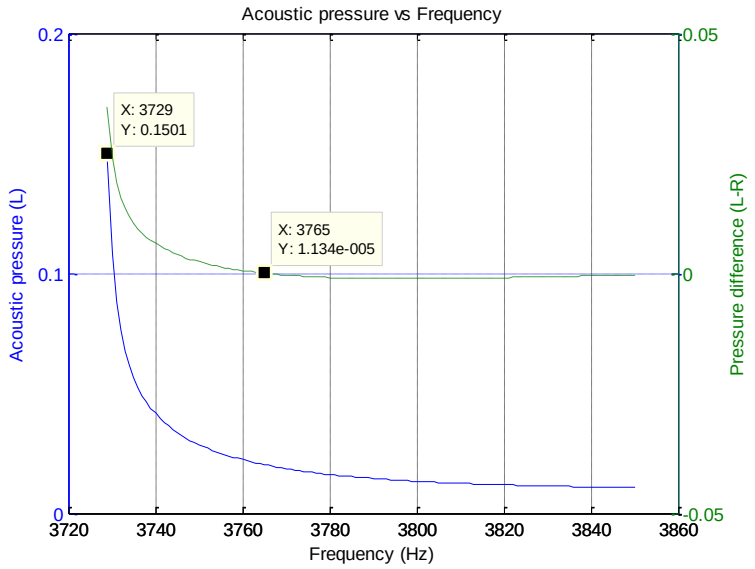

Figure 6.12 – Plots of acoustic pressure magnitude at infinite duct side (left side) and pressure difference between left and right sides of duct in frequency domain for Case 2(b).

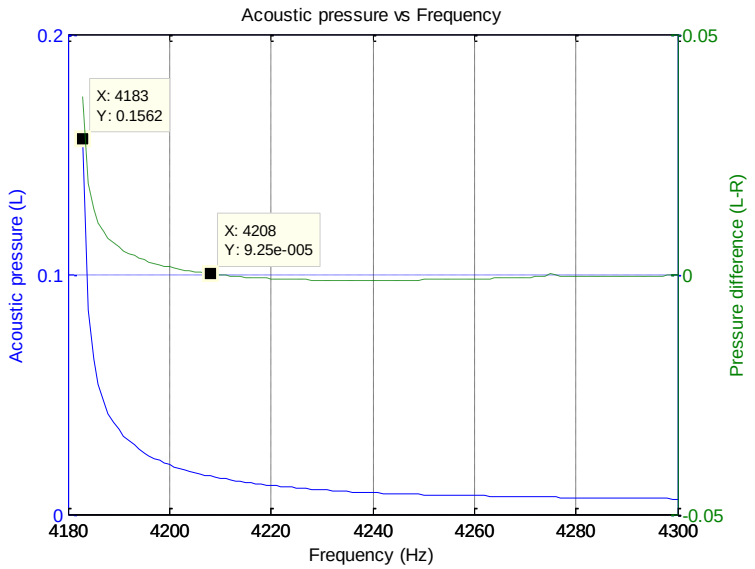

Figure 6.13 – Plots of acoustic pressure magnitude at infinite duct side (left side) and pressure difference between left and right sides of duct in frequency domain for Case 2(c).

Table 6.2 – Results of tuning-point frequency

Mode	Eigen-frequency of infinitely long duct	Frequency at which the pressure different between both sides are close to zero (turning-point)	
		4.5mm square	*9mm square*
(0,1)	1864.1Hz	1952Hz	1956Hz
(0,2)	3728.3Hz	3762Hz	3765Hz
(2,0)	4182.9Hz	4205Hz	4208Hz

Table 6.2 shows the results of turning-point frequencies of this case study. It is noted that duct sound pressures above the turning-point frequency are not dominant and shall not be discussed further. The above findings shall be the criterion of setting the frequency ranges for predicting complex wave-numbers for the slot cases. The frequency

range is set between the duct eigen-frequency and the turning-point frequency of each mode, so-called "leaky duct mode". That is, 1865Hz to 1952Hz, 3729Hz to 3762Hz and 4183Hz to 4205Hz are the ranges to be focused for the (0,1), (0,2) and (2,0) mode respectively in the next Section 6.4.

6.4 The open slot cases

The acoustic model of interest is set to be the same as the one in Chapter 5 except different slot sizes are proposed for the study. Under the square air piston size restriction in the present model, h/λ or $\frac{kh}{2\pi}$ is set to be less than 1/6 and kh is controlled to be smaller than unity $(kh < 1)$. Thus, the slot height (h) is focused up to around $a/6$ (say $2 \times 9\text{mm} = 18\text{mm}$) and three values of the slot length (L) are fixed for the 3-D numerical models. The first element of each slot is commenced from the position at $x_1 = 0.162\text{m}$ ($x_1 = 9\text{mm} \times 18$) and at the top of the side wall. The element is represented by a square air piston in the mathematical model. The cases are tabulated as in Table 6.3. Figure 6.14 illustrates a typical model with a slot on the side wall of the duct.

Table 6.3 - Selected cases for 3-D numerical models

Slot sizes	L=0.045	L=0.09	L=0.18
h=4.5mm	Case 1	Case 2	Case 3
	(4.5mm×10 elements)	(4.5mm×20 elements)	(4.5mm×40 elements)
h=9mm	Case 4	Case 5	Case 6
	(9mm×5 elements)	(9mm×10 elements)	(9mm×20 elements)
h=18mm	-	Case 7	Case 8
		(18mm×5 elements)	(18mm×10 elements)

Remark:

L: slot length, h: slot height, 1 element = 1 square air piston

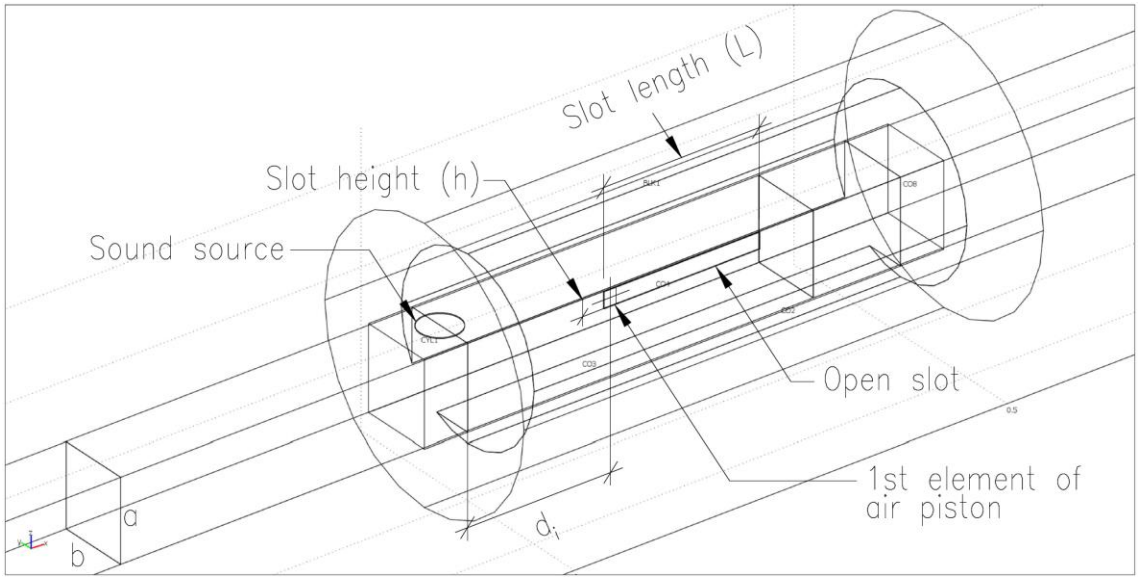

Figure 6.14 – An isometric view of the computational slot model.

The same modal decomposition technique as per Chapter 5 is used to analyse the numerical results of sound pressure over the concerned internal cross-sections. The same interval of cross-section along x direction and the frequency resolution are adopted. The

computed duct pressures from finite element models were collected. The numbers of duct cross-sectional planes included for each cases are shown in Table 6.4.

Table 6.4 - Selected cases for computations

Case	Number of cross-sectional plane for computation
1 (a, b, c)	91
2 (a, b, c)	111
3 (a, b, c)	151
4 (a, b, c)	45
5 (a, b, c)	55
6 (a, b, c)	75
7 (a)	27
8 (a)	37

Remark: a, b, c denote the (0,1), (0,2) and (2,0) mode respectively.

The selected frequency range of interest is narrowed down for the analysis of the slot cases. It is focused on the range between eigen-frequency of infinitely long duct and the turning-point frequency (leaky duct mode) stated in Table 6.2. The frequency interval is 10Hz and Table 6.5 sets out the particular ranges of each mode. Numerical results obtained shall form part of the functions to predict the complex wave-number. Eight cases of (0,1) mode with 5 frequencies, 6 cases of (0,2) mode with 3 frequencies and 6 cases of (2,0) mode with 2 frequencies (total 70 sets of result) are computed.

Table 6.5 – Frequency range of open slot models

	Mode	Frequency range	Number of data set	Number of case
(a)	(0,1)	1870-1910Hz	5	8
(b)	(0,2)	3740-3760Hz	3	6
(c)	(2,0)	4190-4200Hz	2	6

6.5 A method for prediction of the complex wave-number

In the slot model, the existence of amplitude adjustment (ε) and phase angle (ϕ) of wave-number is stated in Chapter 3. The question is how to find ε and ϕ effectively? Basically, they can be found if the theoretical predictions tend to be the numerical results. However, such functions involve numerous sets of simultaneous equations together with the finite element computational results. It is unlikely to solve them analytically. Numerical iterative method can offer approximate solutions to predict the complex wave-number.

6.5.1 Numerical iterative technique

The deviation between the theoretical prediction and finite element computational results should be equal to zero if an appropriate complex wave-number or adjustment to real wave-number ($D = \varepsilon e^{i\phi}$) is inserted to the mathematical model. One expects that the root of the function of this study can be found by:

$$f(D) = 0 \tag{6.3}$$

where D is the complex number with the dimensionless variables ε and ϕ.

Eq. (6.3) presents $f(D)$ the cost function explicitly for reaching the optimal deviation.

Recall the Eq. (5.7) showing the deviation:

$$\text{Deviation} = \sqrt{\frac{1}{s}\sum_{t=1}^{s}\left(\frac{|V_C|-|V_M|}{|V_C|}\right)_t^2}$$

where s is number of fitted points, V_C are the values obtained from COMSOL 3-D numerical model and V_M are the prediction values calculated by mathematical model (MATLAB).

The prediction values are evaluated by several associated functions in Chapter 3 and 4. An iterative technique is used to find the root of formulas numerically. A well-known technique is the Newton's method.

$$D_{i+1} = D_i - \frac{f(D_i)}{f'(D_i)} \tag{6.4}$$

where the subscript i represents the ith ilteration for root of f and f' its derivative.

In order to solve the dimensionless variables of a complex number in polar form, a specific method are derived in the current research on the basis of Newton's method. Observing that:

$$\Delta f = \frac{\partial f}{\partial \varepsilon}\cdot \Delta\varepsilon + \frac{\partial f}{\partial \phi}\cdot \Delta\phi \tag{6.5}$$

the numerical approximation of the derivative can be presented as:

$$f'(D_i) = \frac{\Delta f}{\Delta D} = \frac{\partial f}{\partial \varepsilon} \cdot \frac{\partial \varepsilon}{\partial D} + \frac{\partial f}{\partial \phi} \cdot \frac{\partial \phi}{\partial D} \tag{6.6}$$

where

$$\frac{\partial f}{\partial \varepsilon} = \frac{f(\varepsilon_i + \Delta\varepsilon) - f(\varepsilon_i)}{\Delta\varepsilon},$$

$$\frac{\partial \varepsilon}{\partial D} = e^{-i\emptyset},$$

$$\frac{\partial f}{\partial \phi} = \frac{f(\phi_i + \Delta\phi) - f(\phi_i)}{\Delta\phi}$$

and

$$\frac{\partial \phi}{\partial D} = -\frac{i}{D}$$

Thus, the derivative of Eq. (6.6) becomes:

$$f'(D_i) = \frac{f(\varepsilon_i + \Delta\varepsilon) - f(\varepsilon_i)}{\Delta\varepsilon} \cdot \left(e^{-i\emptyset}\right) - \frac{f(\phi_i + \Delta\phi) - f(\phi_i)}{\Delta\phi} \cdot \left(\frac{i}{D}\right) \tag{6.7}$$

6.5.2 Findings of different slot cases

An input initial guess point should be provided for the iteration. A matrix of dimensionless variables ε and ϕ are manipulated in the iteration. One can expect that ε should be close to zero in resonance and small for leaky duct mode. According to Eq. (3.23), the modified wave-number is as below:

$$k\sqrt{1 - D^2} = k\sqrt{1 - \varepsilon^2 e^{i2\emptyset}}$$

ε is set to be between 0 to 0.3 and the range of the phase angle ϕ is from 0 to π. The intervals of ε and ϕ are fixed to 0.01 and $\pi/32$ respectively. Value of minimum deviation is recognized in the matrix. Such preliminary approach is reliable and can obtain the pair of initial point relatively close to the root. It is interested to visualize the model behaviour as a function of ε and ϕ. The contour of the cost function from an example for Case 4 at 1890Hz is illustrated in Figure 6.15. It is not surprising that a single root is observed at the loci around the minimum.

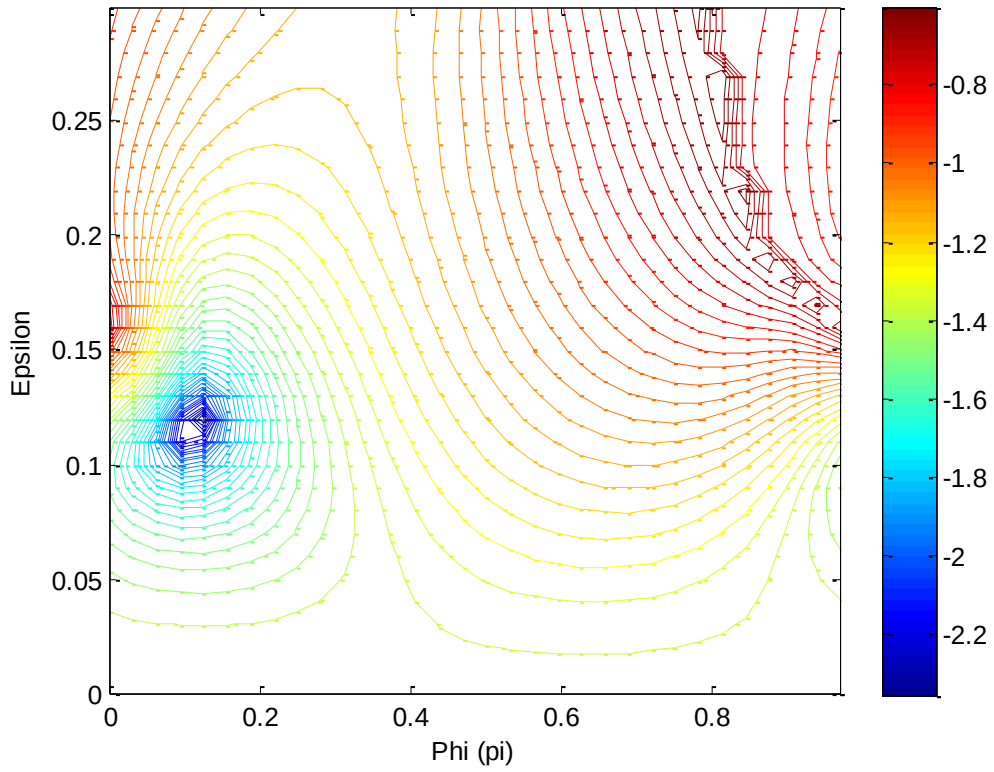

Figure 6.15 – An example of contour of deviation (anti-$\log_{10}$) for Case 4, 1890Hz2

Subsequently, the abovementioned Newton's method is implemented. The step difference $\Delta\varepsilon$ $(1 \cdot 10^{-5})$ and $\Delta\phi$ $(\pi \cdot 10^{-5})$ are adopted. The criterions to exit the iteration of different cases are tabulated in Table 6.6 to 6.13.

Table 6.6 – Solutions of ε and ϕ for Case 1

Case	Mode	Frequency (Hz)	ε	ϕ (π)	Deviation
1	(0,1)	1870	0.050002	0.160550	0.0013003
1	(0,1)	1880	0.100560	0.138282	0.0009051
1	(0,1)	1890	0.141529	0.120295	0.0003346
1	(0,1)	1900	0.177032	0.107166	0.0009799
1	(0,1)	1910	0.208774	0.095898	0.0017381
1	(0,2)	3740	0.057710	0.080758	0.0012045
1	(0,2)	3750	0.085556	0.066554	0.0018260
1	(0,2)	3760	0.107384	0.057928	0.0032322
1	(2,0)	4190	0.032639	0.086162	0.0021605
1	(2,0)	4200	0.064744	0.053926	0.0025035

Table 6.7 – Solutions of ε and ϕ for Case 2

Case	Mode	Frequency (Hz)	ε	ϕ (π)	Deviation
2	(0,1)	1870	0.039225	0.168205	0.0018452
2	(0,1)	1880	0.080604	0.154351	0.0011910
2	(0,1)	1890	0.114301	0.146718	0.0008752
2	(0,1)	1900	0.144856	0.142241	0.0013354
2	(0,1)	1910	0.173846	0.139548	0.0022326
2	(0,2)	3740	0.046057	0.087000	0.0010758
2	(0,2)	3750	0.069831	0.080669	0.0019276
2	(0,2)	3760	0.088866	0.076456	0.0042347
2	(2,0)	4190	0.025457	0.109491	0.0045374
2	(2,0)	4200	0.051157	0.094415	0.0031983

In Table 6.6, ε increases with the frequency while ϕ commonly decreases as the frequency increases. The deviations are small, representing that the predictions from the mathematical model are close to the numerical results. Comparing the results shown in Tables 6.7 and 6.8, the increase of slot length does not result in increase of ε. For instance, at the same frequency 1890Hz, ε are 0.141529, 0.114301 and 0.081075 for Case 1, 2 and 3 respectively. Similar interpretations apply to other cases (Tables 6.9 to 6.13).

Table 6.8 – Solutions of ε and ϕ for Case 3

Case	Mode	Frequency (Hz)	ε	ϕ (π)	Deviation
3	(0,1)	1870	0.027088	0.204715	0.0065735
3	(0,1)	1880	0.055870	0.179405	0.0078411
3	(0,1)	1890	0.081075	0.170517	0.0091827
3	(0,1)	1900	0.104960	0.165588	0.0106749
3	(0,1)	1910	0.128048	0.171996	0.0125268
3	(0,2)	3740	0.030671	0.097758	0.0127923
3	(0,2)	3750	0.051028	0.088494	0.0170756
3	(0,2)	3760	0.066909	0.104416	0.0237729
3	(2,0)	4190	0.017016	0.122394	0.0061705
3	(2,0)	4200	0.037308	0.105536	0.0031742

Table 6.9 – Solutions of ε and ϕ for Case 4

Case	Mode	Frequency (Hz)	ε	ϕ (π)	Deviation
4	(0,1)	1870	0.040342	0.127920	0.0022485
4	(0,1)	1880	0.083165	0.118270	0.0010723
4	(0,1)	1890	0.117220	0.111040	0.0005008
4	(0,1)	1900	0.147620	0.106460	0.0009234
4	(0,1)	1910	0.175930	0.103070	0.0017754
4	(0,2)	3740	0.055808	0.051302	0.0014834
4	(0,2)	3750	0.082710	0.042256	0.0018331
4	(0,2)	3760	0.103930	0.036018	0.0034546
4	(2,0)	4190	0.032136	0.013114	0.0025759
4	(2,0)	4200	0.063567	0.010490	0.0026903

Table 6.10 – Solutions of ε and ϕ for Case 5

Case	Mode	Frequency (Hz)	ε	ϕ (π)	Deviation
5	(0,1)	1870	0.033340	0.129150	0.0024639
5	(0,1)	1880	0.068047	0.123800	0.0018982
5	(0,1)	1890	0.096512	0.121140	0.0015222
5	(0,1)	1900	0.121840	0.121050	0.0016959
5	(0,1)	1910	0.145390	0.124030	0.0024518
5	(0,2)	3740	0.047052	0.060271	0.0018237
5	(0,2)	3750	0.071089	0.056242	0.0018941
5	(0,2)	3760	0.090233	0.054611	0.0041807
5	(2,0)	4190	0.026953	0.043987	0.0043021
5	(2,0)	4200	0.051983	0.036869	0.0036455

Table 6.11 – Solutions of ε and ϕ for Case 6

Case	Mode	Frequency (Hz)	ε	ϕ (π)	Deviation
6	(0,1)	1870	0.021257	0.159898	0.0079068
6	(0,1)	1880	0.046170	0.132081	0.0097814
6	(0,1)	1890	0.067557	0.128073	0.0116425
6	(0,1)	1900	0.088457	0.125304	0.0133291
6	(0,1)	1910	0.109920	0.128533	0.0154116
6	(0,2)	3740	0.030426	0.066938	0.0241434
6	(0,2)	3750	0.052128	0.058368	0.0312978
6	(0,2)	3760	0.069508	0.069091	0.0398578
6	(2,0)	4190	0.018704	0.007866	0.0135612
6	(2,0)	4200	0.040210	0.050348	0.0093968

Table 6.12 – Solutions of ε and ϕ for Case 7

Case	Mode	Frequency (Hz)	ε	ϕ (π)	Deviation
7	(0,1)	1870	0.033375	0.102955	0.0037974
7	(0,1)	1880	0.068595	0.102108	0.0028998
7	(0,1)	1890	0.096849	0.102363	0.0024230
7	(0,1)	1900	0.122108	0.103202	0.0024322
7	(0,1)	1910	0.145657	0.105276	0.0031345

Table 6.13 – Solutions of ε and ϕ for Case 8

Case	Mode	Frequency (Hz)	ε	ϕ (π)	Deviation
8	(0,1)	1870	0.022650	0.120926	0.0111846
8	(0,1)	1880	0.048020	0.109933	0.0137240
8	(0,1)	1890	0.070308	0.107173	0.0162007
8	(0,1)	1900	0.091807	0.106856	0.0182738
8	(0,1)	1910	0.112833	0.111948	0.0206468

6.5.3 Formulated complex wave-number

In Chapter 3, the theoretical models are derived to demonstrate the wave mechanism along the duct with an open slot. According to Eq. (3.6) and (3.12), the slot interface vibrates radially with an oscillating component of velocity distribution as:

$$U(x) = U_0 e^{-ik_{xo}x}$$

$$k_{xo} = k\varepsilon e^{i\phi}$$

This model suggests that the oscillating interface in wave form propagates downstream from the leading edge of open slot in the x direction.

$$U(x) = U_0 e^{-ik\varepsilon e^{i\phi}x} \tag{6.8}$$

The value of ε is of interest in this research. One can consider that ε is a dimensionless variable which is a function of duct propagation constant k_x, L (length of slot) and h (height of slot):

$$\varepsilon = f\left(\frac{k_x}{k}, \frac{L}{a}, \frac{h}{a}\right) \tag{6.9}$$

The ε and ϕ are computed by numerical iterative technique presented in Section 6.5.2. A population of 70-set data is collected in various cases from the previous section. Graphical presentation of ε is considered useful. A regression analysis can show a predicting function with respect to the parameter(s). By using the software TableCurve 3D, three data sets can be examined. In the current study, the dependent variable is ε. Then, what are the two independent variables appropriate for analysis?

In view of Eq. (6.9), there are three parameters considered in the function. Therefore, two parameters have to be combined in the graphical analysis. One can consider that the equivalent radius of the rectangular opening with notation R_e as stated by Howe (1996) can be one of the parameter.

$$R_e = \sqrt{\frac{S}{\pi}} \tag{6.10}$$

where slot area, $S = L \times h$. As observed from the trend of iteration results shown in Tables 6.8 to 6.13, it is noted that ε is unlikely to increase with the slot length or area. Therefore, the dimensionless parameter $k\sqrt{S}$ is set as the denominator of one of the independent variable. The function ε is then revised to the form given in Eq. (6.11) for the 3-D curve fitting exercise.

$$\varepsilon = f\left(\frac{k_x a}{k\sqrt{S}}, \frac{h}{a}\right) \tag{6.11}$$

Since all data sets are evaluated from various combinations of frequency ranges and slot dimensions, it is quite surprising that a single formula can be obtained with rather good coefficient of determination (R^2) and fit standard error. Results are shown as follows:

Table 6.14 – A summary of 3-D curve fitting exercise results

	Formula	R^2	Fit Standard Error
All cases	$\varepsilon = 0.5690(\frac{k_x a}{k\sqrt{S}})^{1.0723}(\frac{h}{a})^{0.4637}$	0.91262146	0.013210689

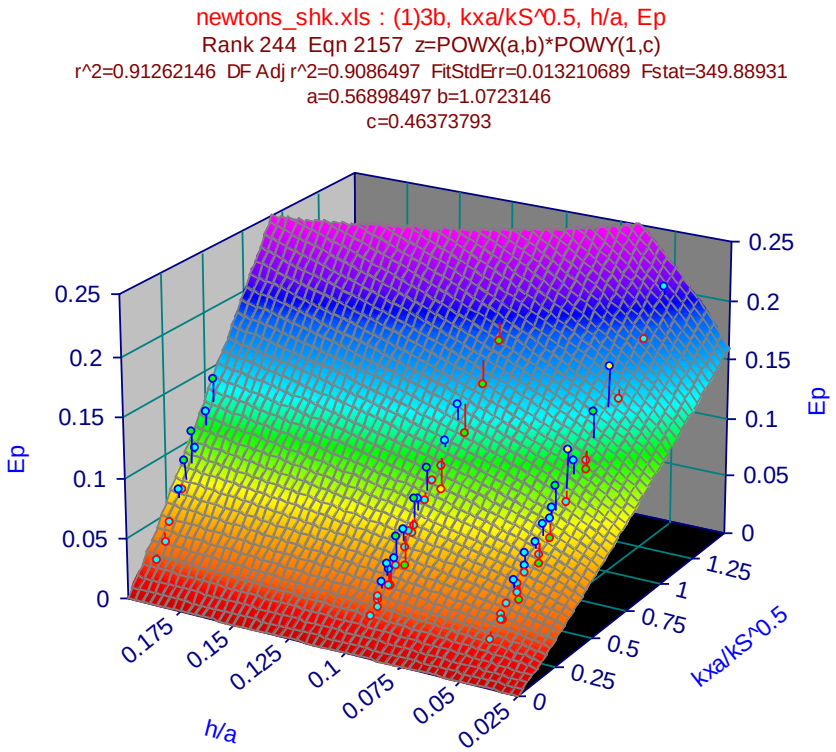

Figure 6.16 – Plot of 3-D curve fitting (z-axis, ε)

One can normalize L with respect to the duct internal height a.

$$\frac{a}{\sqrt{S}} = \left(\frac{a}{L}\right)^{0.5} \times \left(\frac{a}{h}\right)^{0.5} \tag{6.12}$$

and then the formula in Table 6.14 becomes:

$$\varepsilon = 0.5690\left(\frac{k_x}{k}\right)^{1.0723}\left(\frac{a}{L}\right)^{0.6086}\left(\frac{a}{h}\right)^{0.0363} \tag{6.13}$$

Eq. (6.13) shows that the magnitude of ε is nearly proportional to k_x/k and tends to zero when k_x/k is zero (resonance of infinitely long duct mode). Moreover, the magnitude of ε is probably reduced with increasing the open slot length connected to the free space.

Since $(\frac{a}{h})^{0.0363} \approx 1$ (approximate 1.06~1.12 for the all study cases), it justifies that the normalized slot height is no longer significant in the model of ε at all. Thus,

$$\varepsilon \approx 0.6(\frac{k_x}{k})(\frac{a}{L})^{0.6} \tag{6.14}$$

$\phi \approx 0.095\pi$ which is the mean value obtained from iteration and shows an approximate phase angle of the complex number.

6.6 Creditability of the formulated complex wave-number

In connection with the above sections and Eq. (6.14), an appropriate modification to real wave-number ($D = \varepsilon e^{i\emptyset}$) is predicted with embedded constants and known parameters in this research. The following formula is substituted into the mathematical model of Eqs. (3.24), (4.24), (4.25), (4.33) and (4.34) for slot cases:

$$D = 0.6(\frac{k_x}{k})(\frac{a}{L})^{0.6} e^{i0.095\pi} \tag{6.15}$$

Figures 6.17 to 6.20 illustrate the comparisons of all the test cases with different slot sizes. The plots show comparisons between mathematical model predictions with D estimated using Eq. (6.15) against numerical model predictions. Good agreements are noted.

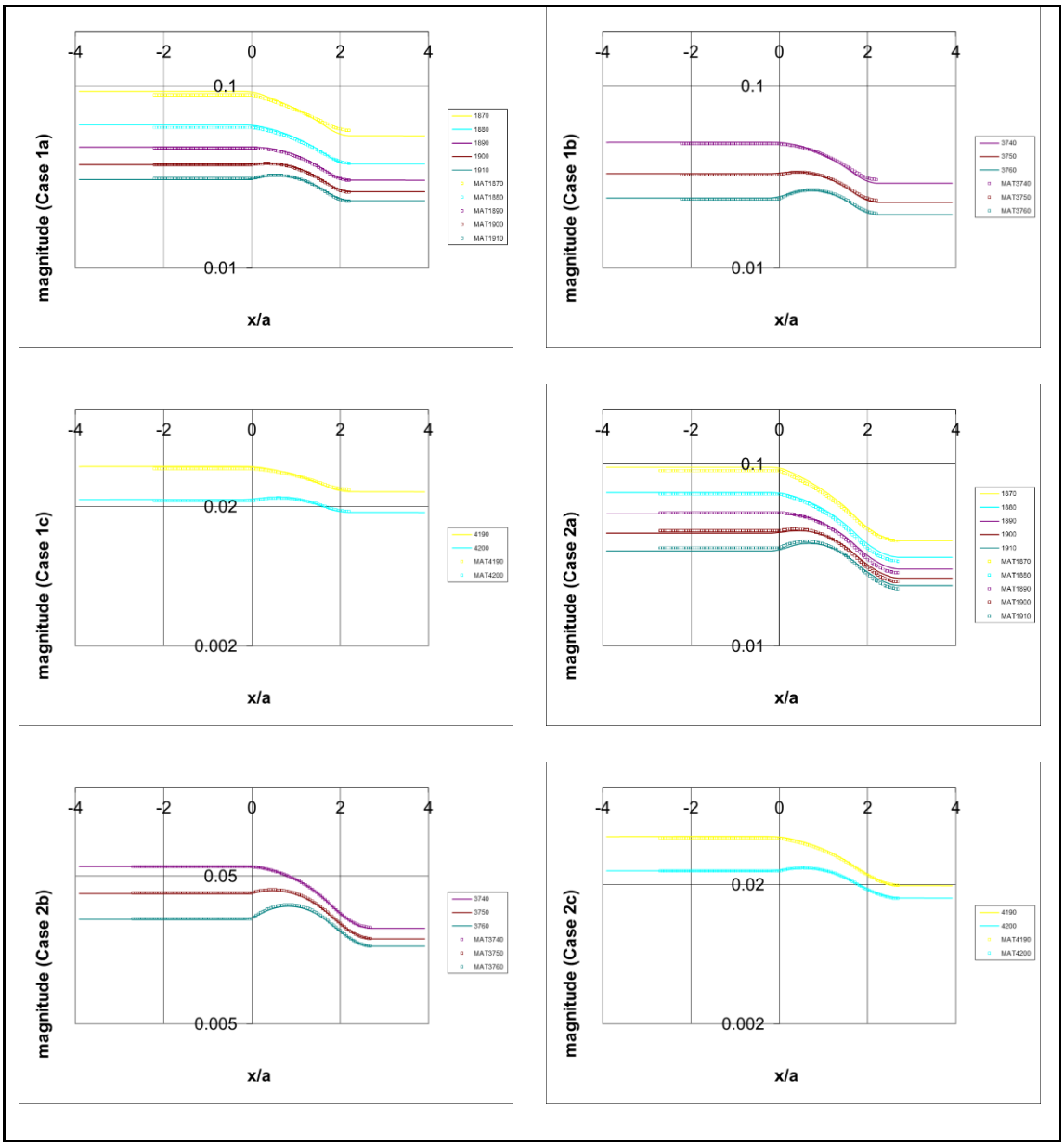

Figure 6.17 – Comparisons of mathematical model with formulated complex wave-number (Eq. 6.15) against finite element simulation by slot model (Case 1 and 2)

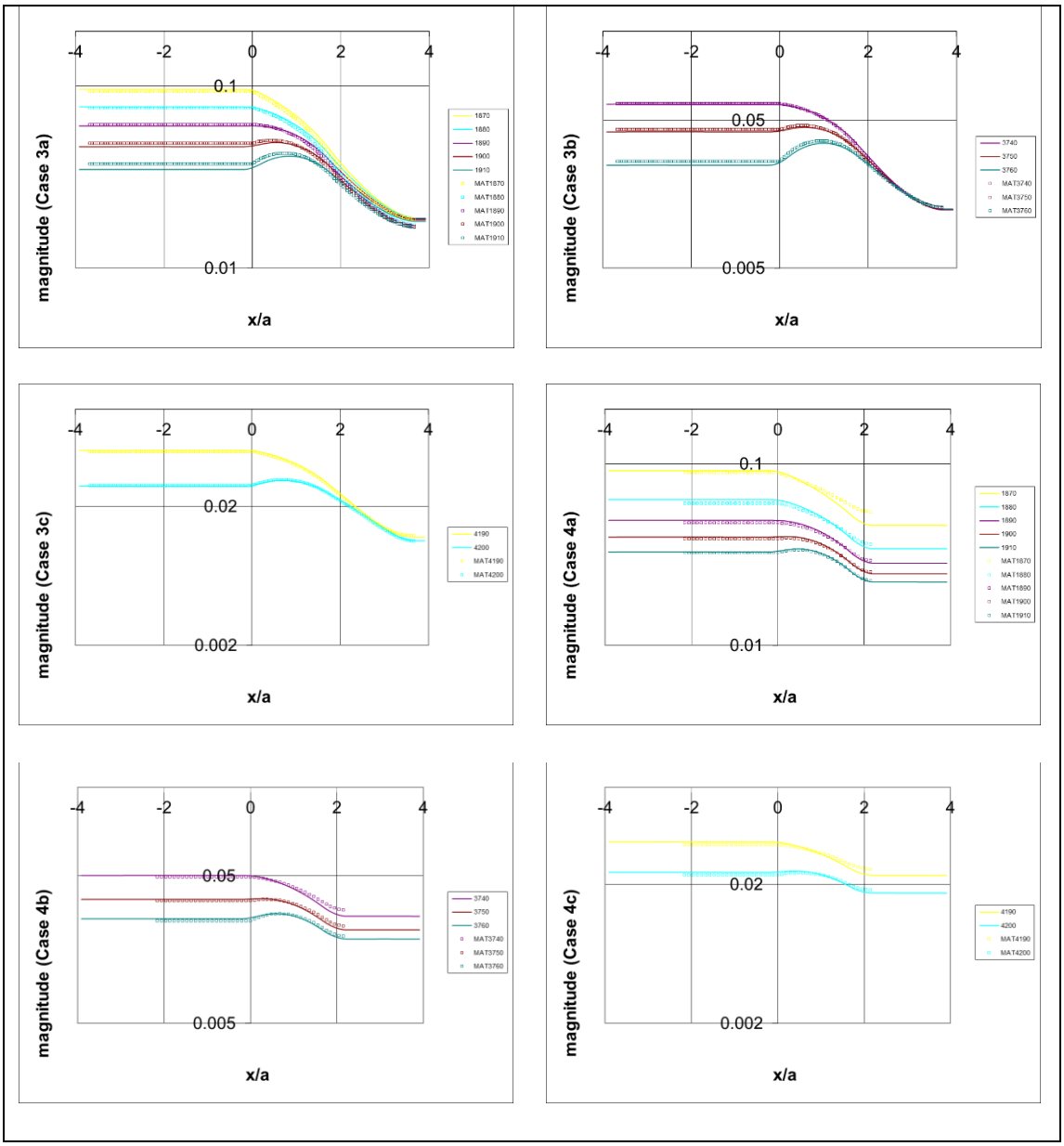

Figure 6.18 – Comparisons of mathematical model with formulated complex wave-number (Eq. 6.15) against finite element simulation by slot model (Case 3 and 4)

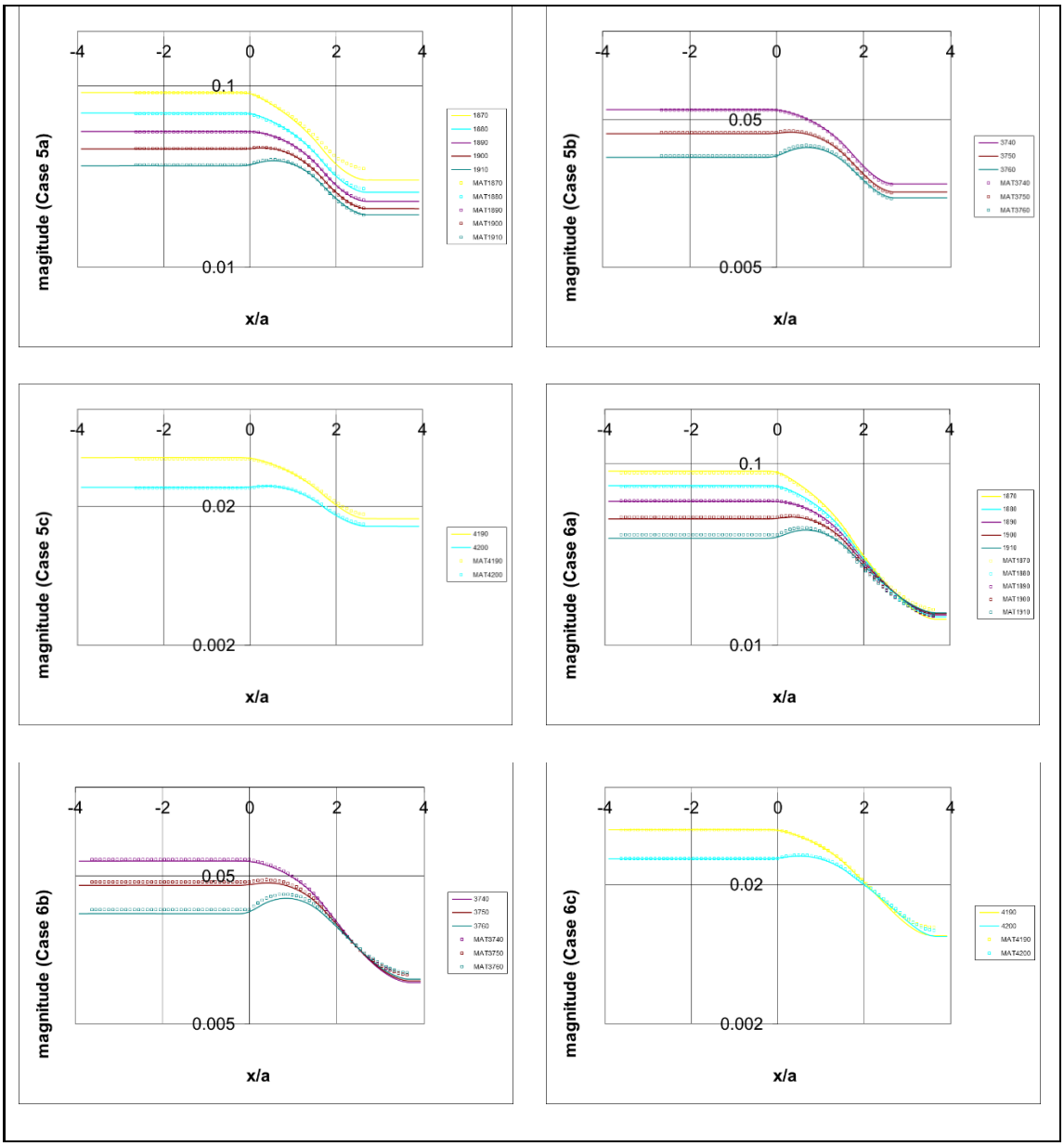

Figure 6.19 – Comparisons of mathematical model with formulated complex wave-number (Eq. 6.15) against finite element simulation by slot model (Case 5 and 6)

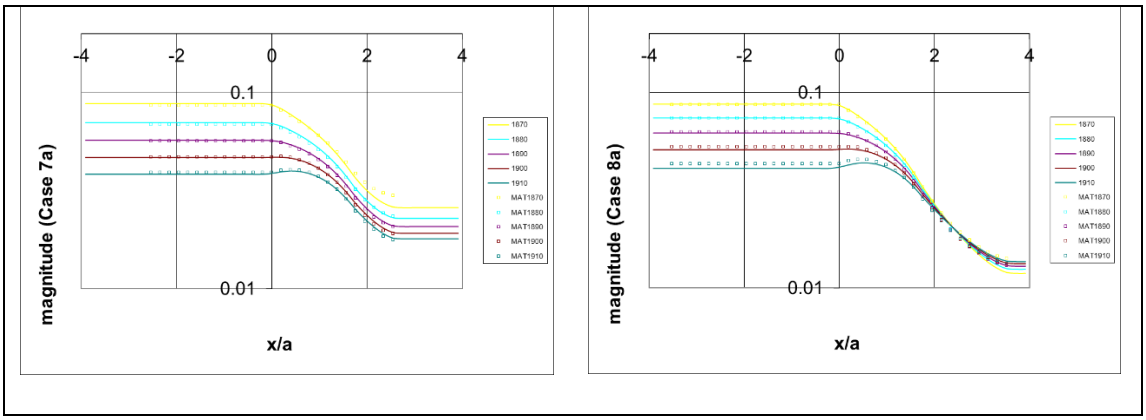

Figure 6.20 – Comparisons of mathematical model with formulated complex wave-number (Eq. 6.15) against finite element simulation by slot model (Case 7a and 8a)

For the sake of completeness of this study, in addition to the percentage deviation, standard error of estimate (SEE) is adopted as a statistical evaluation of the final results.

$$\text{Standard error of estimate (SEE)} = \sqrt{\frac{1}{s}\sum_{t=1}^{s}(|V_C| - |V_M|)_t^2} \qquad (6.16)$$

where s is number of fitted points,

V_C are the values obtained from COMSOL 3-D numerical model and

V_M are the prediction values calculated by mathematical model (MATLAB).

Table 6.15 – Percentage deviation of results and standard error of estimate from mathematical model with formulated complex wave-number (Eq. 6.15) against finite element simulation by slot models

Case		Percentage deviation	SEE
1 (h= 0.0045, L= 0.045)	a	2.12%	0.001437
	b	2.01%	0.000686
	c	2.71%	0.000891
2 (h= 0.0045, L= 0.09)	a	3.16%	0.001881
	b	1.00%	0.000329
	c	1.80%	0.000763
3 (h= 0.0045, L= 0.18)	a	4.93%	0.001925
	b	2.95%	0.000919
	c	1.32%	0.000562
4 (h= 0.009, L= 0.045)	a	4.29%	0.002207
	b	3.58%	0.001113
	c	4.72%	0.001343
5 (h= 0.009, L= 0.09)	a	2.24%	0.001232
	b	2.59%	0.000736
	c	2.68%	0.000718
6 (h= 0.009, L= 0.18)	a	2.94%	0.001017
	b	5.05%	0.001504
	c	3.73%	0.000480
7 (h= 0.018, L= 0.09)	a	2.80%	0.001028
8 (h= 0.018, L= 0.18)	a	3.50%	0.001100

Remark: a, b, c denote (0,1), (0,2) and (2,0) mode respectively.

Table 6.15 shows the evidence that the mathematical model with complex wave-number given by Eq. (6.15) has good accuracy at leaky duct modes. Is this complex wave-number universal for the prediction?

The aim of the following study is to further examine whether such empirical model is applicable to other physical dimensions. The original duct cross-section is rectangular with height-to-width ratio around 1.12:1. A different geometry of numerical model is prepared for estimating the internal sound field of the duct hereinafter. The geometrical changes are highlighted as follows:

- Uniform rectangular duct section is horizontally oriented in aspect ratio around 2.39:1 (0.134m in width and 0.056m in height). The cross-sectional area is approximately $7.5 \times 10^{-3}\text{m}^2$ as in previous cases.
- Open slot length is 0.12m (L/a = 2.143).
- Open slot height is 6mm (h/a = 0.107).
- The first element at leading edge of the slot is in positive x direction at 0.216m (x_1/a = 3.857).

The sound source is kept at the centre of top wall of the duct. The other physical dimensions remain unchanged. Figure 6.21 illustrates the new model of the abovementioned case.

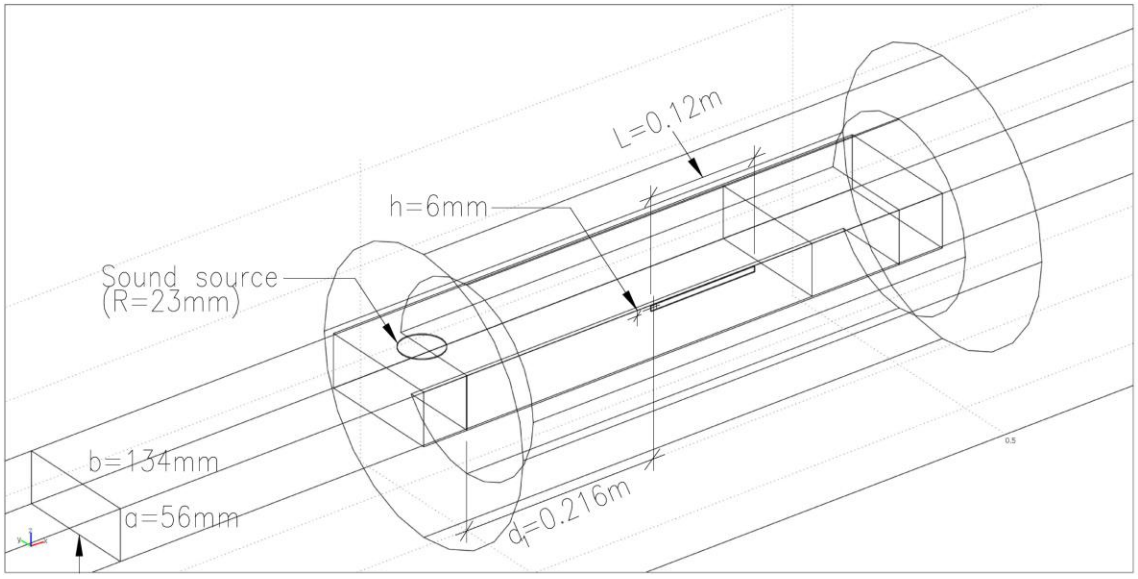

Figure 6.21 – An isometric view of the computational model for horizontal rectangular duct

The frequency range of interest should be above and near to eigen-frequency of infinitely long duct. The same frequency interval (10Hz) is adopted and Table 6.16 sets out the frequency ranges of the analysis. There are three sets of frequency computed for individual (2,0), (0,1) and (2,1) mode, where (2,1) mode is not catered in the previous slot models.

Table 6.16 – Frequency range of horizontal rectangular duct model

Mode	Frequency range	Nos. of data set
(2,0)	2570-2590Hz	3
(0,1)	3070-3090Hz	3
(2,1)	4000-4020Hz	3

Due to the sound source location at the centre of relatively long span of new duct width and the odd spanwise modes are not excited, the first excitation in numerical model is at (2,0) mode. Such mode pattern is captured and presented in Figure 6.22 for reference (at 2570Hz where x = 0.216m). This pattern is similar to that of the infinitely long duct mode, but a nodal line nearer to the opening is distorted.

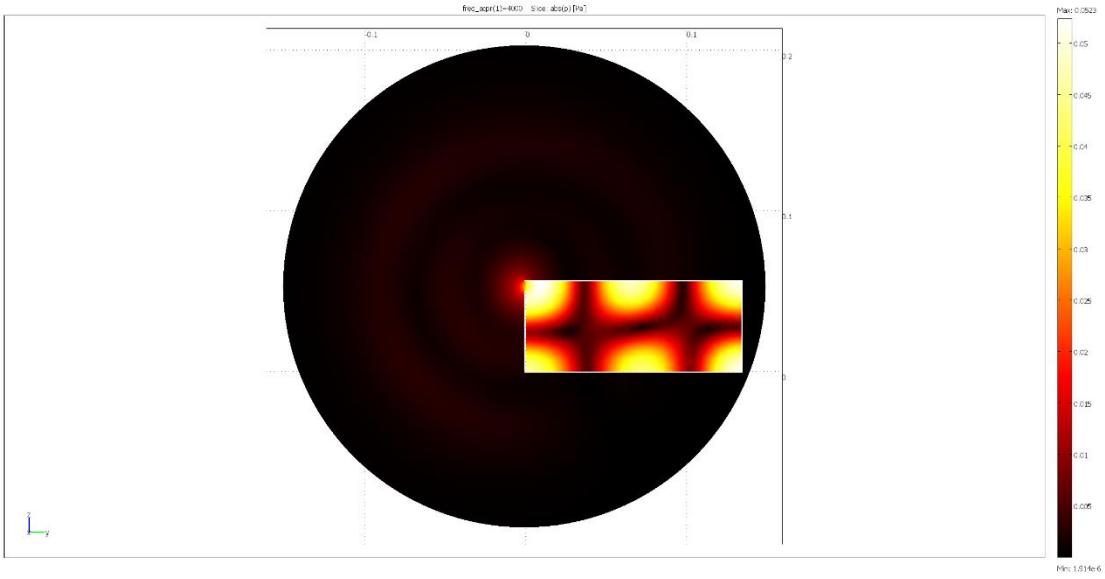

Figure 6.22 – Sound field pattern excited at (2,1) mode for horizontal rectangular duct model

Figure 6.23 shows comparisons between results from mathematical model with the complex wave-number estimated using Eq. (6.15) and the numerical results for the 3 modes of the new duct model. Again, the plots including that of the higher order mode (2,1) illustrate good agreements of results.

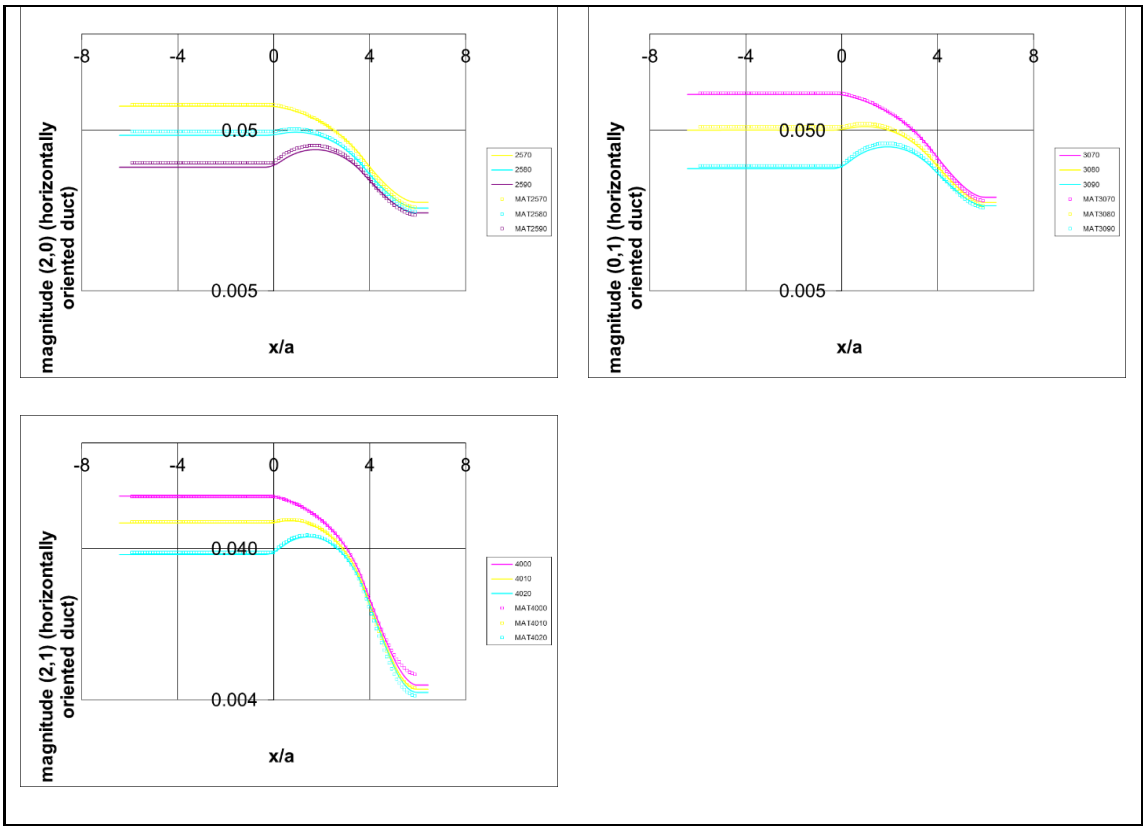

Figure 6.23 – Comparisons of mathematical model with formulated complex wave-number (Eq. 6.15) against the finite element simulation, (2,0), (0,1) and (2,1) mode for horizontally oriented duct model

Table 6.17 – Percentage deviation of results and standard error of estimate from COMSOL against MATLAB (horizontal rectangular duct section)

Mode	Percentage deviation	SEE
(2,0)	4.55%	0.001674
(0,1)	3.27%	0.001369
(2,1)	3.47%	0.000685

The outcomes of percentage deviation and standard error shown in Table 6.17 are expected. Despite changes of the slot length, slot height, distance from the slot to sound

source and aspect ratio of duct section, the predictions of sound field from the mathematical model are tallied with that of the finite element model. It is believed that the present mathematical model with complex wave-number is reliable for similar geometry of partial enclosures.

6.7 Concluding remarks

This chapter demonstrates an application of 3-D finite element method for sound propagation along an infinitely long duct with small/ narrow wall opening. The acoustical behaviour of a uniform duct with an infinitely long gap connected to an external free field is studied. Modal frequencies are found by using the 3-D numerical modelling. These modal frequencies are identified to be near to and above the duct eigen-frequencies. Moreover, the sound field inside the duct with single aperture in frequency domain is calculated by the mathematical model. Results show that the mode magnitude along the duct downstream of the aperture is not always lower than that in the side without an opening. This situation occurs at a transitional frequency, called turning-point frequency in this study, at which the pressure difference between both sides is zero. Such phenomenon can be explained by the differences in the modal frequencies on the two sides of the duct.

A method to predict the complex wave-number introduced in Chapter 3 for different slot size is derived. Finite element modelling is employed to assist the prediction. The complex wave-numbers are determined simultaneously by the numerical iterative method. Results are collected for regression analysis by 3-D curve fitting exercise.

Findings indicate that the complex wave-number correlates closely with the propagation constant k_x and the slot length. The effect of slot height is found insigificant to the magnitude. The predictions from the mathematical model are concluded to be reliable.

Chapter 7

Conclusions

7.1 Summary of achievements

A broad literature survey in this thesis specifies that researches of interaction between sound and long partial enclosures have deficiency in consideration of leaky duct sound behaviour. Results of this research fills the missing portions to predict the sound fields inside the leaky ducts.

The former part of this thesis formulates the mathematical models for the sound field generated by a flush-mounted circular piston (sound source) in an infinitely long and rigid rectangular duct with aperture(s). The configurations of apertures include a single rectangular opening, multiple square openings and an open slot. The derived theoretical model for sound field inside the infinitely long duct (without an aperture) shows that the spanwise odd modes are not excited. Larger the source radius and/or spanwise mode index can moderate the mode amplitude excited near to and above the eigen-frequencies. The side opening(s) are modelled as vibrating air pistons. Simultaneous equations for estimating the air piston velocities are derived. By solving these equations, the sound fields in the duct with side opening(s) can be obtained. The radiation impedance of a

square air piston in terms of piston size, wave-number and aperture thickness is also derived.

The leaky sound behaviour due to an open slot on the duct wall is investigated. The air in the slot is modelled as a linear array of air pistons, which oscillate under the action of the sound excitation. A theory is developed to model the asymmetric sound radiation from the slot. This theory leads to the introduction of a complex wave-number which is used to model the sound propagation inside the leaky duct. This complex number comprises of an amplitude adjustment (ε) and a phase angle (ϕ).

This study also derives a method to predict the complex wave-number for different slot sizes. The finite element modelling is adopted to assist the prediction. The in-duct modal decomposition technique is adopted to analyse the computed sound pressures. Contributions of discrete propagating modes are examined. The numerical models are validated. Numerical results show excellent agreement with the acoustical theory of the infinitely long duct model. The grid sensitivity test by a long duct with two-apertures is executed as well. Moreover, the mathematical predictions derived for the single/ two aperture(s) cases in the first part of the thesis show good agreement with numerical results.

Both magnitude and phase angle of the complex wave-number are determined simultaneously by a numerical iterative method. The computed complex numbers for different slot cases are collected for regression analysis. Interesting findings show that ε is nearly proportional to k_x/k (the normalized propagation constant) and tends to be zero at the resonance of duct eigen-modes. ε is also proportional to a certain power of L/a (the normalized slot length) but not closely related to the slot height.

The creditability of the predicted complex wave-number is verified by setting up another numerical model with different duct settings. The geometrically differences consist of the changes of slot size, the distance from the slot to sound source and the aspect ratio of duct section. The predictions from the mathematical model indicate good agreement with numerical results. The complex wave-number is able to explain the physical propagation phenomenon of a leaky duct. The results of the present investigation generalize current understanding on the fundamentals of sound propagation in tube-like cavity. This research offers significant contributions and construction framework for the investigation of related subjects of sound propagation along partial/ discontinuous enclosures.

7.2 Suggestions for further work

The sound behaviours of leaky ducts have been studied in the thesis. One can expect that the review of embedded constants in the predicted complex wave-number is interesting. The exact theoretical model and experimental studies are considered valuable.

Succi *et al.* (1978) was interested in the research of interactions between turbulent-jet noise source and a rectangular duct experimentally. The jet area was much smaller than that of the duct cross-section. They demonstrated that the simple source model can predict the resonance frequencies and the acoustic modes. The scale model experiment of the sound radiation from railway tunnel opening was studied (Heutschi & Bayer 2006). Acoustic propagating modes and non-rigid boundaries were concerned.

It is suggested that experimental models can be derived in the future. The measured sound data can be evaluated by modal analysis. The experimental test rig can be in the form of a physical scaled down model simulating a long duct and the one with a slot or gap with different sizes. Studies in the laboratory can offer a further evaluation on the predictions by the mathematical model derived in this research.

Measurement outside the model can be carried out so as to understand the overall directivity of sound radiation in free field condition for the partial enclosures. It is expected that the acoustic array beamforming technique is useful for such purpose (Flynn & Kinns 1976). For reverberant exterior, sound power can be measured. The stationary source can be a small loudspeaker or electric spark. The latter is especially helpful in understanding the impulse response of the enclosure cavity (Picaut & Simon 2001). Moving source can be a small point source mounted on a trolley inside the model duct. The investigation could recognize the fundamental know-how on the effects of source movements on the sound propagation in a cavity and its control.

Furthermore, squeal noise can be heard near to locations where train turns. However, the exact location of generation is usually not precisely known. The characteristics (spectral and magnitude) of the sequel noise are not repeatable even for the same set of train and track (Thompson & Jones 2000 and Ruiten 1988). This makes passive control not cost effective at all. The present results would allow the development of an active control strategy (Martin & Bodrero 1997, Lacour *et al.* 2000) for the noise which propagates in the long partial enclosure. An application is to control the propagation of the wheel/rail and train sequel noise problem.

References

Aarts, Ronald M. and Augustus J. E. M. Janssen. 2003. "Approximation of the Struve Function H[sub 1] Occurring in Impedance Calculations." *The Journal of the Acoustical Society of America* 113(5):2635–37.

Åbom, Mats. 1989. "Modal Decomposition in Ducts Based on Transfer Function Measurements between Microphone Pairs." *Journal of Sound and Vibration* 135(1):95–114.

Alfredson, R. J. 1972. "The Propagation of Sound in a Circular Duct of Continuously Varying Cross-Sectional Area." *Journal of Sound and Vibration* 23(4):433–42.

Allam, Sabry and Mats Åbom. 2006. "Investigation of Damping and Radiation Using Full Plane Wave Decomposition in Ducts." *Journal of Sound and Vibration* 292:519–34.

Amir, N., V. Pagneux, and J. Kergomard. 1997. "A Study of Wave Propagation in Varying Cross-Section Waveguides by Modal Decomposition. Part II. Results." *The Journal of the Acoustical Society of America* 101(5):2504–17.

Arase, E. M. 1964. "Mutual Radiation Impedance of Square and Rectangular Pistons in a Rigid Infinite Baffle." *The Journal of the Acoustical Society of America* 36(8):1521–25.

Bank, G. and J. R. Wright. 1990. "Radiation Impedance Calculations for a Rectangular Piston." *Journal of the Audio Engineering Society* 38(5):350–53.

Benade, A. H. 1960. "On the Mathematical Theory of Woodwind Finger Holes." *The*

Journal of the Acoustical Society of America 32(12):1591–1608.

Berenger, J. P. 1996. "Three-Dimensional Perfectly Matched Layer for the Absorption of Electromagnetic wave." *Journal of Computational Physics* 127: 363-379.

Bladel, J. Van. 1967. "Low Frequency Scattering through an Aperture in a Rigid Screen." *Journal of Sound and Vibration* 6(3):386–95.

Bokor, A. 1969. "Attenuation of Sound in Lined Ducts." *Journal of Sound and Vibration* 10(3):390–403.

Börgers, Christoph, Claude Greengard, and Enrique Thomann. 1992. "The Diffusion Limit of Free Molecular Flow in Thin Plane Channels." *SIAM Journal on Applied Mathematics* 52(4):1057–75.

Burnett, D. S. and W. W. Soroka. 1972. "Tables of Rectangular Piston Radiation Impedance Functions, with Application to Sound Transmission Loss through Deep Apertures." *The Journal of the Acoustical Society of America* 51(5):1618–23.

Cabelli, A. and I. C. Shepherd. 1984. "Duct acoustics—A Numerical Technique for the Higher Order Mode Solution of Three-Dimensional Problems with Rigid Walls and No Flow." *Journal of Sound and Vibration* 92(3):149–426.

Chapman, C. J. 1994. "Sound Radiation from a Cylindrical Duct. Part 1. Ray Structure of the Duct Modes and of the External Field." *Journal of Fluid Mechanics* 281:293–311.

Chen, Kuo Tsai. 1995. "Study of Acoustic Transmission through Apertures in a Wall." *Applied Acoustics* 46:131–51.

Chen, X. X., X. Zhang, C. L. Morfey, and P. A. Nelson. 2004. "A Numerical Method for Computation of Sound Radiation from an Unflanged Duct." *Journal of Sound and Vibration* 270(3):573–86.

Cheong, C. and S. Lee. 2001. "The Effects of Discontinuous Boundary Conditions on the Directivity of Sound From a Piston." *Journal of Sound and Vibration* 239(3):423–43.

COMSOL. 2012. *COMSOL Multiphysics Users Guide. Ver. 4.3*. COMSOL AB.

COMSOL 2012a. "Optical Scattering off of a Gold Nanosphere." *Wave Optics Module. Ver. 4.2a*. COMSOL AB.

Copley, L. G. 1968. "Fundamental Results Concerning Integral Representations in Acoustic Radiation." *The journal of the acoustical society of America* 44(1):1–5.

Cummings, A. 1974. "Sound Transmission in Curved Duct Bends." *Journal of sound and vibration* 35:451–77.

Cummings, A. 1978. "Low Frequency Acoustic Transmission through the Walls of Rectangular Ducts." *Journal of Sound and Vibration* 61(3):327–45.

Cummings, A., H. J. Rice, and R. Wilson. 1999. "Radiation Damping in Plates, Induced by Porous Media." *Journal of sound and vibration* 221(1):143–67.

Dalmont, J. P. and C. J. Nederveen. 2002. "Experimental Determination of the Equivalent Circuit of an Open Side Hole: Linear and Non Linear Behaviour." *Acta Acustica united with Acustica* 88:567–75.

Davy, John L. 2009. "The Directivity of the Sound Radiation from Panels and Openings."

The Journal of the Acoustical Society of America 125(6):3795–3805.

Declercq, Nico F., Joris Degrieck, and Oswald Leroy. 2005. "Diffraction of Complex Harmonic Plane Waves and the Stimulation of Transient Leaky Rayleigh Waves." *Journal of Applied Physics* 98(11):1–10.

Doak, P. E. 1973a. "Excitation, Transmission and Radiation of Sound from Source Distributions in Hard-Walled Ducts of Finite Length (I): The Effects of Duct Cross-Section Geometry and Source Distribution." *Journal of Sound and Vibration* 31(1):1–72.

Doak, P. E. 1973b. "Excitation, Transmission and Radiation of Sound from Source Distributions in Hard-Walled Ducts of Finite Length (II): The Effects of Duct Length." *Journal of Sound and Vibration* 31(2):137–74.

Dubos, V. and J. Kergomard. 1999. "Theory of Sound Propagation in a Duct with a Branched Tube Using Modal Decomposition." *Acta Acustica united with Acustica* 85:153–69.

Environmental Protection Department. 2002. *Technical Memorandum for the Assessment of Noise from Places Other than Domestic Premises, Public Places or Construction Sites*. HKSAR Government.

Feit, D. 1970. "Sound Radiation from Orthotropic Plates." *The Journal of the Acoustical Society of America* 47(1):388–89.

Filippi, P. J. T. 1977. "Layer Potentials and Acoustic Diffraction." *Journal of Sound and Vibration* 54(4):473–500.

Floody, S. E., R. Venegas, and F. C. Leighton. 2010. "Optimal Design of Slit Resonators for Acoustic Normal Mode Control in Rectangular Room." *Proceedings of the Comsol Users Conference 2010 Paris*.

Flynn, O. E. and R. Kinns. 1976. "Multiplicative Signal Processing for Sound Source Location on Jet Engines." *Journal of Sound and Vibration* 46(1):137–50.

Fontaine, R. F. La and I. C. Shepherd. 1985. "The Influence of Waveguide Reflections and System Configuration on the Performance of an Active Noise Attenuator." *Journal of Sound and Vibration* 100(4):569–79.

Furue, Y. 1990. "Sound Propagation from the inside to the outside of a Room through an Aperture." *Applied Acoustics* 31:133–46.

Gomperts, M. C. 1965. "Comments on 'Approximation to the Diffraction of Sound by a Circular Aperture in a Rigid Wall of Finite Thickness'[GP Wilson and WW Soroka, J. Acoust." *The Journal of the Acoustical Society of America* 38:877.

Grace, S. M., K. P. Horan, and M. S. Howe. 1998. "The Influence of Shape on the Rayleigh Conductivity of a Wall Aperture in the Presence of Grazing Flow." *Journal of Fluids and Structures* 12(3):335–51.

Gradshteyn, I. S. and I. M. Ryzhik. 2007. *Table of Integrals, Series, and Products*. 7th ed. USA Academic Press.

Hastings, F. D., J. B. Schneider, and S. L. Broschat. 1996. "Application of the Perfectly Matched Layer (PML) Absorbing Boundary Conditions to Elastic Wave Propagation." *The Jounrnal of the Acoustical Society of America* 100(5): 3061-3069.

Heutschi, Kurt and R. Bayer. 2006. "Sound Radiation from Railway Tunnel Openings." *Acta acustica united with acustica* 92:567–73.

Hocter, S. T. 1999. "Exact and Approximate Directivity Patterns of the Sound Radiated from a Cylindrical Duct." *Journal of sound and vibration* 227(2):397–407.

Hocter, S. T. 2000. "Sound Radiated From a Cylindrical Duct With Keller'S Geometrical Theory." *Journal of Sound and Vibration* 231(5):1243–56.

Homicz, G. F. and J. A. Lordi. 1975. "A Note on the Radiative Directivity Patterns of Duct Acoustic Modes." *Journal of Sound and Vibration* 41(3):283–90.

Hongo, Kohei and Hirohide Serizawa. 1999. "Diffraction of an Acoustic Plane Wave by a Rectangular Hole in an Infinitely Large Rigid Screen." *The Journal of the Acoustical Society of America* 106(1):29–35.

Horoshenkov, V. K., C. D. Hothersall, and E. S. Mercy. 1999. "Scale Modelling of Sound Propagation in a City Street Canyon." *Journal of sound and vibration* 223(5):795–819.

Howe, M. S. 1980. "On the Diffraction of Sound by a Screen with Circular Apertures in the Presence of Low Mach Number Grazing Flow." *Proceedings of the Royal Society of London* 370:523–44.

Howe, M. S. 1981. "On the Theory of Unsteady Shearing Flow over a Slot." *Proceedings of the Royal Society of London* 303:151–80.

Howe, M. S. 1997. "Low Strouhal Number Instabilities of Flow over Apertures and Wall Cavities." *The Journal of the Acoustical Society of America* 102(2):772.

Hsu, T. S. and K. A. Poornima. 2001. "Loudspeaker Failure Modes and Error Correction Techniques." *Applied Acoustics* 62:717–34.

Huang, Chaang, Ralph D. Kodis, and Harold Levine. 1955. "Diffraction by Apertures." *Journal of Applied Physics* 26(2):151–65.

Huang, Lixi. 1999. "A Theoretical Study of Duct Noise Control by Flexible Panels." *The Journal of the Acoustical Society of America* 106(4):1801.

Huang, Lixi. 2000. "A Theory of Reactive Control of Low-Frequency Duct Noise." *Journal of Sound and Vibration* 238(4):575–94.

Huang, Lixi. 2006. "Broadband Sound Reflection by Plates Covering Side-Branch Cavities in a Duct." *The Journal of the Acoustical Society of America* 119(5):2628–38.

Huang, Lixi, Y. S. Choy, R. M. C. So, and T. L. Chong. 2000. "Experimental Study of Sound Propagation in a Flexible Duct." *The Journal of the Acoustical Society of America* 108(2):624.

Ismail, M. R. and D. J. Oldham. 2005. "A Scale Model Investigation of Sound Reflection from Building Facades." *Applied Acoustics* 66(2):123–47.

Iu, K. K. and K. M. Li. 2002. "The Propagation of Sound in Narrow Street Canyons." *The Journal of the Acoustical Society of America* 112(2):537–50.

Jayachandran, V., S. M. Hirsch, and J. Q. Sun. 1998. "On the Numerical Modelling of Interior Sound Fields by the Modal Function Expansion Approach." *Journal of sound and vibration* 210(2):243–54.

Johnston, G. W. and K. Ogimoto. 1980. "Sound Radiation from a Finite Length Unflanged Circular Duct with Uniform Axial Flow. I. Theoretical Analysis." *The Journal of the Acoustical Society of America* 68(6):1858–70.

Johnson, S. G. 2007. "Notes on Perfectly Matched Layers (PMLs)." *Online MIT Course Notes*.

Joseph, Phillip and C. L. Morfey. 1999. "Multimode Radiation from an Unflanged, Semi-Infinite Circular Duct." *The Journal of the Acoustical Society of America* 105(5):2590–2600.

Kang, Jian. 1996a. "Reverberation in Rectangular Long Enclosures with Geometrically Reflecting Boundaries." *Acta Acustica united with Acustica* 82:509–16.

Kang, Jian. 1996b. "Sound Attenuation in Long Enclosures." *Building and environment* 31(3):245–53.

Kang, Jian. 2000. "Sound Propagation in Street Canyons: Comparison between Diffusely and Geometrically Reflecting Boundaries." *The Journal of the Acoustical Society of America* 107(3):1394–1404.

Kang, Jian. 2002a. "Numerical Modelling of the Sound Fields in Urban Streets With Diffusely Reflecting Boundaries." *Journal of Sound and Vibration* 258(5):793–813.

Kang, Jian. 2002b. "Reverberation in Rectangular Long Enclosures with Diffusely Reflecting Boundaries." *Acta Acustica United with Acustica* 88:77–87.

Kang, Jian. 2005. "Urban Acoustics." *Applied Acoustics* 66(2):121–22.

Kang, Jian. 2007. *Urban Sound Environment*. Taylor & Francis, New York.

Kang, S. W. and Y. H. Kim. 1997. "Active Intensity Control for the Reduction of Radiated Duct Noise." *Journal of sound and vibration* 201(5):595–611.

Katz, D. S., E. T. Thiele, and A. Taflove. 1994. "Validation and Extension to Three Dimensions of the Berenger PML Absorbing Boundary Condition for FD-TD Meshes." *IEEE Microwave and Guided Wave Letters* 4(8): 268-270.

Keefe, Douglas H. 1982. "Theory of the Single Woodwind Tone Hole." *The Journal of the Acoustical Society of America* 72(3):676–87.

Kerwin, E. M. 1961. "Acoustic Damping Mechanisms." *Wright Air Development Center under Contracts AF 33(616)-5426 and AF 33(616)-6340*.

Kim, Y. H. 2010. *Sound Propagation: An Impedance Based Approach*. Singapore, John Wiley & Sons (Asia) Pte Ltd.

Kim, Y. H. and S. M. Kim. 2002. "Solution of Coupled Acoustic Problems: A Partially Opened Cavity Coupled With a Membrane and a Semi-Infinite Exterior Field." *Journal of Sound and Vibration* 254(2):231–44.

Kinsler, L. E., A. R. Frey, A. B. Coppens, and J. V. Sanders. 2000. *Fundamental of Acoustics*. New York, Chichester: John Wiley & Sons, INC.

Ko, N. W. M. and C. P. Tang. 1978. "Reverberation Time in a High-Rise City." *Journal of Sound and Vibration* 56(3):459–61.

Koch, W. 2005. "Acoustic Resonances in Rectangular Open Cavities." *AIAA journal* 43(11):2342–49.

Komkin, A. I. and M. A. Mironov. 2013. "Radiation Impedance of a Piston at the Wall of

a Rectangular Duct." *Acoustical Physics* 59(3):257–60.

Kriegsmann, G. A. and C. L. Scandrett. 1989. "Assessment of a New Radiation Damping Model for Structural Acoustic Interactions." *The Journal of the Acoustical Society of America* 86(2):788–94.

Kubota, Y. and E. H. Dowell. 1992. "Asymptotic Modal Analysis for Sound Fields of a Reverberant Chamber." *The Journal of the Acoustical Society of America* 92(2):1106–12.

Kung, Chaw-hua and Rajendra Singh. 1985. "Experimental Modal Analysis Technique for Three-dimensional Acoustic Cavities." *The Journal of the Acoustical Society of America* 77(2):731–38.

Kurze, U. J. and I. L. Vér. 1972. "Sound Attenuation in Ducts Lined with Non-Isotropic Material." *Journal of Sound and Vibration* 24(2):177–87.

Lacour, O., M. A. Galland, and D. Thenail. 2000. "Preliminary Experiments on Noise Reduction in Cavities Using Active Impedance Changes." *Journal of sound and vibration* 230(1):69–99.

Lam, P. M. and K. M. Li. 2007. "A Coherent Model for Predicting Noise Reduction in Long Enclosures with Impedance Discontinuities." *Journal of Sound and Vibration* 299(3):559–74.

Lapin, A. D. 2000. "Radiation Impedance of a Piston in a Waveguide." *Acoustical Physics* 46(3):427–29.

Lau, C. K. and S. K. Tang. 2005. "Sound Transmission across Duct Constrictions with

and without Tapered Sections." *The Journal of the Acoustical Society of America* 117(6):3679–85.

Lau, S. K. and S. K. Tang. 2000. "Sound Fields in a Slightly Damped Rectangular Enclosure Under Active Control." *Journal of Sound and Vibration* 238(4):637–60.

Lee, J. and I. Seo. 1996. "Radiation Impedance Computations of a Square Piston in a Rigid Infinite Baffle." *Journal of sound and vibration* 198(3):299–312.

Levine, H. 1983. "On the Radiation Impedance of a Rectangular Piston." *Journal of Sound and Vibration* 89(4):447–55.

Li, Y. Y. and L. Cheng. 2004. "Modifications of Acoustic Modes and Coupling due to a Leaning Wall in a Rectangular Cavity." *The Journal of the Acoustical Society of America* 116(6):3312–18.

Malbéqui, P., C. Glandier, and C. Reyner. 1996. "Sound Propagation and Radiation in a Curved Duct." *AIAA journal* 34(9):1778–84.

Mangiarotty, R. A. 1963. "Acoustic Radiation Damping of Vibrating Structures." *The Journal of the Acoustical Society of America* 35(3):369–77.

Mangulis, V. 1965a. "Radiation Impedance of a Rectangular Piston on a Corner." *Journal of the Franklin Institute* 279(3):200–208.

Mangulis, V. 1965b. "The Radiation of Sound from a Rectangular Piston on a Corner." *Journal of the Franklin Institute* 279(2):124–35.

Martin, V. and A. Bodrero. 1997. "An Introduction to the Control of Sound Fields by Optimising Impedance Locations on the Wall of an Acoustic Cavity." *Journal of*

sound and vibration 204(2):331–57.

Martin, V., A. Cummings, and C. Gronier. 2004. "Discrimination of Coupled Structural/acoustic Duct Modes by Active Control: Principles and Experimental Results." *Journal of Sound and Vibration* 274:583–603.

Mechel, F. P. 1988. "Notes on the Radiation Impedance, Especially of Piston-like Radiators." *Journal of sound and vibration* 123(3):537–72.

Mellow, Tim and Leo Kärkkäinen. 2011. "On the Sound Fields of Infinitely Long Strips." *The Journal of the Acoustical Society of America* 130(1):153–67.

Molinet, F. 2011. *Acoustic High-Frequency Diffraction Theory*. Momentum Press.

Montazeri, Allahyar, Javad Poshtan, and M. H. Kahaei. 2007. "Modal Analysis for Global Control of Broadband Noise in a Rectangular Enclosure." *Journal of low frequency noise, vibration and active control* 26(2):91–104.

Morfey, C. L. 1969a. "A Note on the Radiation Efficiency of Acoustic Duct Modes." *Journal of Sound and Vibration* 9(3):367–72.

Morfey, C. L. 1969b. "Acoustic Properties of Openings at Low Frequencies." *Journal of Sound and Vibration* 9(3):357–66.

Morse, P. M. 1976. *Vibration and Sound*. The American Institute of Physics.

Morse, P. M. and H. Feshbach. 1953. *Methods of Theoretical Physics. Vol. 1*. New York, McGraw Hill.

Morse, P. M. and K. U. Ingard. 1968. *Theoretical Acoustics*. USA McGraw-Hill.

Morse, P. M. and P. J. Rubenstein. 1938. "The Diffraction of Waves by Ribbons and by Slits." *Physical Review* 54(11):895–98.

Nelisse, H., O. Beslin, and J. Nicolas. 1998. "A Generalized Approach for the Acoustic Radiation from a Baffled or Unbaffled Plate with Arbitrary Boundary Conditions, Immersed in a Light or Heavy Fluid." *Journal of Sound and Vibration* 211(2):207–25.

Nieter, J. J. and Rajendra Singh. 1982. "Acoustic Modal Analysis Experiment." *The Journal of the Acoustical Society of America* 72(2):319–26.

Oldham, D. J. and X. Zhao. 1993. "Measurement of the Sound Transmission Loss of Circular and Slit-Shaped Apertures in Rigid Walls of Finite Thickness by Intensimetry." *Journal of sound and vibration* 161(1):119–35.

Ortiz, Santiago, Cyprien Le Plenier, and Pedro Cobo. 2013. "Efficient Modeling and Experimental Validation of Acoustic Resonances in Three-Dimensional Rectangular Open Cavities." *Applied Acoustics* 74(7):949–57.

Pagneux, V., N. Amir, and J. Kergomard. 1996. "A Study of Wave Propagation in Varying Cross-section Waveguides by Modal Decomposition. Part I. Theory and Validation." *The Journal of the Acoustical Society of America* 100(4):2034–48.

Pàmies, T., J. Romeu, M. Genescà, and A. Balastegui. 2011. "Sound Radiation from an Aperture in a Rectangular Enclosure under Low Modal Conditions." *The Journal of the Acoustical Society of America* 130(1):239–48.

Pan, J., S. J. Elliott, and K. H. Baek. 1999. "Analysis of Low Frequency Acoustic

Response in a Damped Rectangular Enclosure." *Journal of Sound and Vibration* 223(4):543–66.

Park, H. H. and H. J. Eom. 1997. "Acoustic Scattering from a Rectangular Aperture in a Thick Hard Screen." *The Journal of the Acoustical Society of America* 101(1):595–98.

Pelat, Adrien, Simon Félix, and Vincent Pagneux. 2009. "On the Use of Leaky Modes in Open Waveguides for the Sound Propagation Modeling in Street Canyons." *The Journal of the Acoustical Society of America* 126(6):2864–72.

Peretti, L. F. and E. H. Dowell. 1992. "Asymptotic Modal Analysis of a Rectangular Acoustic Cavity Excited by Wall Vibration." *AIAA journal* 30(5):1191–98.

Picaut, J., T. Le Pollès, P. L'Hermite, and V. Gary. 2005. "Experimental Study of Sound Propagation in a Street." *Applied Acoustics* 66(2):149–73.

Picaut, J. and L. Simon. 2001. "A Scale Model Experiment for the Study of Sound Propagation in Urban Areas." *Applied Acoustics* 62(3):327–40.

Pierce, Allan D., Robin O. Cleveland, and Mario Zampolli. 2002. "Radiation Impedance Matrices for Rectangular Interfaces within Rigid Baffles: Calculation Methodology and Applications." *The Journal of the Acoustical Society of America* 111(2):672–84.

Piippo, K. E. and S. K. Tang. 2011. "The Characteristics of Acoustic Line Array Prototypes for Scale Model Experiments." *Applied Acoustics* 72(11):884–88.

Le Polles, Thierry, Judicaël Picaut, Michel Berengier, and Claude Bardos. 2004. "Sound Field Modeling in a Street Canyon with Partially Diffusely Reflecting Boundaries

by the Transport Theory." *The Journal of the Acoustical Society of America* 116(5):2969–83.

Potel, Catherine and Michel Bruneau. 2008. "Modes Coupling due to Nonhomogeneously Shaped Walls in Duct Acoustics." *Journal of Sound and Vibration* 313:738–59.

Pretlove, A. J. 1965. "Note on the Virtual Mass for a Panel in an Infinite Baffle." *The Journal of the Acoustical Society of America* 113:266–70.

Pritz, T. 2004. "Frequency Power Law of Material Damping." *Applied Acoustics* 65:1027–36.

Rayleigh, J. W. S. 1945. *The Theory of Sound. Vol.2*. Dover Publications, New York.

Rice, E. A. P. 1978. "Multimodal Far-Field Acoustic Radiation Pattern Using Mode Cutoff Ratio." *AIAA Journal* 16(9):906–11.

Richards, S. K., X. Zhang, X. X. Chen, and P. A. Nelson. 2004. "The Evaluation of Non-Reflecting Boundary Conditions for Duct Acoustic Computation." *Journal of Sound and Vibration* 270(3):539–57.

Van Ruiten, C. J. M. 1988. "Mechanism of Squeal Noise Generated by Trams." *Journal of Sound and Vibration* 120(2):245–53.

Sadamoto, Akira, Yasuji Tsubakishita, and Yoshinori Murakami. 2004. "Sound Attenuation in Circular Duct Using Slit-like Short Expansion of Eccentric And/or Serialized Configuration." *Journal of Sound and Vibration* 277(4–5):987–1003.

Sauter, A. and W. W. Soroka. 1970. "Sound Transmission through Rectangular Slots of Finite Depth between Reverberant Rooms." *The Journal of the Acoustical Society of*

America 47(1):5–11.

Schröder, Christoph T. and Waymond R. Scott. 2001. "On the Complex Conjugate Roots of the Rayleigh Equation: The Leaky Surface Wave." *The Journal of the Acoustical Society of America* 110(6):2867–77.

Schultz, Todd. 2006. "Modal Decomposition Method for Acoustic Impedance Testing in Square Ducts." *The Journal of the Acoustical Society of America* 120(6):3750–58.

Seo, H. S. and Y. H. Kim. 2005. "Directional Radiation Pattern in Structural–acoustic Coupled System." *The Journal of the Acoustical Society of America* 118(1):92–103.

Sgard, Franck, Hugues Nelisse, and Noureddine Atalla. 2007. "On the Modeling of the Diffuse Field Sound Transmission Loss of Finite Thickness Apertures." *The Journal of the Acoustical Society of America* 122(1):302–13.

Sha, Kan, Jun Yang, and Woon Seng Gan. 2005. "A Simple Calculation Method for the Self- and Mutual-Radiation Impedance of Flexible Rectangular Patches in a Rigid Infinite Baffle." *Journal of Sound and Vibration* 282:179–95.

Shepherd, I. C. 1986. "Characteristics of Loudspeakers Operating in an Active Noise Attenuator." *Journal of sound and vibration* 110(3):471–81.

Sinayoko, Samuel, Phillip Joseph, and Alan McAlpine. 2010. "Multimode Radiation from an Unflanged, Semi-Infinite Circular Duct with Uniform Flow." *The Journal of the Acoustical Society of America* 127(4):2159–68.

Snakowska, A. 1996. "Modal Analysis of the Acoustic Field Radiated from an Unflanged Cylindrical Duct–theory and Measurement." *Acta Acustica united with Acustica*

82:201–6.

Stepanishen, P. R. 1971. "The Time-Dependent Force and Radiation Impedance on a Piston in a Rigid Infinite Planar Baffle." *The Journal of the Acoustical Society of America* 49(3):841–49.

Stepanishen, P. R. 1977. "The Radiation Impedance of a Rectangular Piston." *Journal of Sound and Vibration* 55(2):275–88.

Succi, G. P., K. J. Baumeister, and K. U. Ingard. 1978. "Interaction of a Turbulent-Jet Noise Source with Transverse Modes in a Rectangular Duct." *NASA Technical Paper 1248*.

Sucheendran, Mahesh M., Daniel J. Bodony, and Philippe H. Geubelle. 2014. "Coupled Structural-Acoustic Response of a Duct-Mounted Elastic Plate with Grazing Flow." *AIAA Journal* 52(1):178–94.

Sum, K. S. and J. Pan. 2006. "Effects of the Inclination of a Rigid Wall on the Free Vibration Characteristics of Acoustic Modes in a Trapezoidal Cavity." *The Journal of the Acoustical Society of America* 119(4):2201–10.

Swenson, G. W. and W. E. Johnson. 1952. "Radiation Impedance of a Rigid Square Piston in an Infinite Baffle." *The Journal of the Acoustical Society of America* 84.

Taflove, A. and S. C. Hagness. 2000. *Computational Electrodynamics: The Finite-Difference Time-Domain Method. Third Edition*. Boston London, Artech House.

Tang, S. K. 2012. "Narrow Sidebranch Arrays for Low Frequency Duct Noise Control." *The Journal of the Acoustical Society of America* 132(5):3086–97.

Tang, S. K. and J. S. F. Cheng. 1998. "On the Application of Active Noise Control in an Open End Rectangular Duct with and without Flow." *Applied Acoustics* 53:193–210.

Tang, S. K. and G. C. Y. Lam. 2008. "On Sound Propagation from a Slanted Side Branch into an Infinitely Long Rectangular Duct." *The Journal of the Acoustical Society of America* 124(4):1921–29.

Tang, S. K. and C. K. Lau. 2002. "Sound Transmission across a Smooth Nonuniform Section in an Infinitely Long Duct." *The Journal of the Acoustical Society of America* 112(6):2602–11.

Tang, S. K., R. C. K. Leung, R. M. C. So, and K. M. Lam. 2005. "Acoustic Radiation by Vortex Induced Flexible Wall Vibration." *The Journal of the Acoustical Society of America* 118(4):2182–89.

The MathsWorks. 1996. *Partial Differential Equation Toolbox User's Guide*. The MathsWorks, INC.

Thompson, D. J. and C. J. C. Jones. 2000. "A Review of the Modelling of Wheel/rail Noise Generation." *Journal of Sound and Vibration*.

Ting, Lu and J. B. Keller. 1977. "Radiation from the Open End of a Cylindrical or Conical Pipe and Scattering from the End of a Rod or Slab." *The Journal of the Acoustical Society of America* 61(6):1438–44.

Trompette, Nicolas, Jean-Louis Barbry, Franck Sgard, and Hugues Nelisse. 2009. "Sound Transmission Loss of Rectangular and Slit-Shaped Apertures: Experimental Results and Correlation with a Modal Model." *The Journal of the Acoustical Society of*

America 125(1):31–41.

Utsumi, M. 1999. "An Efficient Method for Sound Transmission in Non-Uniform Circular Ducts." *Journal of sound and vibration* 227(4):735–48.

Utsumi, M. 2001. "Sound Transmission in Circular Ducts of Continuously Varying Cross-Sectional Area." *Journal of Sound and Vibration* 242(2):369–76.

Wallace, C. E. 1987. "The Acoustic Radiation Damping of the Modes of a Rectangular Panel." *The Journal of the Acoustical Society of America* 81(6):1787–94.

Wassef, W. A. 1985. "Acoustic Emission Spectra due to Leaks from Circular Holes and Rectangular Slits." *The Journal of the Acoustical Society of America* 77(3):916–23.

Wilson, G. P. and W. W. Soroka. 1965a. "Approximation to the Diffraction of Sound by a Circular Aperture in a Rigid Wall of Finite Thickness." *The Journal of the Acoustical Society of America* 37(2):286–97.

Wilson, G. P. and W. W. Soroka. 1965b. "Reply to 'Comments on "Approximation to the Diffraction of Sound by a Circular Aperture in a Rigid Wall of Finite Thickness"'[MC Gomperts, J. Acoust. Soc. Am. 38, 877(L)]" *The Journal of the Acoustical Society of America* 878.

Wood, J. K. and G. B. Thurston. 1953. "Acoustic Impedance of Rectangular Tubes." *The Journal of the Acoustical Society of America* 25(5):858–60.

Yang, L. N. and B. M. Shield. 2000. "Development of a Ray Tracing Computer Model for the Prediction of the Sound Field in Long Enclosures." *Journal of Sound and Vibration* 229(1):133–46.

Yu, Xiang, Li Cheng, and Jean Louis Guyader. 2014. "On the Modeling of Sound Transmission through a Mixed Separation of Flexible Structure with an Aperture." *The Journal of the Acoustical Society of America* 135(5):2785–96.

Zorumski, W. E. 1973. "Generalized Radiation Impedances and Reflection Coefficients of Circular and Annular Ducts." *The Journal of the Acoustical Society of America* 54(6):1667–73.